AD-A137 409 AN EXPERIMENTAL STUDY ON THE EFFECT OF BOW SHAPE ON THE SEAWORTHINESS OF A SHIP(U) CALIFORNIA UNIV BERKELEY DEPT OF NAVAL ARCHITECTURE W C WEBSTER ET AL. SEP 83 1/2

UNCLASSIFIED N00014-80-C-0226 F/G 13/10 NL

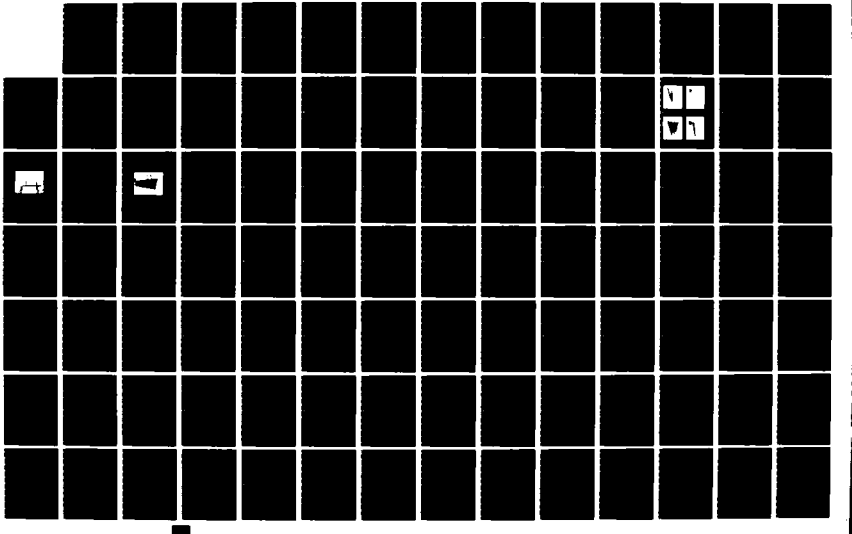

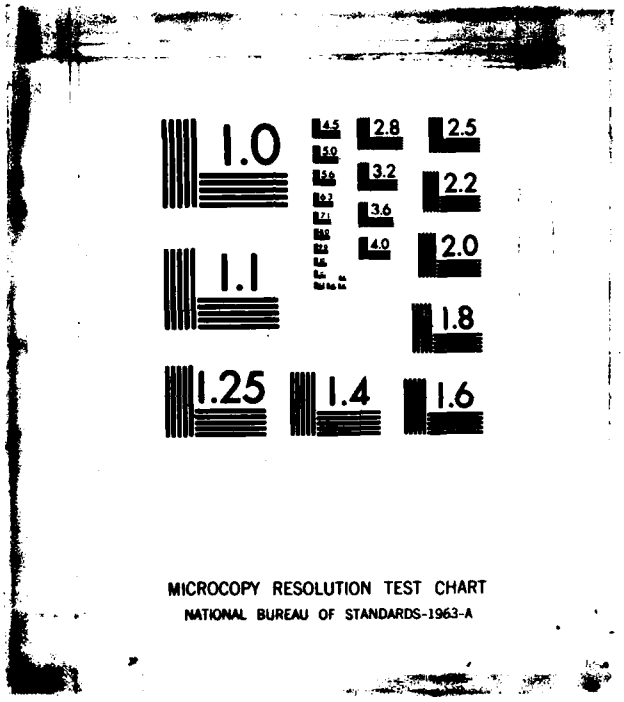
1.0
1.1
1.25
1.4
1.6
1.8
2.0
2.2
2.5
2.8
3.2
3.6
4.0
4.5
5.0
5.6
6.3
7.1
8.0
9.0
MICROCOPY RESOLUTION TEST CHART
NATIONAL BUREAU OF STANDARDS-1963-A

AN EXPERIMENTAL STUDY ON THE EFFECT OF BOW SHAPE ON THE SEAWORTHINESS OF A SHIP

by

William C. Webster[1] and Ying-Fu Zhu[2]

prepared for

David W. Taylor Naval Research & Development Center
General Hydrodynamic Research Program
under Contract N00014-80-C-0226

(In accordance with the Department of Defense Distribution Statement A)

[1] Professor of Naval Architecture, University of California, Berkeley.

[2] Visiting Scholar at Department of Naval Architecture & Offshore Engineering, University of California, Berkeley, on leave from Wuhan Ship Design & Development Institute.

SECURITY CLASSIFICATION OF THIS PAGE *(When Data Entered)*

REPORT DOCUMENTATION PAGE		READ INSTRUCTIONS BEFORE COMPLETING FORM
1. REPORT NUMBER	2. GOVT ACCESSION NO.	3. RECIPIENT'S CATALOG NUMBER
4. TITLE *(and Subtitle)* AN EXPERIMENTAL INVESTIGATION OF THE EFFECT OF BOW SHAPE TO THE SEAKEEPING QUALITIES OF HIGH SPEED DISPLACEMENT TYPE SHIPS		5. TYPE OF REPORT & PERIOD COVERED FINAL 6. PERFORMING ORG. REPORT NUMBER
7. AUTHOR(s) WILLIAM C. WEBSTER & YING-FU ZHU		8. CONTRACT OR GRANT NUMBER(s) N00014-80-C-0226
9. PERFORMING ORGANIZATION NAME AND ADDRESS Naval Architecture & Offshore Engr Dept University of California/Berkeley Berkeley, CA 94720		10. PROGRAM ELEMENT, PROJECT, TASK AREA & WORK UNIT NUMBERS 61153N Ro2301 SR 023 01 01
11. CONTROLLING OFFICE NAME AND ADDRESS David W. Taylor Naval Ship R&D Center (Code 1505) Bethesda, MD 20084		12. REPORT DATE September 1983 13. NUMBER OF PAGES 96
14. MONITORING AGENCY NAME & ADDRESS*(if different from Controlling Office)* Office of Naval Research 800 N. Quincy Street Arlington, Virginia 22217		15. SECURITY CLASS. *(of this report)* Uncl 15a. DECLASSIFICATION/DOWNGRADING SCHEDULE

16. DISTRIBUTION STATEMENT *(of this Report)*

APPROVED FOR PUBLIC RELEASE; DISTRIBUTION UNLIMITED

17. DISTRIBUTION STATEMENT *(of the abstract entered in Block 20, if different from Report)*

N/A

18. SUPPLEMENTARY NOTES

Supported by the Naval Sea Systems Command General Hydromechanics Research Program administered by David Taylor Naval Ship R&D Center, Code 1505, Bethesda, MD 20084

19. KEY WORDS *(Continue on reverse side if necessary and identify by block number)*

(U) Bow Shape Effects (U) GHR Program (U) Seaworthiness

20. ABSTRACT *(Continue on reverse side if necessary and identify by block number)*

(U) This experimental study concentrates on the effects of the above-water shape of a ship's bow on the seaworthiness of the ship. Detailed measurements were made on four ship models, all of which had the same underwater hull form, that of the Series 60/0.69 parent. The four bows included the parent bow, a bow with practically no flare, a bow with very large flare and a bow with compound flare. All of the bows had the standard sheer line. The models were tested in regular head seas of moderately severe height corresponding to waves

DD FORM 1 JAN 73 1473 EDITION OF 1 NOV 65 IS OBSOLETE
S/N 0102-LF-014-6601

SECURITY CLASSIFICATION OF THIS PAGE *(When Data Entered)*

Abstract

This experimental study concentrates on the effect of the above-water shape of a ship's bow on the seaworthiness of the ship. Detailed measurements were made on four ship models, all of which had the same underwater hull form, that of the Series 60 / 0.60 parent. The four bows included the parent bow, a bow with practically no flare, a bow with very large flare and a bow with compound flare. All of the bows had the standard sheer line. The models were tested in regular head seas of moderately severe height, corresponding to waves with a height to length ratio of 1:40. The results showed that all four bow shapes had nearly identical added resistance in waves and nearly identical pitch transfer functions. Increases in the bow flare lead to reductions in the heave and relative water motion transfer functions. Detailed examination of the records indicated that the higher harmonic character of the pitch motions was also affected. Finally, it was determined that the vertical accelerations of the bow were minimized with the small flare bow.

AN EXPERIMENTAL STUDY ON THE EFFECT OF BOW SHAPE ON THE SEAWORTHINESS OF A SHIP

by

William C. Webster and Ying-Fu Zhu

Introduction

When observing the motions of a ship in a seaway, one notices that much of the "action" appears to take place at the bow, particularly in head seas. The pitch and heave motions combine in such a way that the motions at the bow are the largest. In moderate to severe head seas the flow of water near the bow becomes spectacular. Sheets of water are sprayed into the air and occasionally a mass of green water may wash across the deck of the ship. Simultaneously with these two very visible effects, there is invariably a substantial increase in the resistance of the ship. Also, if one measures it, large dynamic pressures occur both on the bottom of the ship's hull and on the flare of the bow. These pressures can lead to local failure of the hull structure and to a dynamic response of the hull called slamming. These phenomena constitute some of the major components of that subjective quality of a ship called "seaworthiness".

It is reasonable to believe, therefore, that the shape of the bow plays a fundamental role in determining seaworthiness in head seas. However, the shape of the bow is important in other aspects of ship design which have nothing to do with behavior in a seaway. For instance, the stillwater resistance of the ship depends critically on the underwater hull shape at the bow, and the maneuvering performance is also affected by this shape. The naval architect must integrate all of these effects into the design of the bow. Unfortunately, although much is known about the relationship of the bow shape to ship resistance, little is known about its relationship to seaworthiness.

It is the aim of the research presented here to explore this relationship. Because we are particularly interested the behavior in moderate to high seas, we expect that the aspects of sea-

worthiness that are of interest here will not be possible to describe or investigate using, say, standard linearized ship motion theories. Rather we can expect that progress at this time can only be made through careful and systematic experiments.

Overview

In order to concentrate more fully on this relationship a special strategy has been adopted. The underwater portion of the ship hull has been kept unchanged throughout this study. This strategy has many benefits. First, since the stillwater resistance depends almost entirely on the underwater shape of the hull, we expect this important design quantity to remain unchanged for all of the bow shapes under consideration. Similarly, we expect the maneuvering performance will also be unaffected. Second, all linear ship motions theories predict that the motions of a ship are completely determined by the underwater shape of the hull together with the inherent inertial characteristics of the ship as a rigid body. In the study reported here we do keep these inertial properties fixed and thus these theories would predict exactly the same motions (and thus exactly the same seaworthiness) for all of the ships under consideration. As a result, any effect of the different bow shapes can be expected to be exhibited only in moderate to severe seas, and that these effects will be higher order in some sense.

Two of the variables in the design of ship's bows are the bow freeboard, the distance from the stillwaterline to the forecastle deck at the bow, and the length of the forecastle deck. If the freeboard is high enough and if the forecastle deck extends far enough aft, then no green water will wash onto the deck. The selection of these two dimensions depends on the relative motion between the bow and the waves, and on the severity of the seaway which the ship can be expected to be exposed. The dynamics of the ship motions might be quite different with a significant amount of green water on the deck and it is problematical whether these dynamics will scale well with the five foot models used in the U. C. Ship Model Towing Tank. Thus, the decision was made not to attempt to consider significant greenwater on deck. The seaways used in testing were selected to be relatively severe, but not so much that the forecastle deck or main deck was immersed in any of the models. A wave steepness of 1:40 proved to be satisfactory for all models used in this study.

The removal of the possibility of green water on the deck does not mean that the relative motion of the waves at the bow and the bow itself is of no interest. Rather, the relative water motion measured during the tests described below can be used as a guide to the naval architect to determine the forecastle deck freeboard and length necessary to avoid green water on the deck.

With the elimination of underwater bow shape, freeboard and forecastle length as principal variables, the effort concentrated simply on the shape of the above water portion of the bow and its effect on the seaworthiness of the ship. The quantities to be measured are the relative water motion at several locations at the bow, the motions of the ship and the resistance of the ship in the seaway.

The Models

The models used for all of the studies presented here were based on the Series 60, block 0.60 parent hull form. As mentioned above, the shape of the underwater portion of the hull was fixed and matched exactly that of the parent Series 60 hull form. In addition, the hull profile, both above and below the waterline, was also maintained constant and equal to that of the Series 60 parent. Thus all of the models had the same freeboard and rake of the stem. The sheer was the standard sheer for Series 60.

The models themselves were all made of wood and were constructed in two pieces. The afterbody, which began at station 6 (30% aft of the forward perpendicular) was the same for all models tested and was identical in every way to the Series 60 parent. Four different forebodies which had the same underwater shape as the Series 60 form were constructed. These bows faired smoothly into the afterbody when they were connected to it. The four bow models were:

a. The Series 60, block 0.60 parent hull.
b. A bow with practically no flare.
c. A bow with extreme flare.
d. A bow with compound flare.

Body plans of the four models are shown in figures 1 through 4. Figure 5 shows photographs of all four of the bow models so that

the differences amongst them can be readily seen. The particulars of all of the models were:

Length between perpendiculars	5.000 ft.
Beam	0.667 ft.
Draft	0.267 ft.
Block Coefficient	0.600
Longitudinal radius of gyration	1.25 ft.

In order to design the large flare and compound flare models, it was of some concern that the flare not begin so close to the waterline that the bow wave in stillwater tests would be deformed. Tests were run in which the bow wave in stillwater for the parent was measured for various Froude numbers. The bow wave for Fr = 0.30 was selected as the reference wave and the shape of the bows c. and d. were allowed to be only marginally different from the Series 60 form in the neighborhood of this wave. The load waterline for the Series 60 form is referred to as the 1.00 waterline. The crest of the bow wave was almost to the 1.50 waterline at a distance 7% aft of the bow at a Fr = 0.30. As a result, the knuckle for the compound flare was chosen to be above the 1.50 waterline (see figure 6).

Stillwater resistance tests were run on all four of the hulls. Results for the total resistance coefficient versus Froude number are shown in figure 7. As hoped for, all of the models had the same resistance (within experimental accuracy) for values of Fr > 0.20. For Fr < 0.20 there was considerable scatter and this was presumably due to variations in the transition to turbulent flow on the hull. The design Froude number for a hull of this block coefficient is about 0.28 to 0.30. However in moderate to severe head seas it seemed unlikely that such a speed could be maintained. It was also desired to conduct tests at a speed well above a value of Fr = 0.20 so that the difficulties with flow transition could be avoided. Therefore a value of Fr = 0.25 was selected as a standard to conduct the bow motions tests.

Test Procedure

Before the test of a model was conducted, the model was ballasted so that it had the correct displacement, center of gravity and longitudinal gyradius. The displacement of the model was measured out of the water on a balance capable of resolving a

weight of 0.01 lbs. The wooden model by itself weighed considerably less than the required displacement so that it was necessary to add lead ballast weights. The longitudinal distribution of these weights was determined by an iterative process since this distribution determined the heel, trim and the longitudinal gyradius of the model. The heel and trim was checked by floating the model in a small tank of water with a mirror behind the model. The gyradius was checked by mounting the model on a bifilar pendulum and checking the period of pendulation. The weights were adjusted towards or away from the center of gravity in order to decrease or increase respectively the longitudinal gyradius. The process of checking for correct heel and trim, and then checking for correct longitudinal gyradius was repeated until all of the quantities were simultaneously correct. At this point the ballast weights were fixed to the model so that they would not move during the tests.

The model was then placed in the ship motions dynomometer as shown in the photograph in figure 8. A schematic diagram of the dynomometer is shown in figure 9. The dynomometer frame is rigidly attached to the towing carriage. The dynomometer has a subcarriage which can translate freely in the longitudinal tank direction and to which a constant towing force can be applied. The towing force is generated by means of a hanging weight and pulley system. The diameter of the pulley to which the ship model is attached 10 times that to which the hanging weight is attached so that reasonable size weights can be used. Compared to the inertia of the ship, the equivalent inertia of the towing weight was small enough to disregard.

In addition to the freedom to surge provided by the dynomometer subcarriage, the model was also allowed to heave and pitch. The model was connected to the subcarriage by a pair of vertical rods which pass through linear ball bushings in the subcarriage. These bushings are rigidly attached to the subcarriage so that only vertical motions of the rods are permitted. The bottoms of the two rods are attached to a bearing which gave the model freedom to pitch. All three motions (heave, pitch and surge) were measured by potentiometer pickups.

Initially, it was attempted to use a constant towing force for all of the wave tests (the force measured during the the stillwater towing tests). However, it was found that the model did appreciably slow down in waves near the pitch resonant

period and this rendered the results somewhat questionable. The tests were then rerun with the towing weight adjusted to maintain a constant forward speed corresponding to Fr = 0.25. This meant that each test had to be conducted at least twice. The first run was needed to determine the proper tow weight and the second to obtain the desired data.

In addition to the motions information and the resistance, other measurements were also made. Wave probes were mounted on the bow of each model at various locations aft of the forward perpendicular. These wave probes were of the resistance type. They were mounted in a special way on the model, as shown in figure 10. The attachment to the hull was made with a plastic fitting which held the probe above the forecastle deck and away from the edge of the hull. Early experience with these gauges indicated that if they were allowed to be contacted by the water on the deck arising from the bow spray, then the measured values of the relative water height were not reliable. Finally an additional wave probe was mounted in the tank itself well in front of the model and reasonably far away from the wave maker, so that the wave enviornment to which the model was exposed could be measured.

All of the measurement signals were amplified and conditioned, and then were recorded in real time on the Department of Naval Architecture's Hewlett-Packhard System 1000 data acquisition computer. These data was sampled at a rate of 50 samples per second and this was more than adequate for these tests. High quality video records were made of almost all of the tests as well.

The test procedure was the same for all models. After the properly ballasted model was installed on the dynomometer, all of the gauges and motions potentiometers were calibrated. Each test consisted of measuring the response of the model to a train of regular waves. These waves were generated with a height to length ratio of 1:40 by the model tank's hydraulic wavemaker. The lengths of the waves used in these tests varied from considerably less than the ship length to several ship lengths. These waves bracketed the pitch and heave resonance of the model. Several additional tests were made using waves at the ship's pitch resonance. In these tests the height of the waves were varied from height to length ratios of 1:60 to 1:30.

Data Analysis

During the model tests two different types of data were recorded. The first type was the resistance of the model during the wave tests. This resistance corresponded to the towing force which was required to maintain the average speed of the model to correspond to a value of Fr = 0.25. Since the model was free to surge, this is the only meaningful measure of resistance. The resistance thus measured was compared with the resistance in stillwater and the difference between the two, the added resistance due to waves, was formed. The added resistance coefficient given by

$$C_{ar} = \delta R / \rho g \zeta_a^2 (B^2/L) \qquad (1$$

was computed for all of the tests. ζ_a is the wave amplitude. The plot shown in figure 11 shows the added resistance for the parent hull form. On this scale the differences amongst the various bow shapes were indiscernable. The fact that the added resistance does not exhibit a strong dependence on the bow shape (as some of the other quantities described below do) seemed at first a bit puzzling. However, even though the added resistance is a non-linear quantity (it varies approximately with the square of the wave amplitude), the leading order terms can be computed from the first-order velocity potential (see Newman [1961]). Since this velocity potential is completely determined by the underwater shape of the hull, and is the same for all of the hulls under consideration here, it is reasonable that the measured added resistance should be the same.

The second, and more interesting type of data consists of the time series recordings of the various motions and relative water heights. The relative water motion at the bow consists of three parts: the piling up of water as the ship proceeds in stillwater (the bow wave), the incoming waves, and the change in these waves caused by the motions of the ship. A careful examination of many of these records revealed that these time series were periodic but not necessarily sinusoidal. Figure 12 shows schematically a typical time series. The mean (or average value) and the median (half way between the maximum and minimum) of the series are offset from zero, the value of the quantity measured when the model was at zero speed and no waves were present. Because the trace is not sinusoidal, the mean value can be different from the median value. If the motions were adequately

represented by linear ship motion theory, then all of the time histories would be pure sinusoidal. The lack of sinusoidal traces is evidence that the nonlinear effects are strong.

The mean displacement from zero is due to three causes. The first is simply the fact that a ship develops a sinkage and trim due to forward way. This causes an offset of all of the measured quantities. Like the added resistance, both of these effects are already well predicted by linear ship resistance theory (Yeung [1972]) and therefore only depend on the underwater shape. Second, as a result of the forward way the ship develops a bow wave which causes an offset of the relative water height measurements. Finally, nonlinear theories predict that inclusion of second-order terms will result in both second harmonic terms in the motions and offsets of the means. A recent paper by Blok and Huisman [1983] claims that, of the three, sinkage and trim effects dominate. If this were true, we should expect little difference amongst the ship models tested here in the mean offsets of the motions.

With this background, it is interesting to examine the data measured during the model tests. For any given quantity (motion or relative wave height) we can characterize the time series by many different statistics. First, we can determine the maximum and minimum values of the given quantity during the interval which the record appears to be periodic. This is particularly appropriate in the case of relative bow motions. If the relative water motion is too large in the up direction, then the chances for green water on the deck increase. If the relative motion is too large in the down direction, then the chances for bottom slamming increase. It is oftentimes true that these two situations are not equally probable. For instance, the former is likely to be dominant for a fully laden ship riding at a deep waterline, whereas the latter is likely to be dominant for a ship in ballast. For the particular model chosen for the basis of this study, the controlling factor appears to be the green water on the deck.

Second, we can perform a Fourier analysis of the time series using the encounter period as the fundamental period. For instance, if the time history in question is given by f(t) then we can determine a Fourier representation of it resulting in

$$f(t) = \sum_{n=1}^{n=N} \{a_{f,n} \cos(n\omega_e t) + b_{f,n} \sin(n\omega_e t)\} \quad (2$$

where ω_e is the encounter frequency. One measure of the size of the motion is the amplitude of the fundamental motion, $A_{f,1}$, where the n^{th} order amplitude is given by

$$A_{f,n} = [a_{f,n}^2 + b_{f,n}^2]^{1/2} \quad (3$$

If the response is truly linear then we expect the fundamental to be the only significant component in the Fourier expansion (2). If the response exhibits nonlinear effects then we can expect that the second and higher harmonics will begin to become significant. A measure of the nonlinear effects then can be formed by taking the ratio of the second harmonic amplitude to the fundamental. If we denote this ratio by t_f, then

$$t_f = A_{f,2} / A_{f,1} \quad (4$$

We do not expect that there will be significant higher harmonics without there being a significant second harmonic. For instance, the second-order perturbation theory of Potash [1971] has only fundamental and second harmonic terms.

The vertical accelerations of the bow (measured in an inertial system) are an important measure of seaworthiness and requires special consideration. These accelerations are uniquely determined from the pitch and heave motions of the ship as a rigid body. If we denote the heave time series by h(t) and the pitch time series by p(t) (pitch and heave measured at the center of gravity), then for a point a distance x forward of the center of gravity the time series of the vertical motion, v(t), is given by

$$v(t) = h(t) + x \cdot p(t) \quad (5$$

Let us assume that a Fourier analysis of the heave and pitch time series has been performed as in (2) above. Then we can rewrite (3)

$$v(t) = \sum_{n=1}^{n=N} \{a_{v,n} \cos(n\omega_e t) + b_{v,n} \sin(n\omega_e t)\} \quad (6$$

where

$$a_{v,n} = a_{h,n} + x \cdot a_{p,n}$$
$$b_{v,n} = b_{h,n} + x \cdot b_{p,n}$$

The vertical acceleration resulting from this motion are given by

$$\ddot{v}(t) = \omega_e^2 \sum_{n=1}^{n=N} n^2 \{a_{v,n} \cos(n\omega_e t) + b_{v,n} \sin(n\omega_e t)\} \quad (7$$

The factor n^2 in this summation gives more weight to the higher harmonics and it is therefore essential to carry these terms. In the data which is presented in the next section, the first three harmonics are retained in the computation of bow acceleration.

Finally, as with all experiments, the data exhibited a certain amount of scatter. In order to better visualize the differences between the various bows curves were fitted to the measured data points. It was found by trial and error that a Laurent series gave a good fit. The data are all plotted as a function of wave length to ship length, r, a parameter which varied from 0.8 to 2.0 during the tests. The following series was fitted in the least-square sense to the any of the resultant quantities, f(r)

$$f(r) = \sum_{n=1}^{n=5} c_n \cdot [r - d]^{(1-n)} \quad (8$$

For the measurements of the amplitude of the fundamental motions and relative water heights a value of d = 0. was selected. For all other results a value of d = 0.4 seem to give a better fit. In all cases the experimental points are presented so that the scatter can be seen.

Test Results

The test results are divided into four separate sets. The first set involves the transfer functions of the two measured motions (pitch and heave) and the transfer functions associated with the relative water motion measured at five different locations (5%, 10%, 15%, 20% and 25% aft of the bow). In the case of heave and the relative water motions, the transfer function used

here is the ratio of the amplitude of the fundamental (see equation 3) to the amplitude of the incoming wave. In the case of the pitch the amplitude of the fundamental angle was divided by the wave slope. This nondimensional presentation has the following advantage. The heave and pitch transfer functions should approach unity for long wave lengths (r large); the relative motion transfer functions should approach zero for long wave lengths. Transfer functions defined this way are a popular presentation for ship motion data. These data are shown in figures 13 through 19. In these figures only the fitted curves are shown. The original data points and the individual curves resulting therefrom are shown in the Appendix.

One quickly sees that the differences in bow shape cause significant differences in the heave transfer functions, but only cause minor differences in the pitch transfer functions. This result was very surprising since it was expected that the dramatic variations in the bow would influence the pitch motions far more significantly than the heave motions. Further, it can be seen that there is a significant variation in the transfer functions of the relative water motion at the various measurement locations with bow shape. There appeared to be a reduction in the relative motion transfer function with increasing bow flare at all of the locations which were measured. In particular, the large flare bow seemed to yield significantly lower relative motions than the other bow shapes. However, since any difference must be due to nonlinear effects, it is not clear how to interpret these differences.

In order to gain a clearer understanding of the nature of the heave and pitch nonlinearity, a second set of curves has been prepared and presented in figures 20 and 21. In these figures the ratio of the second harmonic amplitude to the fundamental amplitude (t in equation 4) is plotted for both the pitch and heave motion. In these plots we see that there is a dramatic increase in second harmonic content in the pitch motions as the flare of the bow increases. The second harmonic content of the heave motions is little affected by the shape of the bow.

Thus, we see that both heave and pitch motions each display significant nonlinear changes resulting from the bow shape, but the character of these changes is very different. The heave motion remains relatively sinusoidal but the amplitude changes as the bow shape changes. The pitch motion becomes increasing non-

sinusoidal as the bow shape changes, but does not undergo a significant change in its fundamental amplitude of motion. It is clear from these two motions that the traditional transfer function presentation does not reliably indicate the presence or nature of significant nonlinearities.

The third set of data are shown in figures 22 through 26. These show the maxima, minima and median (the average of the two previous quantities) of the relative water motion measured at 5%, 10%, 15%, 20% and 25% of the length aft of the bow. These figures show only the fitted curves, the actual data points are, as before, shown in the Appendix. These quantities are important in determining the susceptability to taking green water on deck or to slamming of the bottom of the bow.

The variations in maximum water height amongst the different bows was less pronounced than was observed for the transfer functions, but the general trends remained. In terms of minimum green water on the deck, the large flare bow seemed to reduce the maximum wave height best, followed by the compound flare bow. One should also notice that for locations forward of 10% aft of the bow, the maximum relative water height is affected by the bow shape but the minimum not. Further aft, one sees that both the maximum and minimum relative water heights are affected. That is, these results show that the above-water shape of the bow can influence the chance of slamming at locations aft of about 10% aft of the bow.

At almost all locations and for all bow shapes, a very marked variation in the median value with the parameter r (wave length/ship length) was observed. Thus this data seems to be in conflict with the assertion of Blok and Huisman [1983] that the offset of relative motions at the bow are principally due to stillwater sinkage and trim.

The final set of data in figure 27 show the computed acceleration at the forward perpendicular (see equation 7). The quantity plotted here is the nondimensional magnification factor. It is computed by determining the acceleration at the bow using the first three terms of the Fourier series representation of the time series divided by an acceleration derived from the wave amplitude ($\zeta_a \omega_e^2$). This represents the ratio of the maximum bow acceleration to that which would be experienced by a point exactly following the wave (at the encounter frequency). This figure

clearly shows that although the large flare model reduced the heave transfer function or extreme relative motions most, it did so only at the expense of much greater peak accelerations at the bow. On the other hand, the small flare bow had the least vertical accelerations.

Conclusions

On the basis of the research presented here, it is possible to draw several conclusions concerning the effect of the above-water bow shape on the seaworthiness of a ship travelling in moderately severe head seas. These can be divided into the various aspects of seaworthiness as follows:

1. Added Resistance. The experiments found practically no difference in the added resistance due to motions amongst all of the bow shapes. These data indicate that the added resistance is primarily due to the underwater shape of the hull, a result which is consistent with linearized ship resistance theory.

2. Ship Motions. The data measured in these experiments show that the above-water bow shape affects the pitch and heave motions in entirely different ways. Increases in the flare of the bow led to a reduction of the heave motions. These motions remained practically sinusoidal. Increases in the flare of the bow dramatically increased the higher harmonic content of the pitch but did not change the amplitude of the fundamental motion.

3. Relative Water Motion at the Bow. The relative water motion at the bow varies considerably with the ratio of wave length to ship length. The largest relative motions occur when the encounter frequency is close to the heave and pitch natural frequencies. For these waves the effect of bow shape was examined in two different ways. First, it was found that increases in the flare of the bow reduced considerably the fundamental amplitude of the relative wave motion. Second, the maximum and minimum water heights measured at the bow decreased with increased bow flare, but not as much as the fundamental motion did. That is, the higher harmonic content of the relative water motions in the large flare bow cases removes much of the apparent advantage of these bows seen in the transfer functions.

The tests also showed that changes in bow shape affect not

only the maximum water height at the bow, but the minimum height as well. The relative water height further aft than 10% of the length aft of the bow showed changes in the minimum water height which were as significant as those for the maximum height. These results indicate that the above water bow shape may play a role in the control of slamming.

4. The Median Relative Water Height. The tests revealed that the median relative water height varied significantly with encounter frequency (i.e. wave length) and varied somewhat with bow shape. The variation with bow shape was much more noticeable very close to the bow. At any rate, the contention of Huisman and Blok that the mean of the relative water height is primarily dependent on the stillwater sinkage and trim was not borne out by these tests.

5. The Accelerations at the Bow. Computations of the maximum accelerations at the bow indicated that the smallest flare bow had the smallest accelerations. The large flare bows which appeared to have a distinct advantage as far as the relative water height was concerned showed accelerations which were as much as 30% larger than the small flare bow.

In conclusion, the tests show that selection of the above-water bow shape is really a trade-off. Increases in flare do reduce the relative motion of the water at the bow, but only at the expense of greatly increased accelerations at the bow. The selection of the bow best suited to a particular application must therefore depend on the relative importance of these two considerations.

Acknowledgement

This research was sponsored by the Naval Sea Systems Command General Hydromechanics Research Program administered by the David Taylor Naval Ship Research and Development Center under Office of Naval Research Contract N00014-80-C-0226.

The experimental part of this research program was initiated and carried out for more than two years by Mr. Osvald Sibul, a research engineer at the University of California. Unfortunately, Mr. Sibul died suddenly before the research was completed. Although much of the data reported here was collected after his death, the authors would like to take this opportunity to express their indebtedness to Mr. Sibul for his substantial input to this program and for his development of the instruments and techniques at U. C. Berkeley which made these experiments possible.

References

Bales, N. K., "Minimum Freeboard Requirements for Dry Foredecks: a Design Procedure", SNAME Spring Meeting - STAR Symposium, Paper No. 3, 1979.

Blok, J. J. and Huisman, J., "Relative Motions And Swell-Up for a Frigate Bow", RINA Spring Meeting, Paper 2, 1983.

Newman, J. N., "A Linearized Theory for the Motion of a Thin Ship in Regular Waves", JSR, Vol. 5, No. 1, 1961, pp.34-55.

Newton, R. N., "Wetness Related to Freeboard and Flare", Trans. RINA 1960.

Potash, R. L. "Second-Order Theory of Oscillating Cylinders", JSR, Vol. 15, 1971,, pp.295-324.

Saunders, H. E., Hydrodynamics in Ship Design, SNAME, New York, Vol. I, p.322.

Swaan, W. A. and Vossers, G., "The Effect of Forebody Section Shape on Ship Behaviour in Waves", International Shipbuilding Progress, Vol. 8, July 1961, No. 83.

Yeung, R. W., "Sinkage and Trim in First-Order Thin-Ship Theory", JSR, Vol. 16, No. 1, 1972, pp. 47-59.

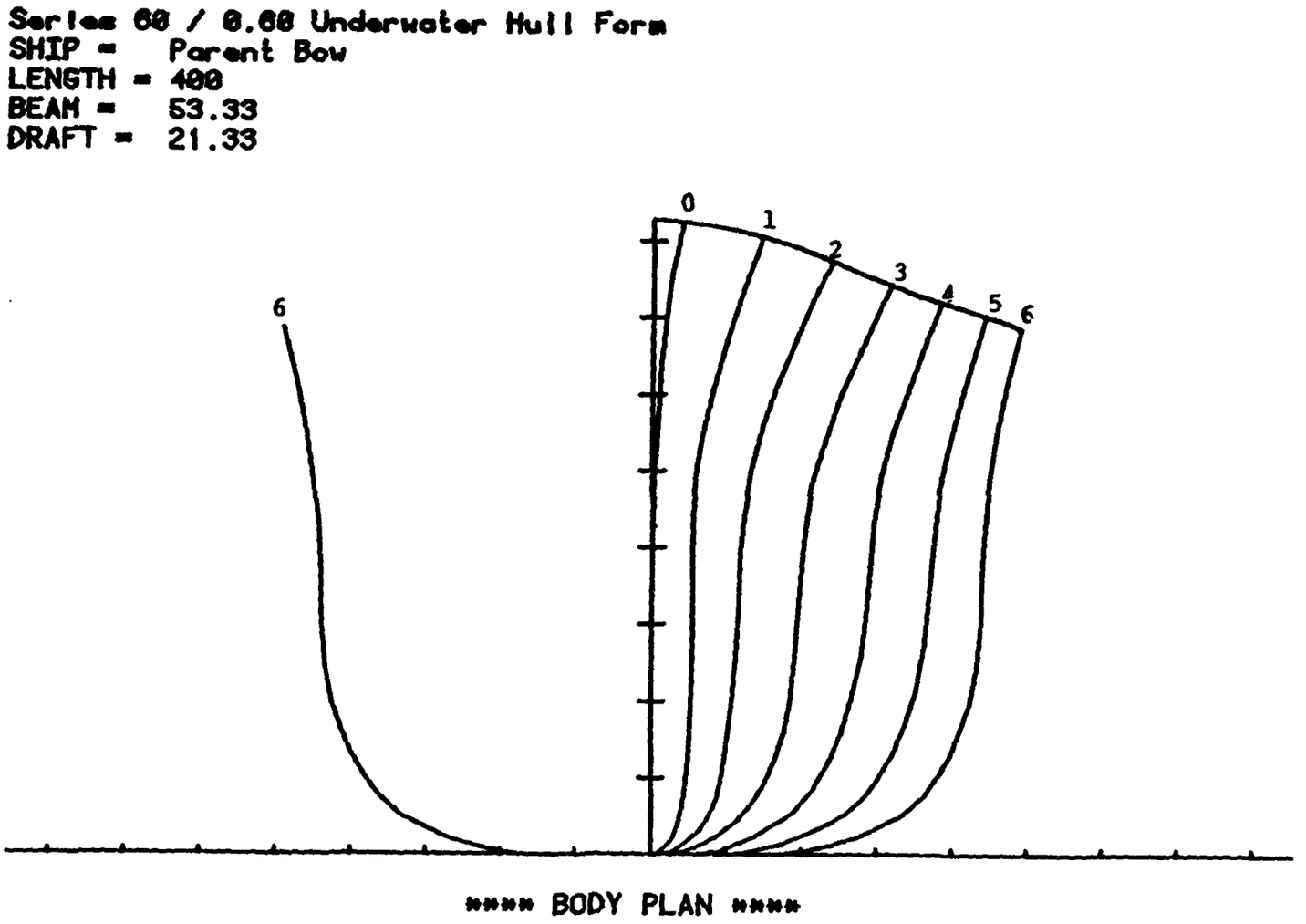

Figure 1. Body Plan of Bow of Series 60 / 0.60 Parent Hull

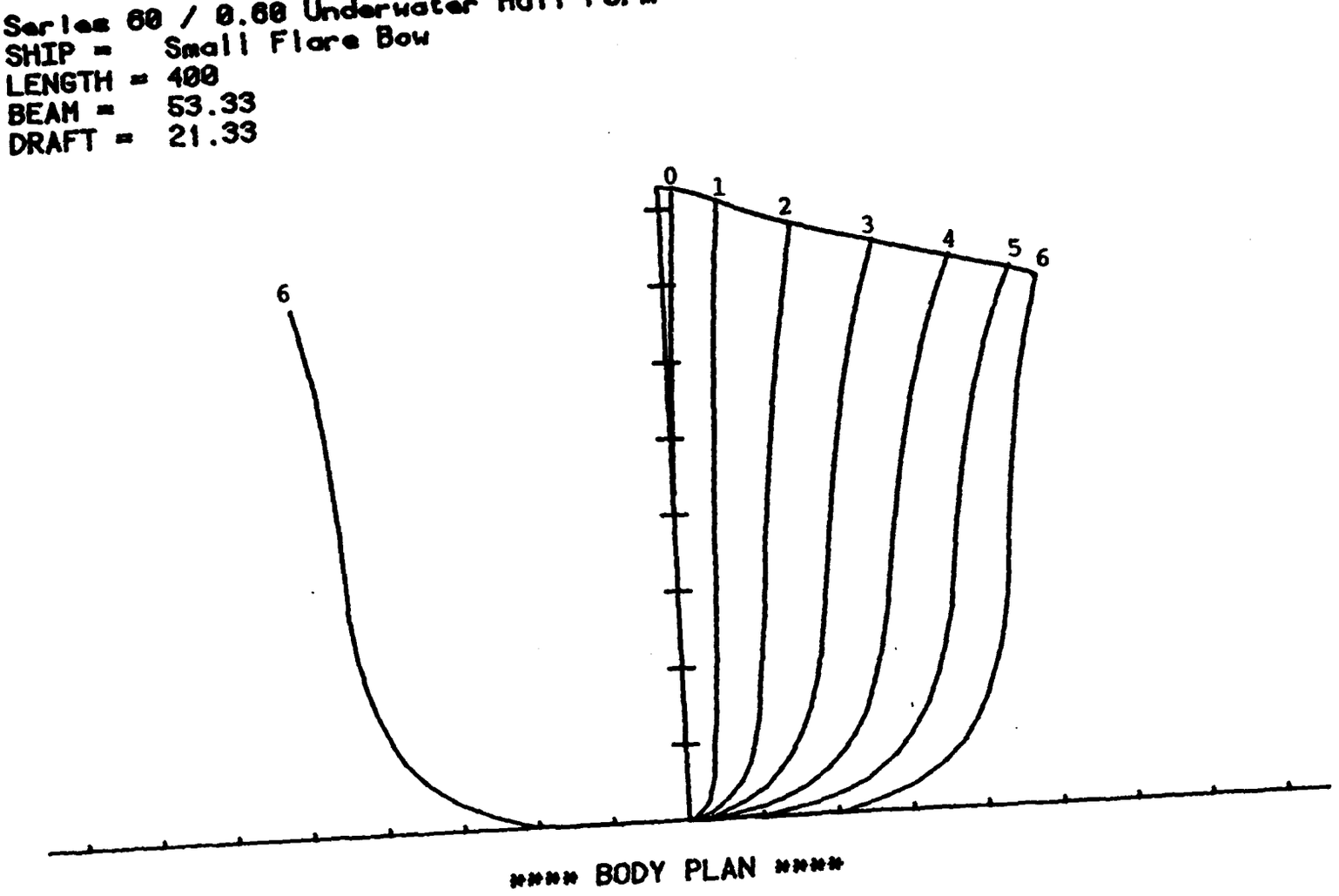

Figure 2. Body Plan of Small Flare Bow

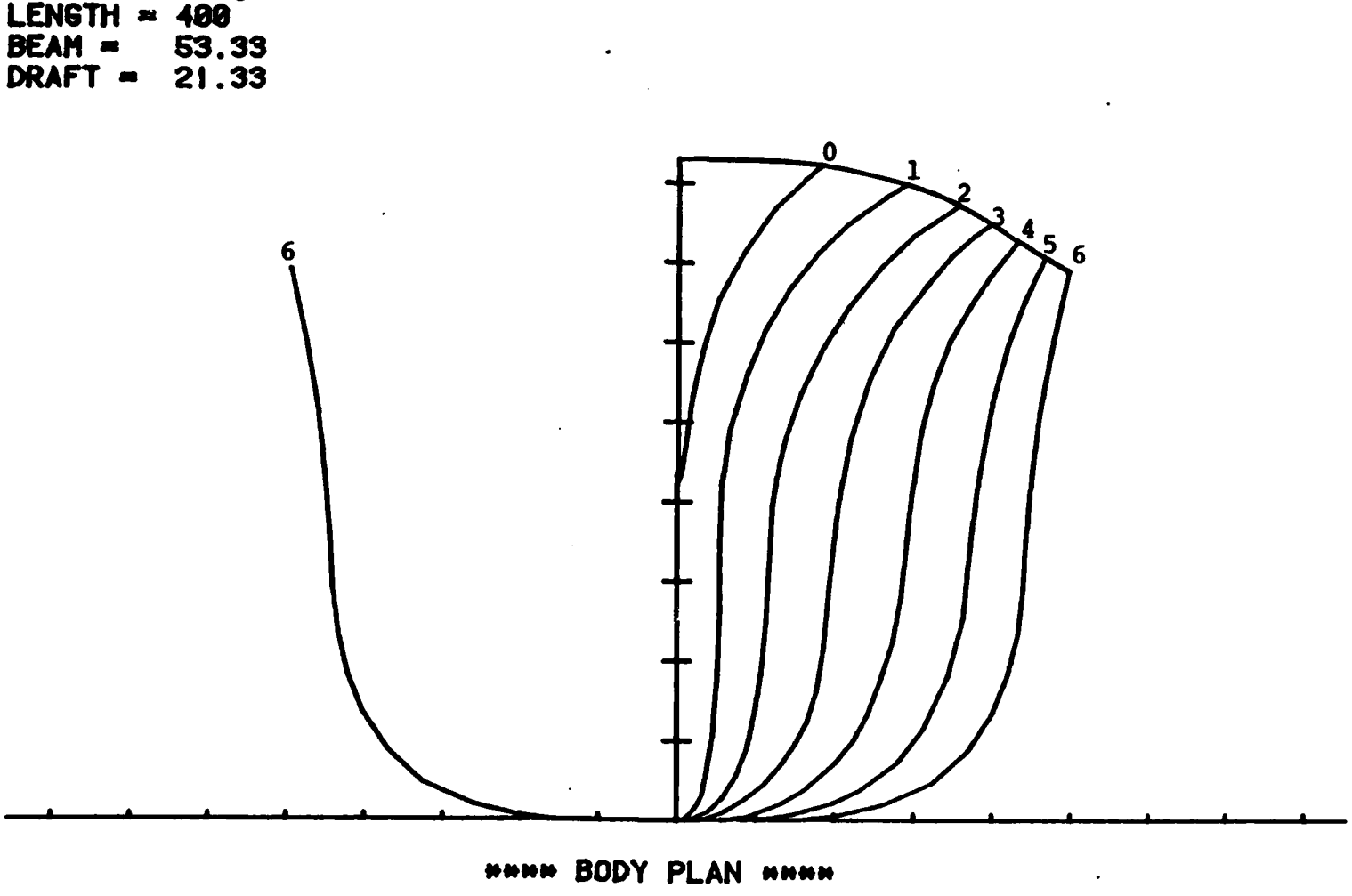

Figure 3. Body Plan of Large Flare Bow

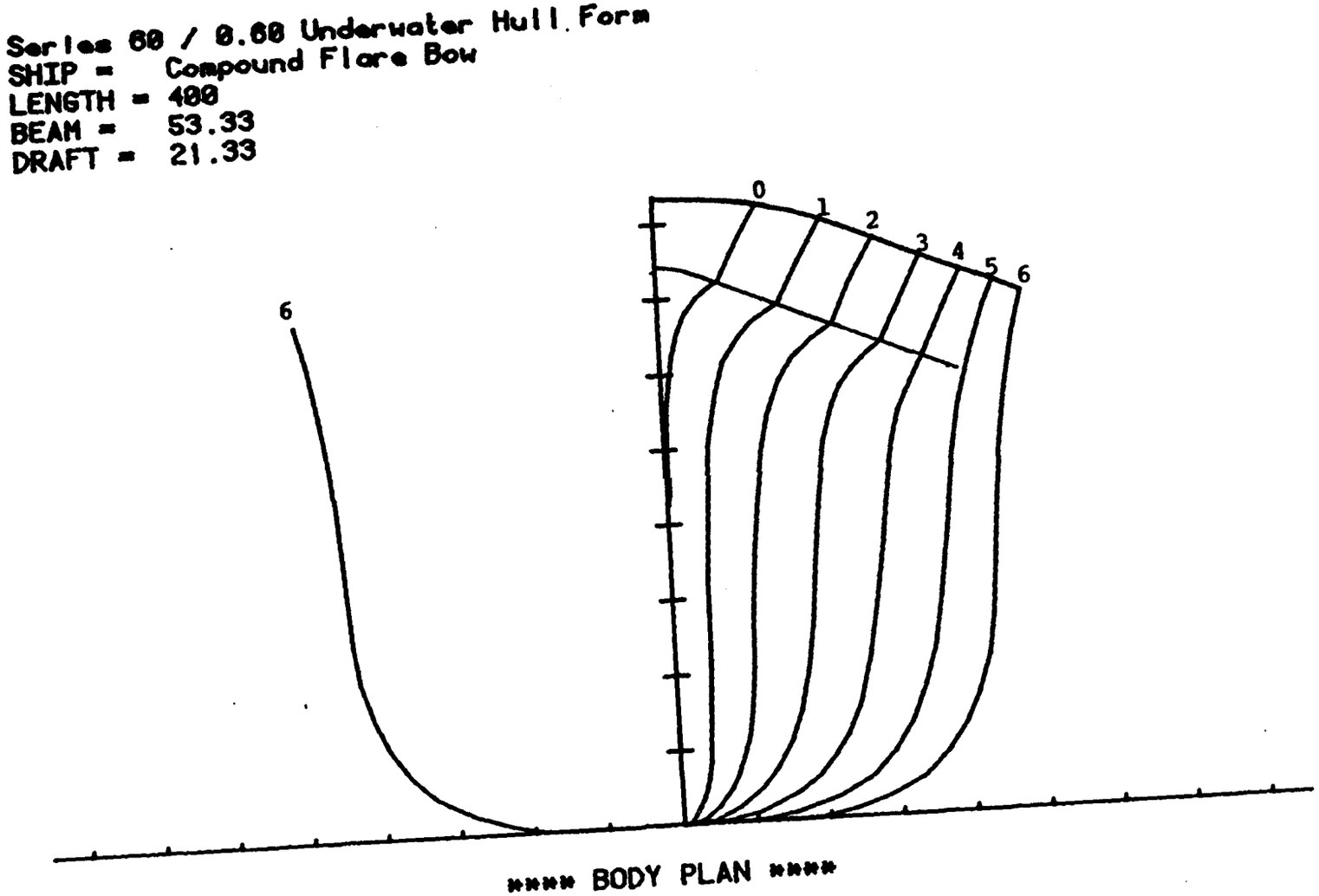

Figure 4. Body Plan of Compound Flare Bow

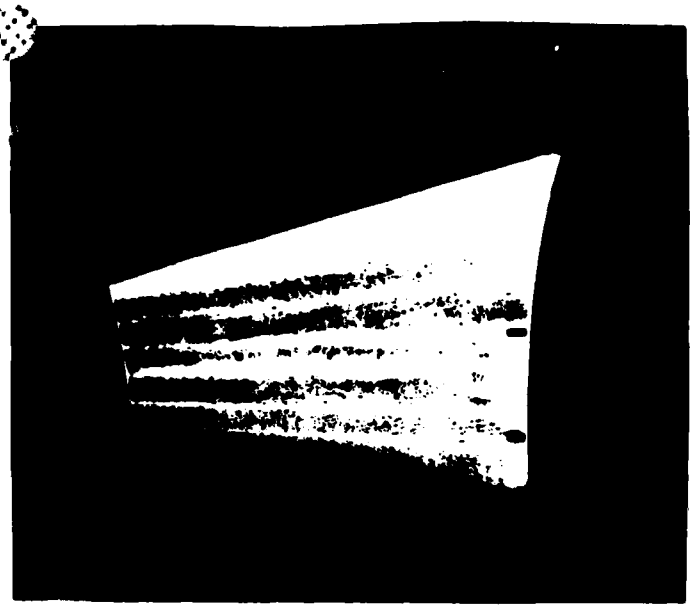

a. Parent Bow

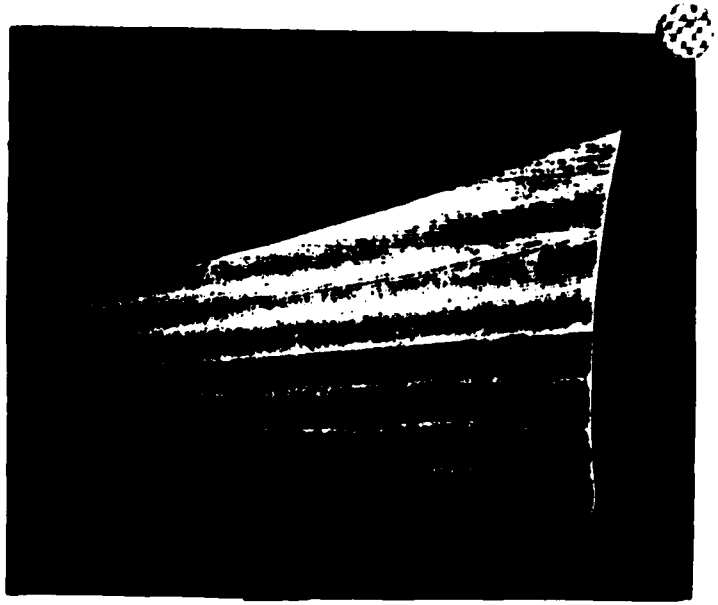

b. Small Flare Bow

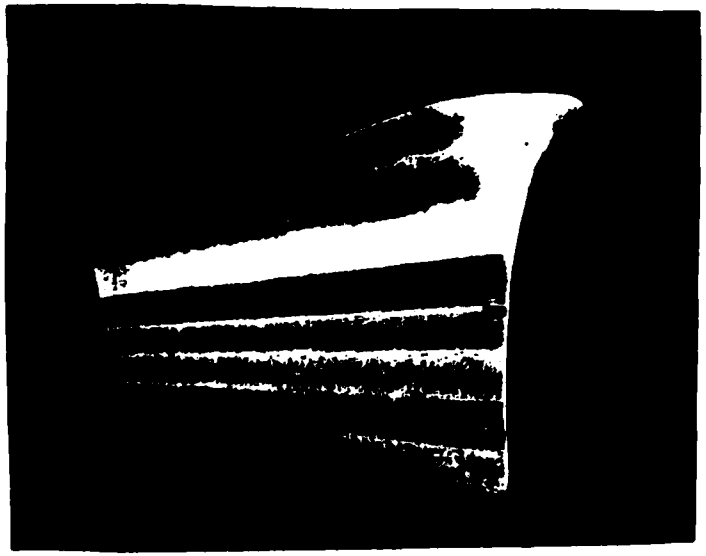

c. Large Flare Bow

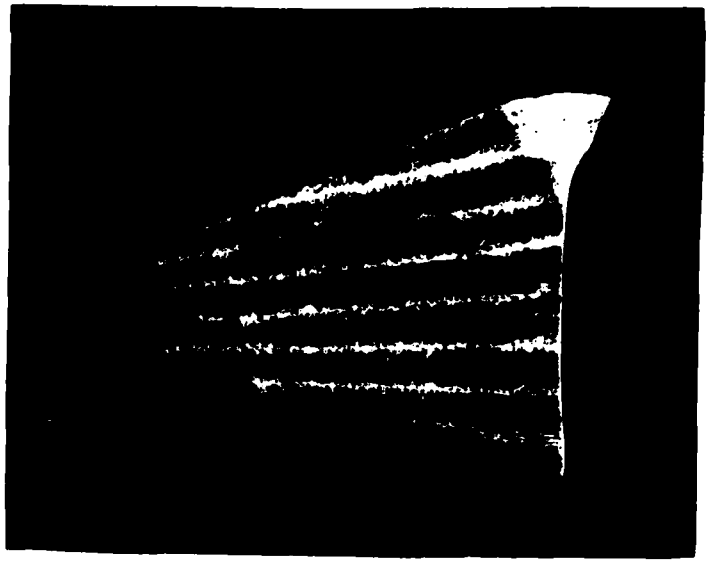

d. Compound Flare Bow

Figure 5. The Four Bows Tested

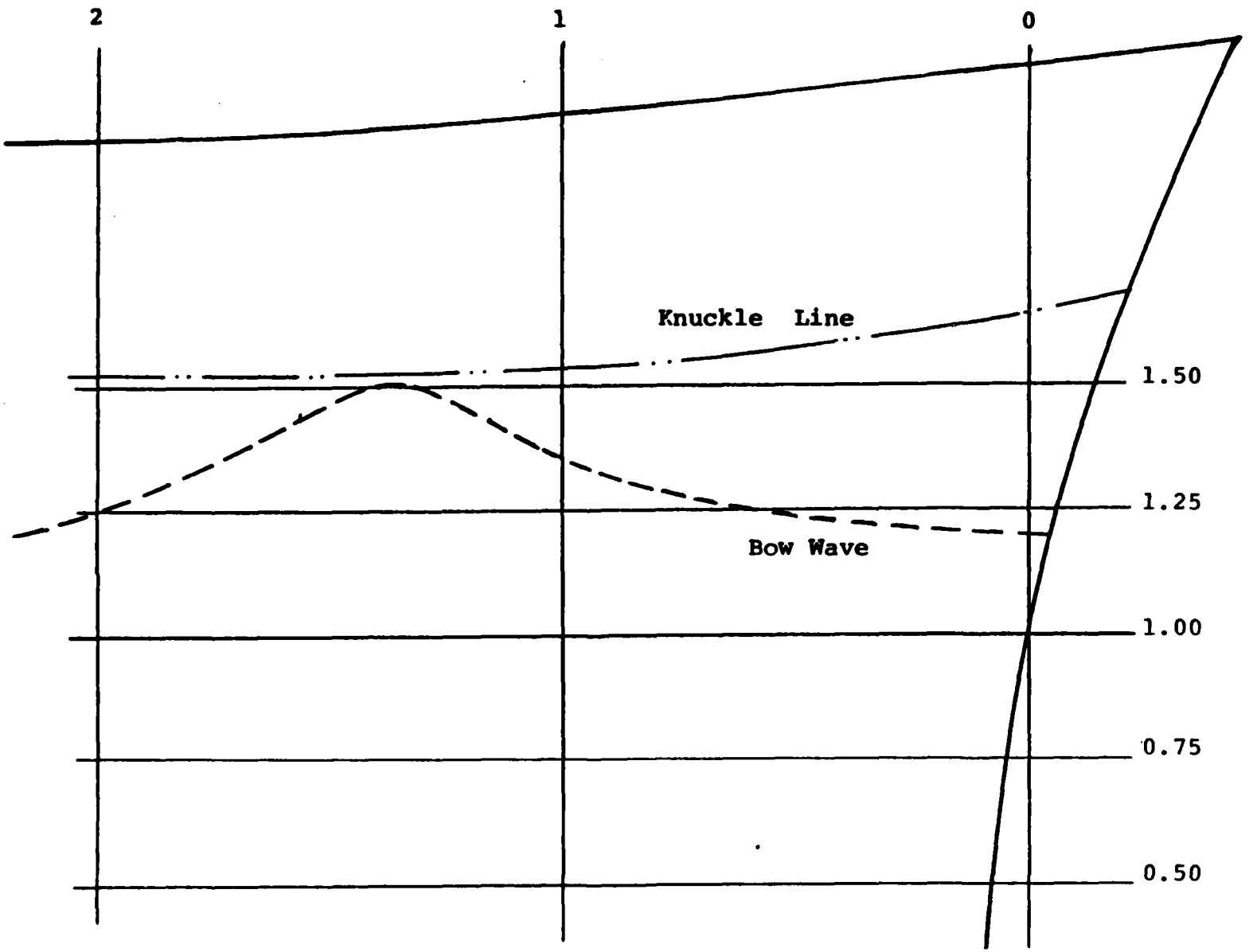

Figure 6. Bow Wave of Series 60 /0.60 Parent Bow at Fr = 0.30

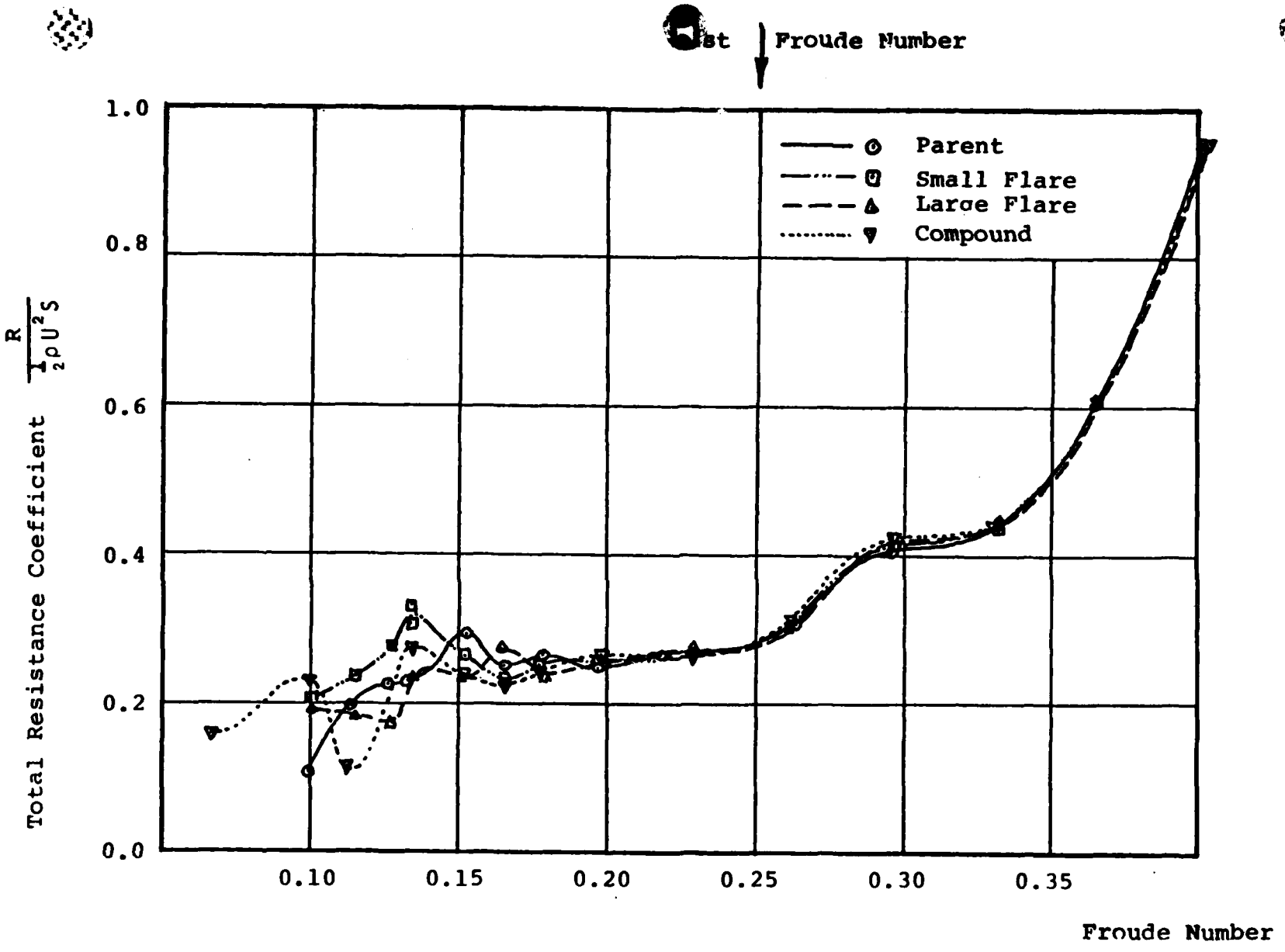

Figure 7. Stillwater Resistance of the Four Bow Forms

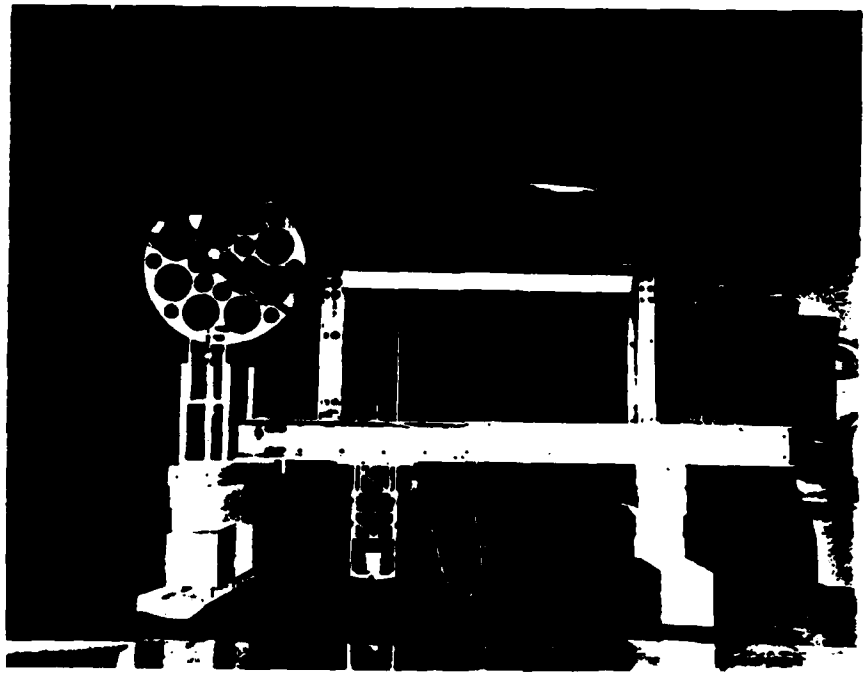

Figure 8. Photograph of Constant Force Dynomometer

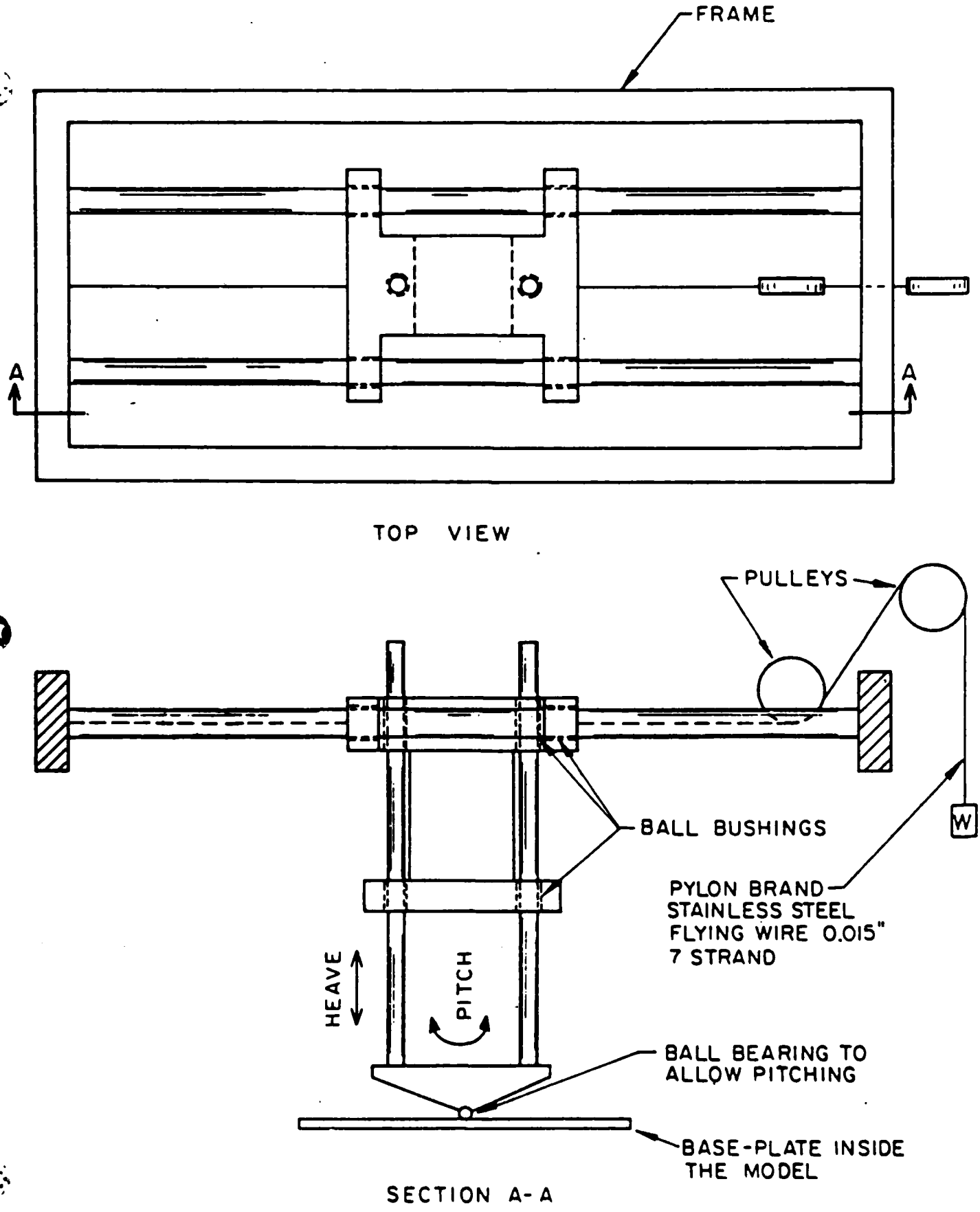

Figure 9. Schematic View of the Constant Force Dynomometer

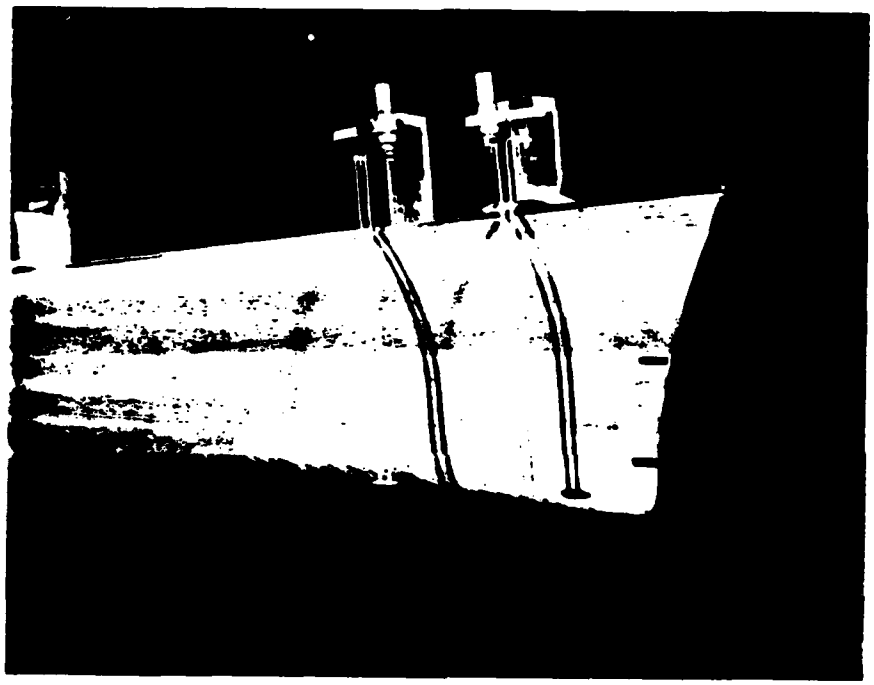

Figure 10. Photograph of Wave Probes Mounted to the Parent Bow

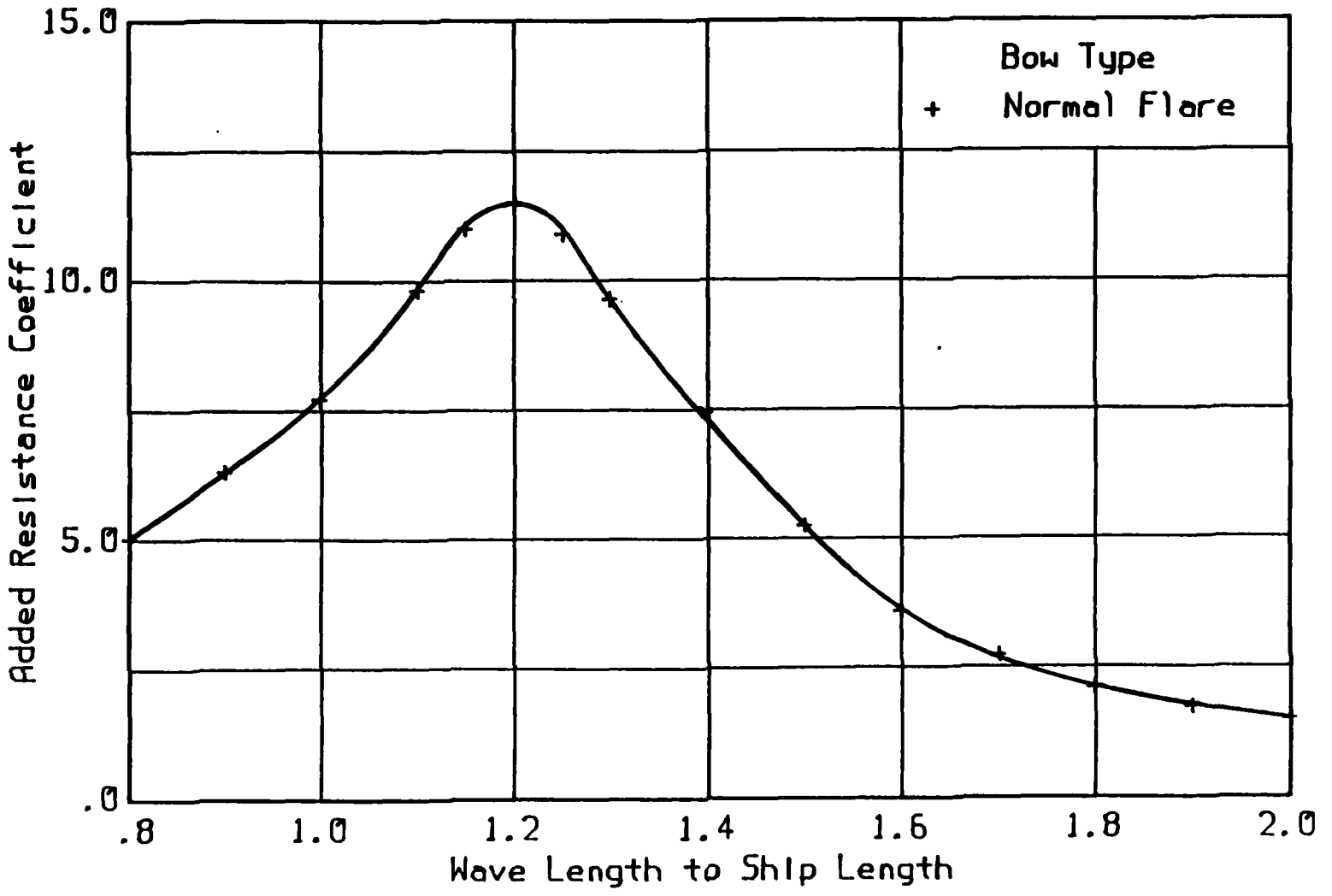

Figure 11. Added Resistance Coefficient for Parent Hull Form

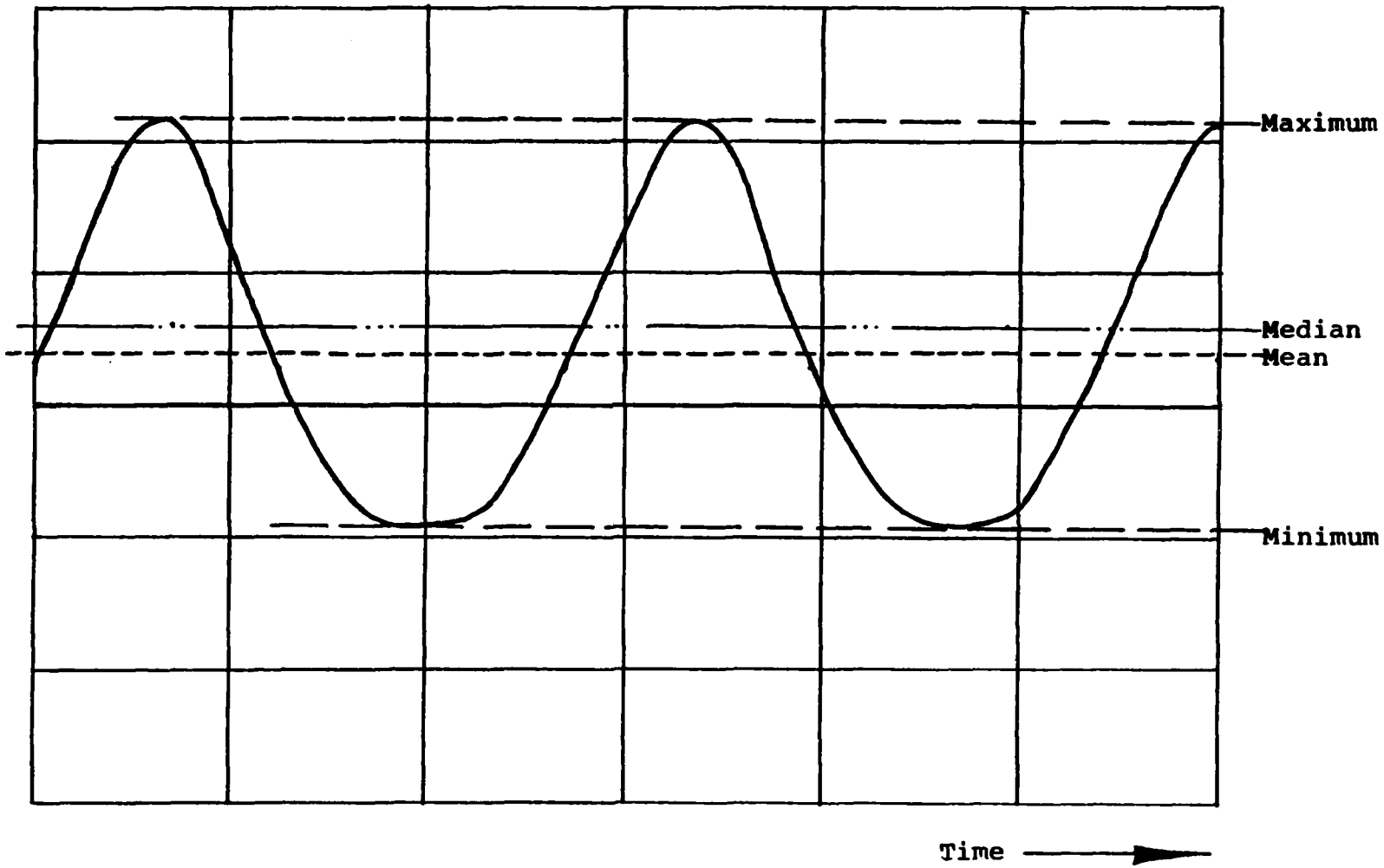

Figure 12. Typical Periodic Time Series

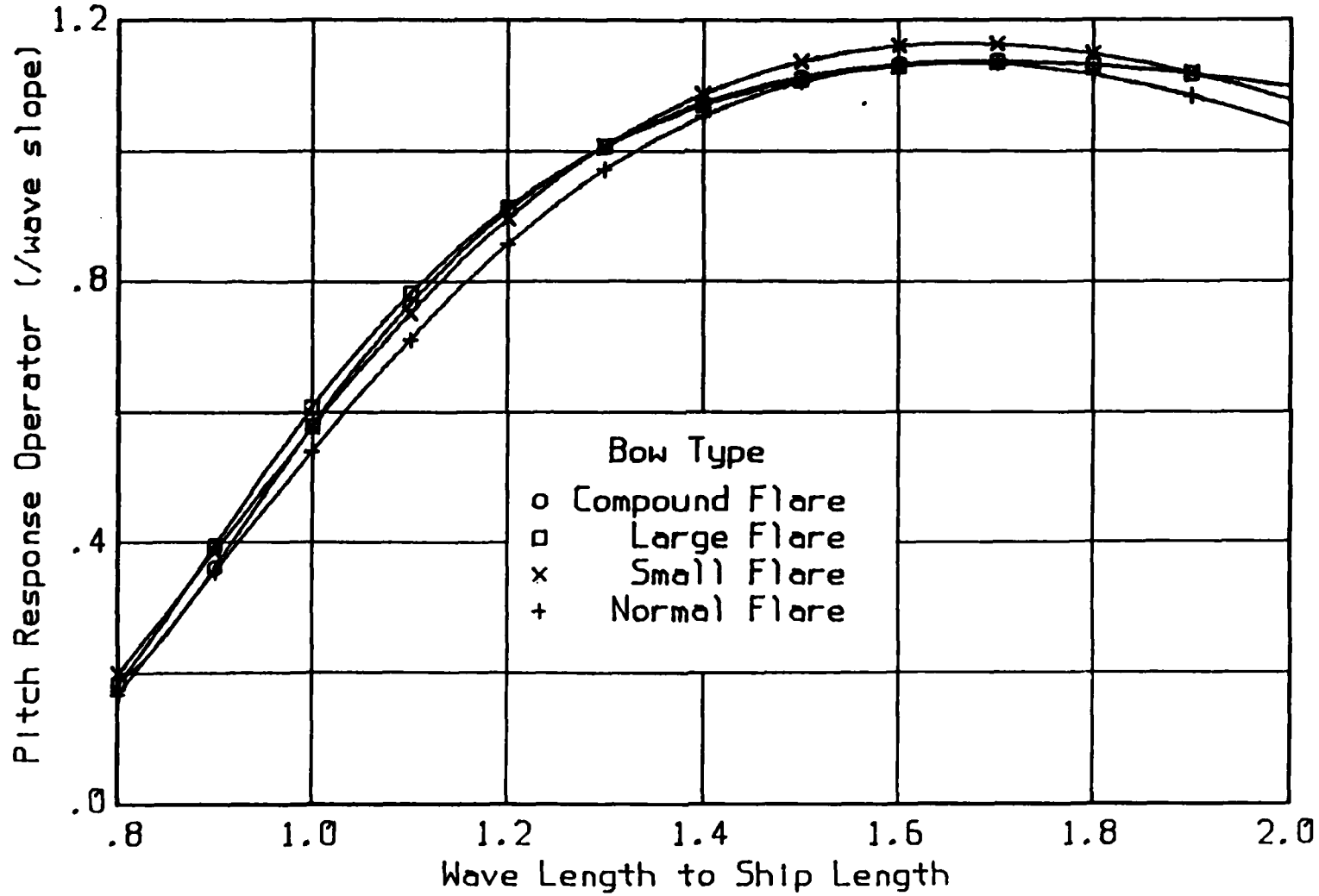

Figure 13. Pitch Transfer Functions in 1:40 Regular Head Seas

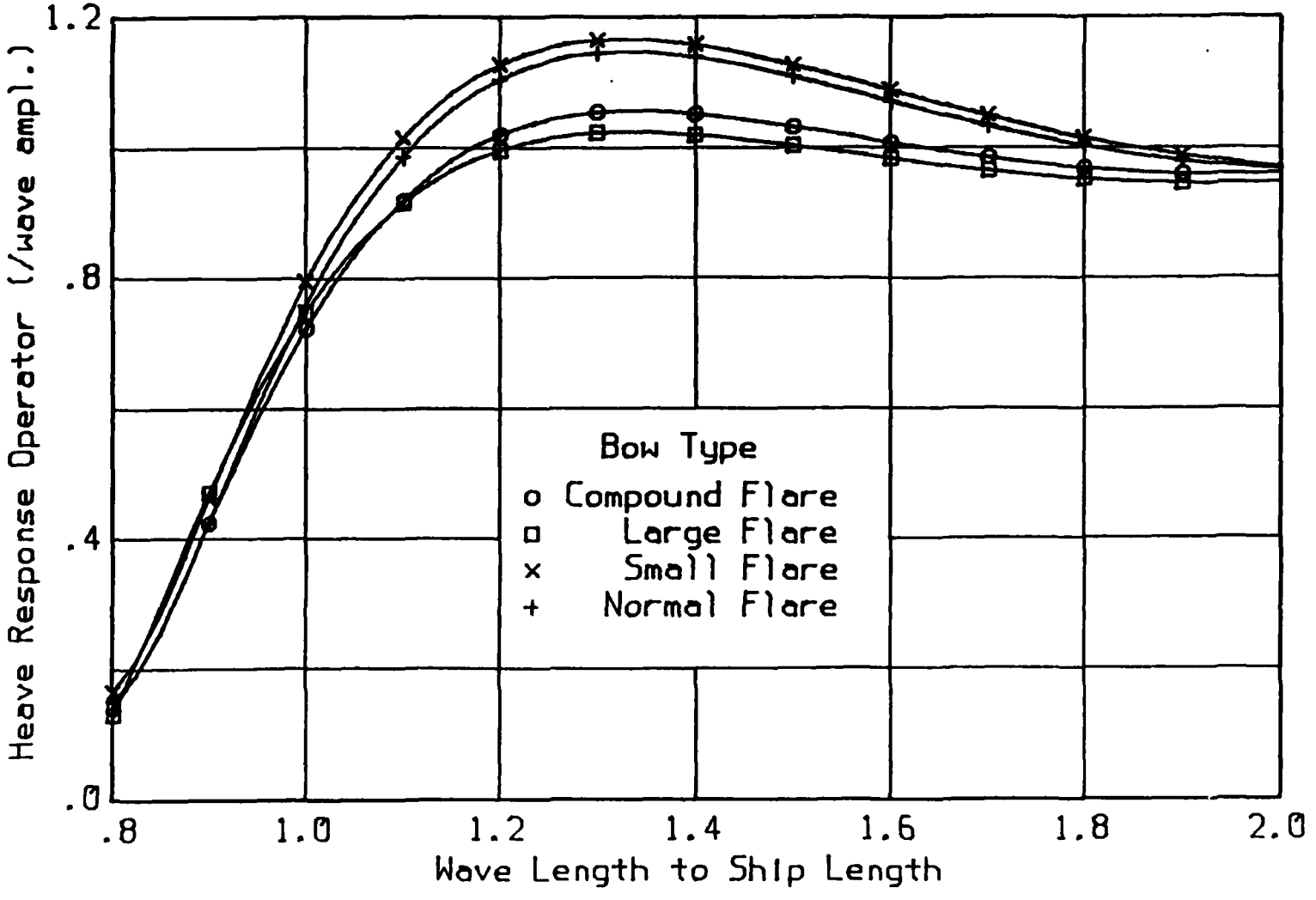

Figure 14. Heave Transfer Functions in 1:40 Regular Head Seas

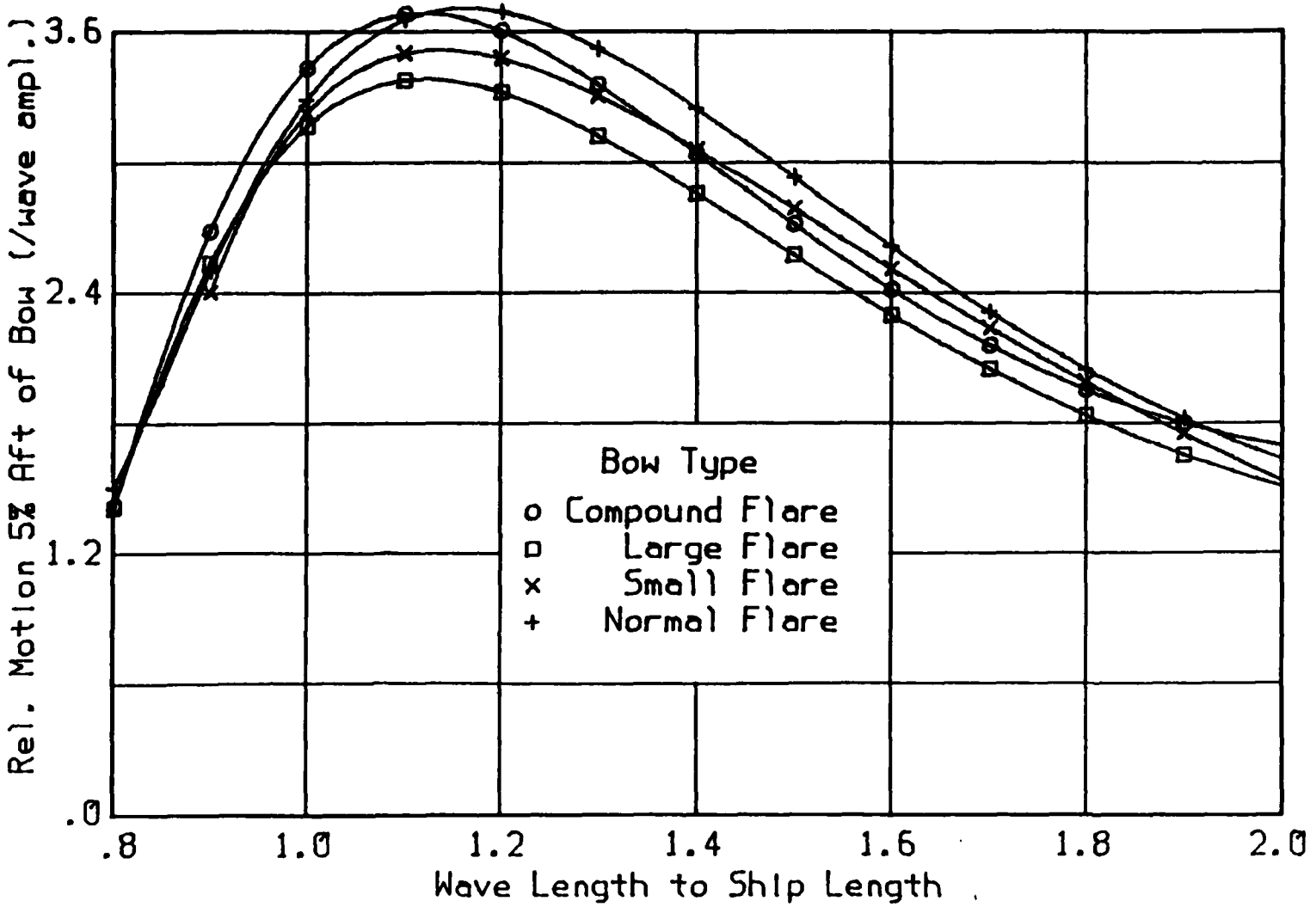

Figure 15. Relative Wave Height Transfer Functions in 1:40 Regular Head Seas - 5% Aft of Bow

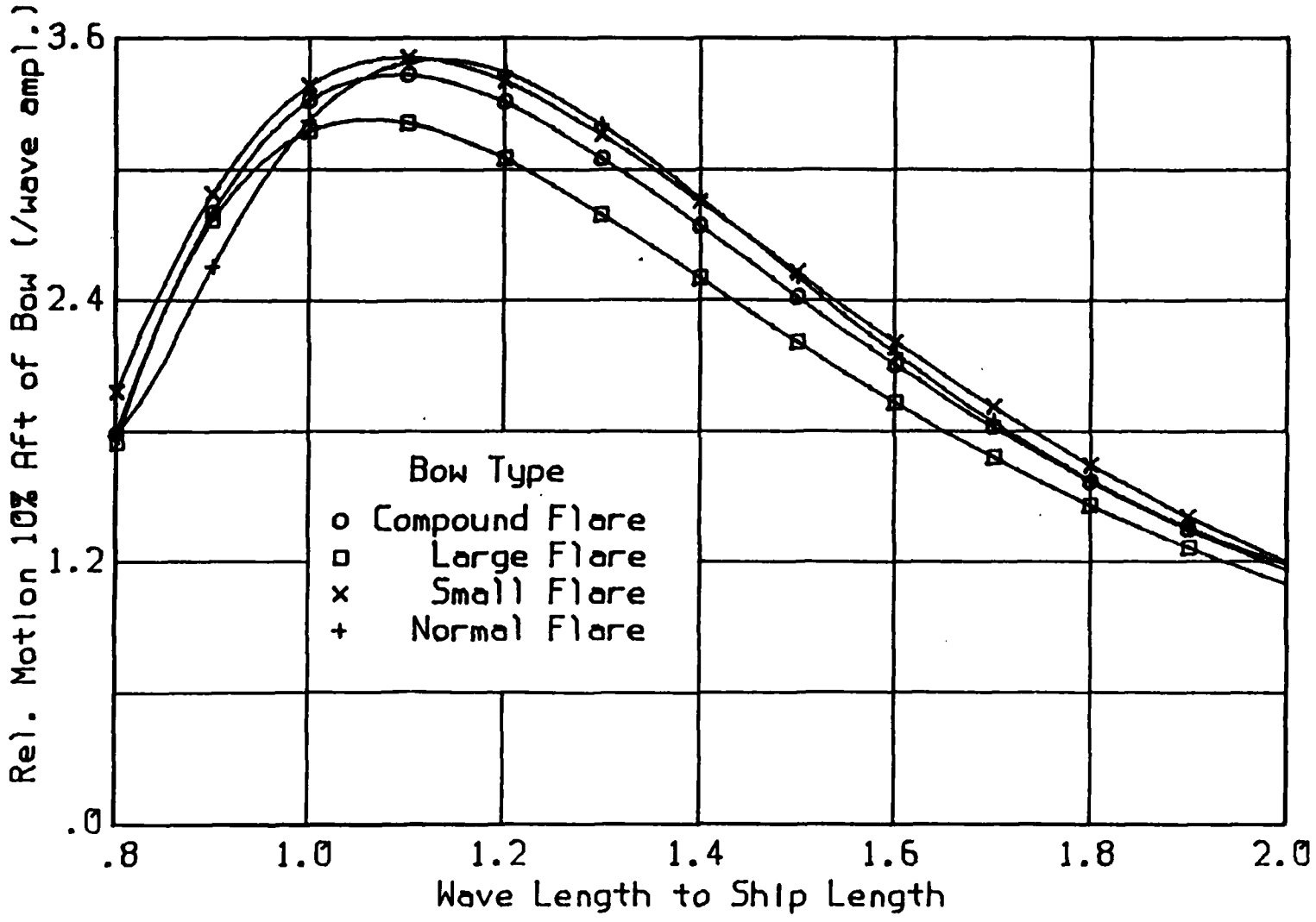

Figure 16. Relative Wave Height Transfer Functions in 1:40 Regular Head Seas - 10% Aft of Bow

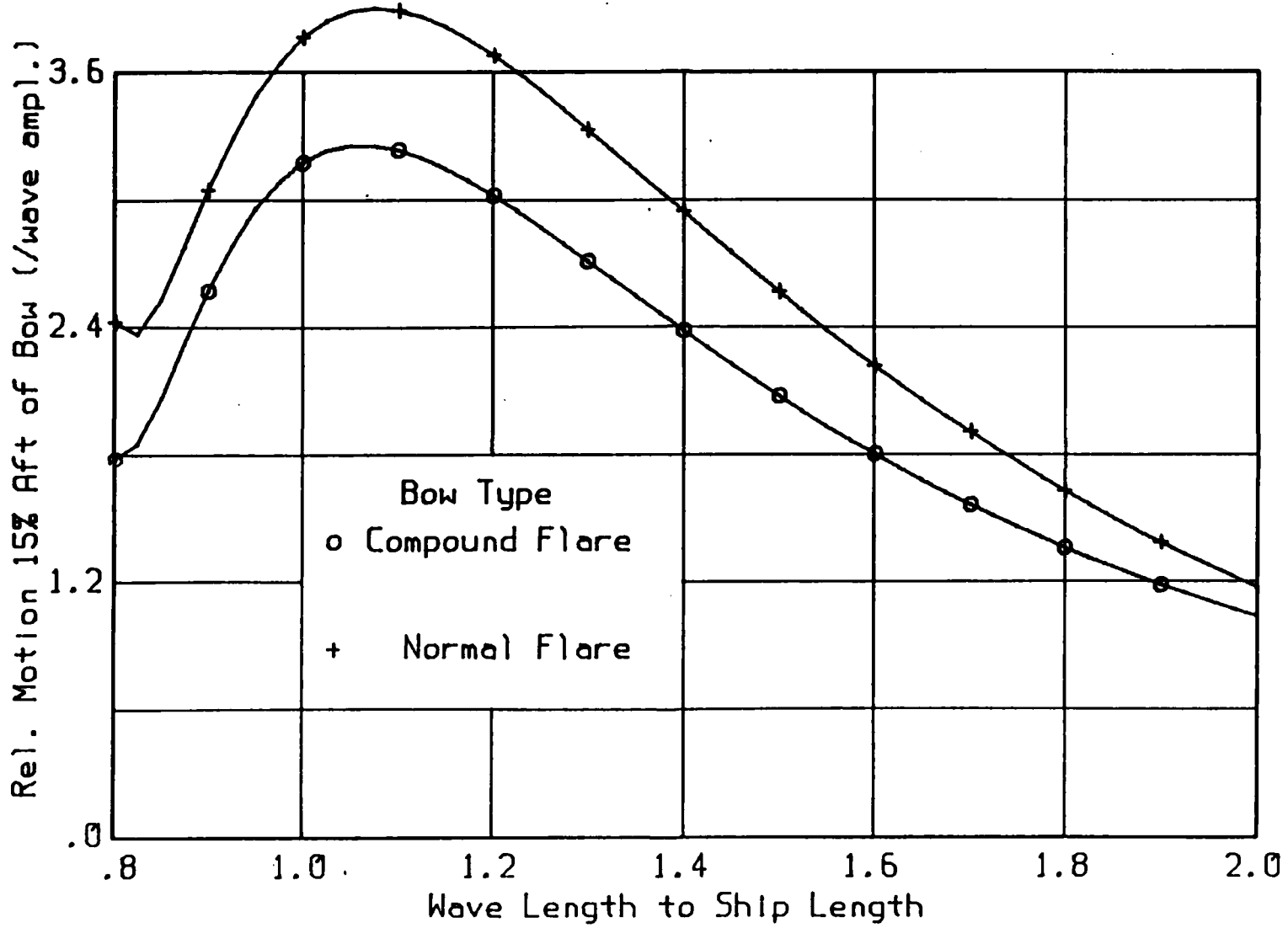

Figure 17. Relative Wave Height Transfer Functions in 1:40 Regular Head Seas - 15% Aft of Bow

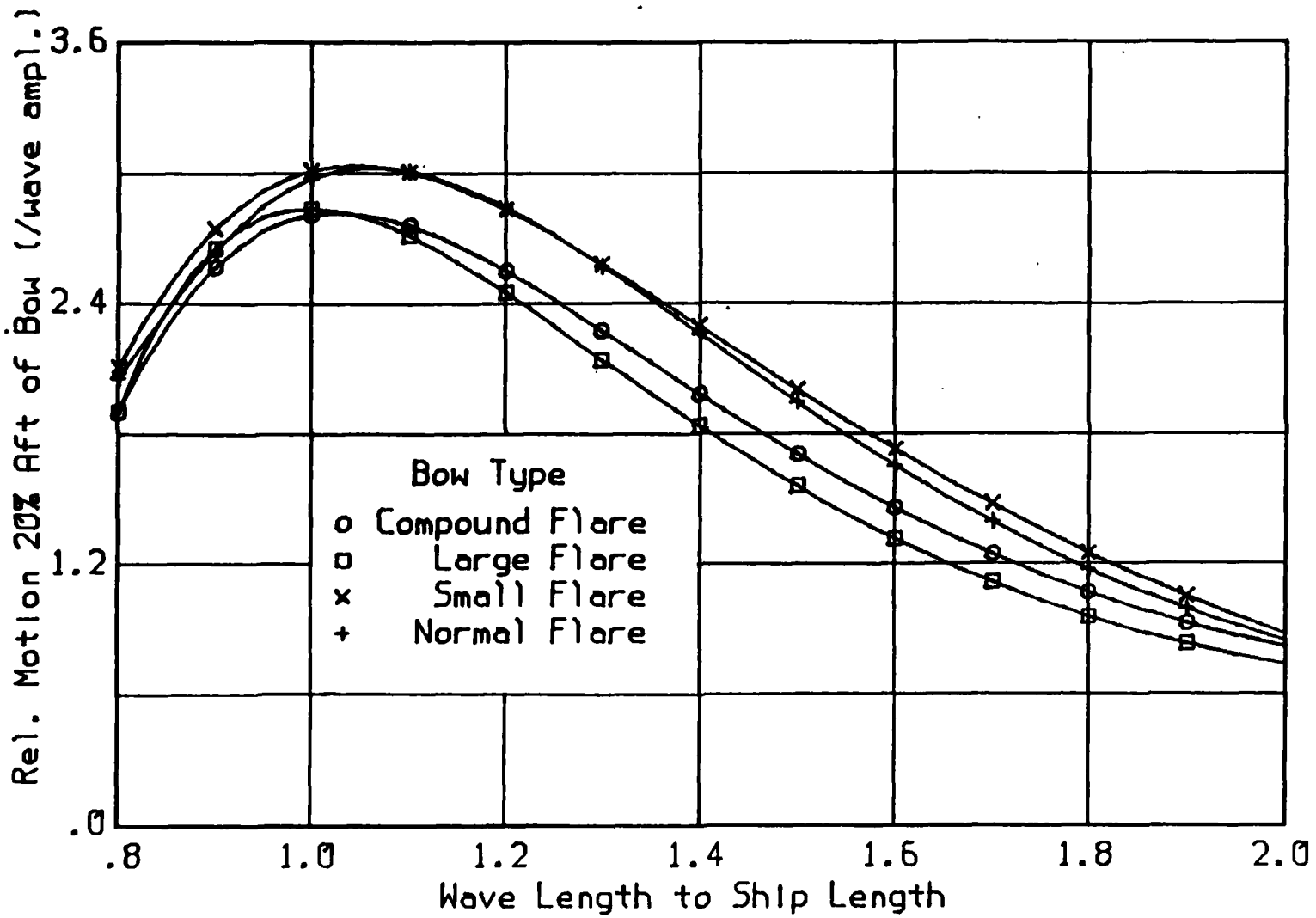

Figure 18. Relative Wave Height Transfer Functions in 1:40 Regular Head Seas - 20% Aft of Bow

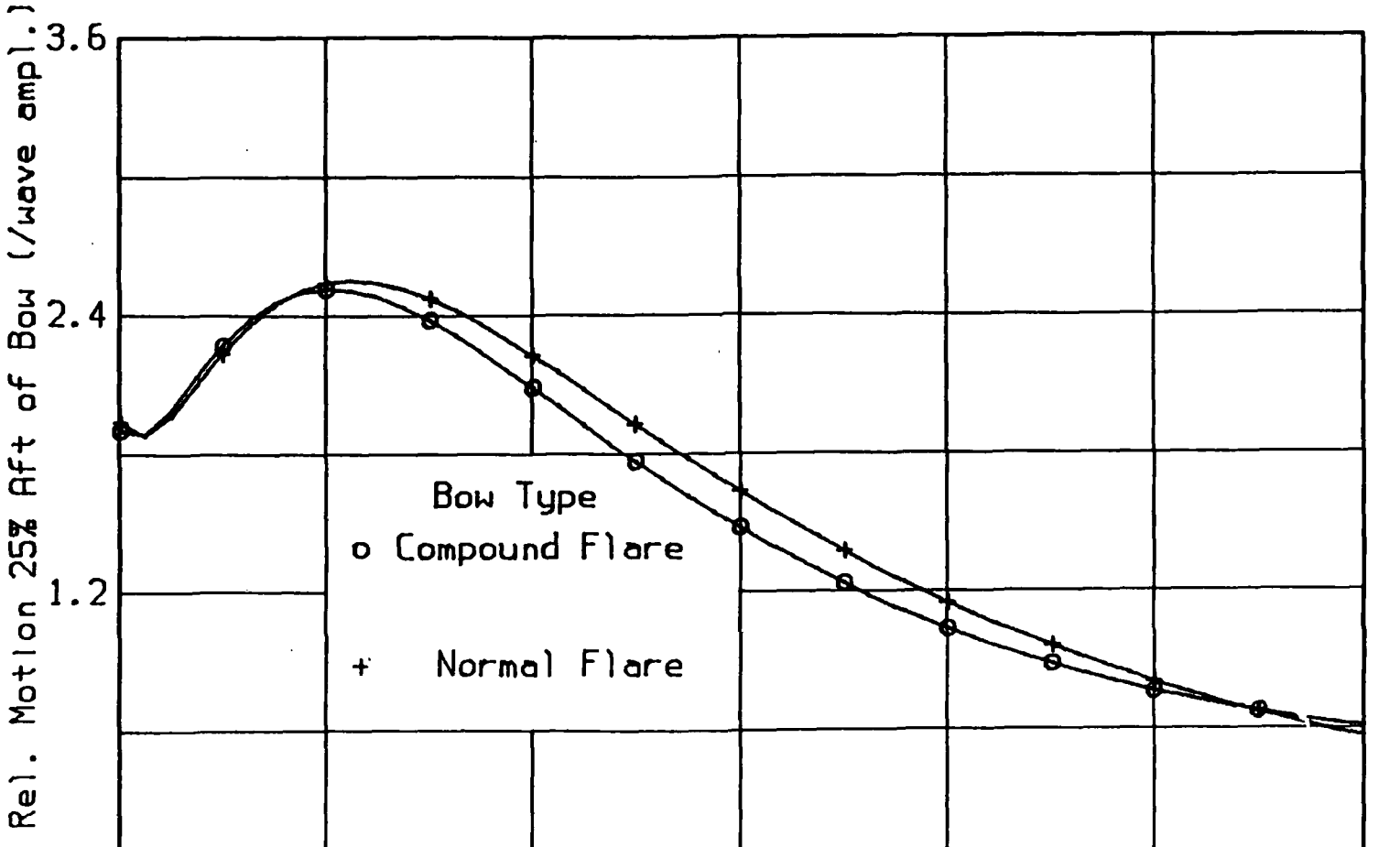

Figure 19. Relative Wave Height Transfer Functions in 1:40 Regular Head Seas - 25% Aft of Bow

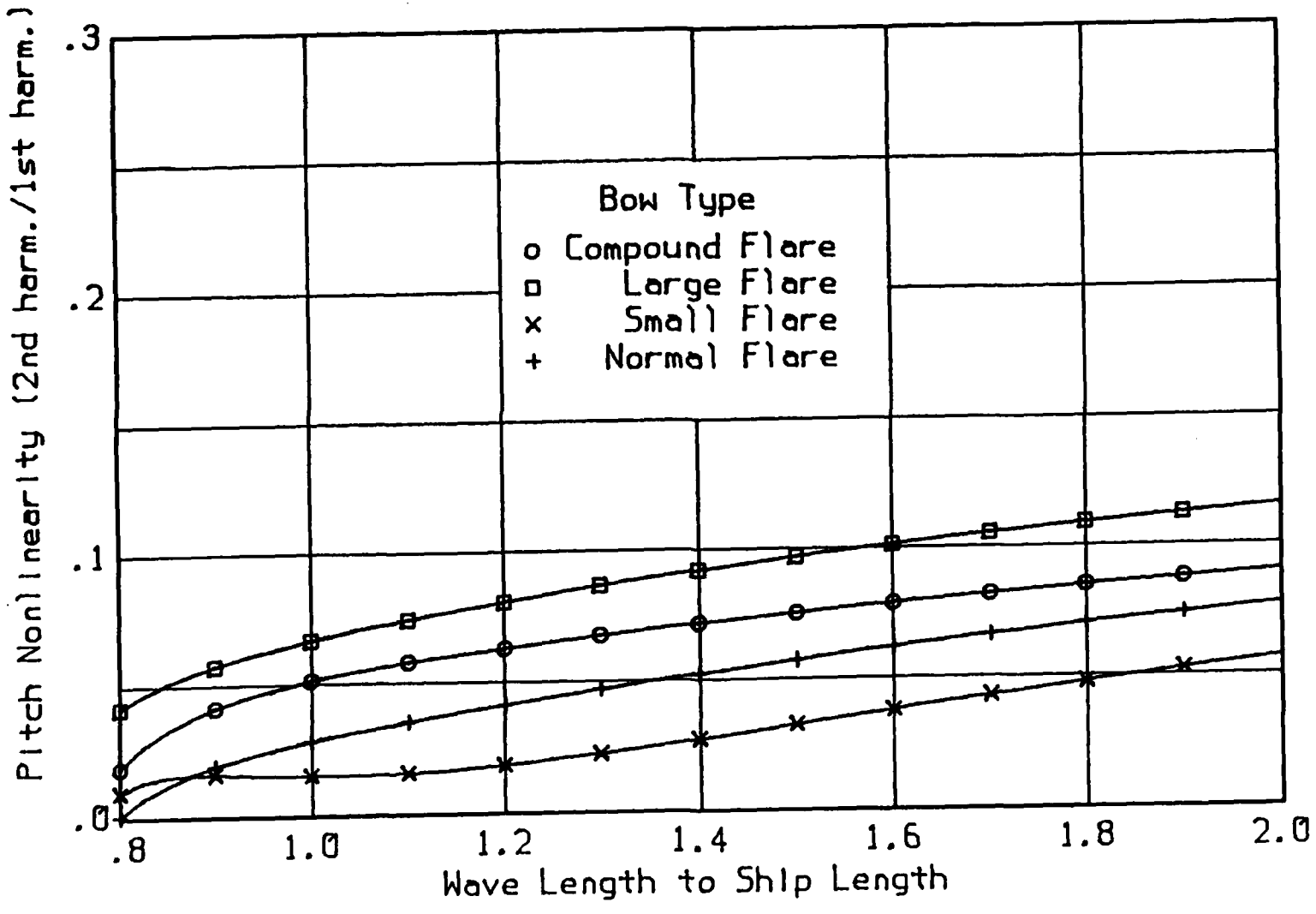

Figure 20. Pitch Motion Nonlinearity Factor

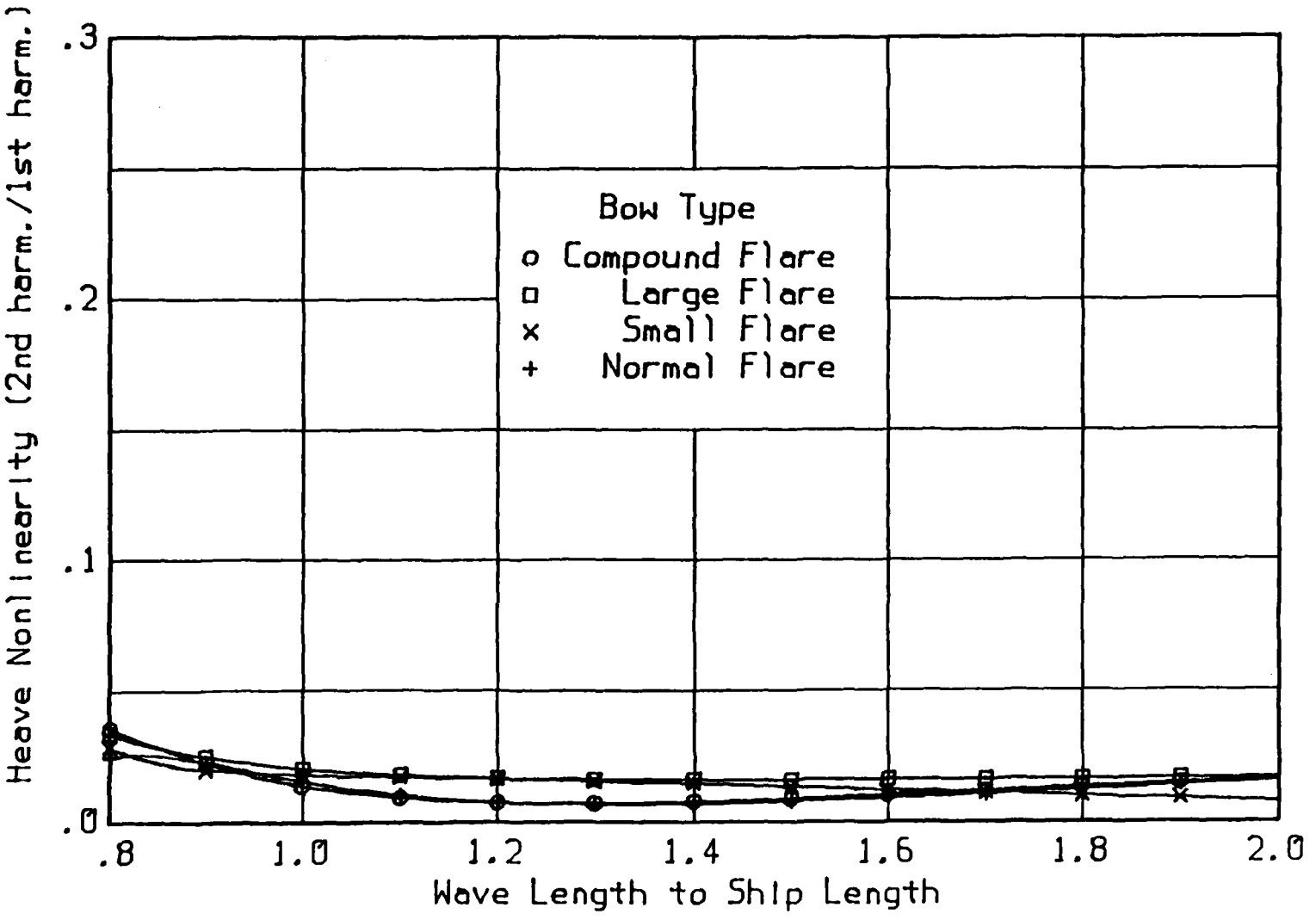

Figure 21. Heave Motion Nonlinearity Factor

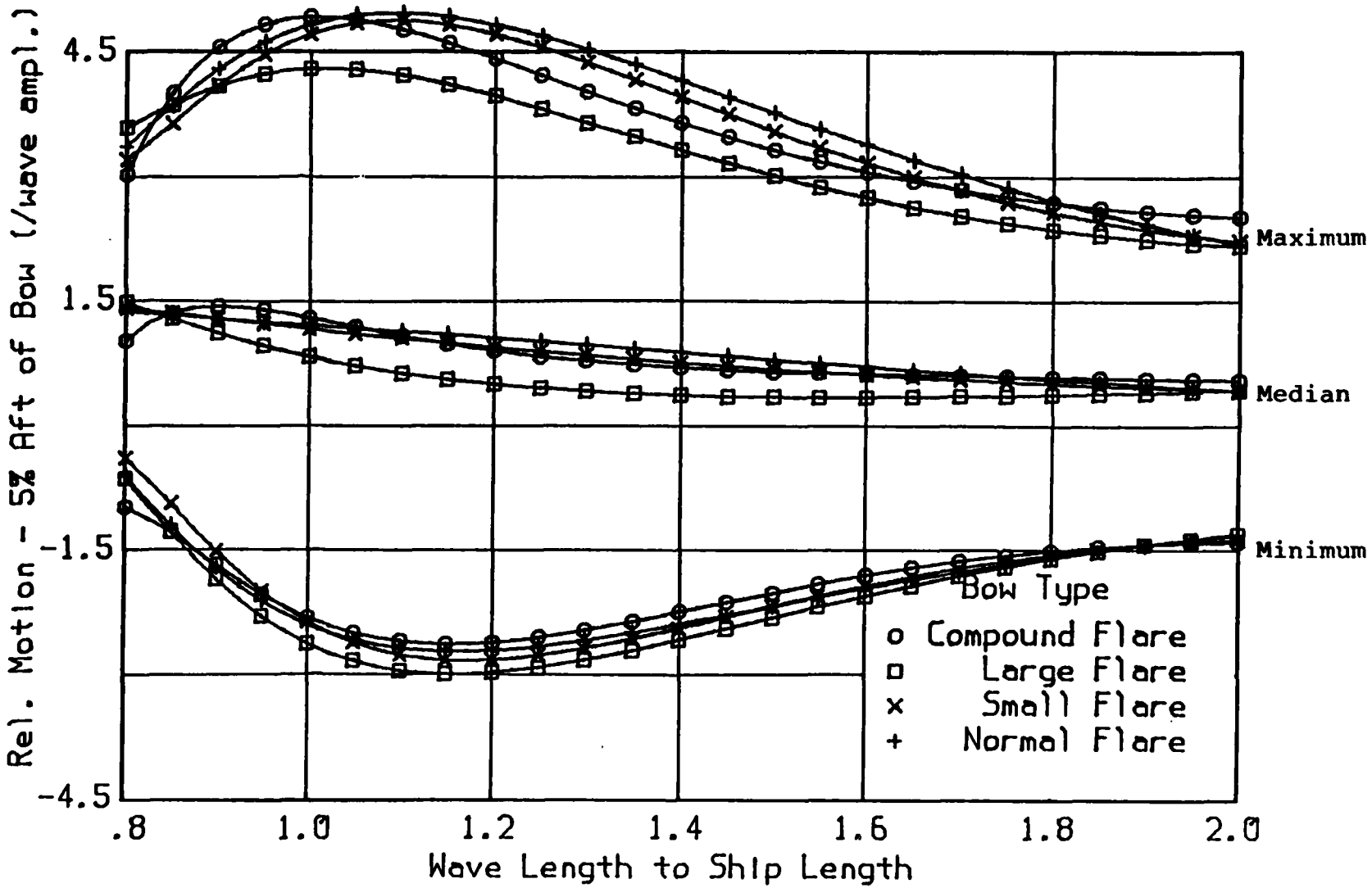

Figure 22. Relative Motion Statistics in 1:40 Head Seas - 5% Aft of Bow.

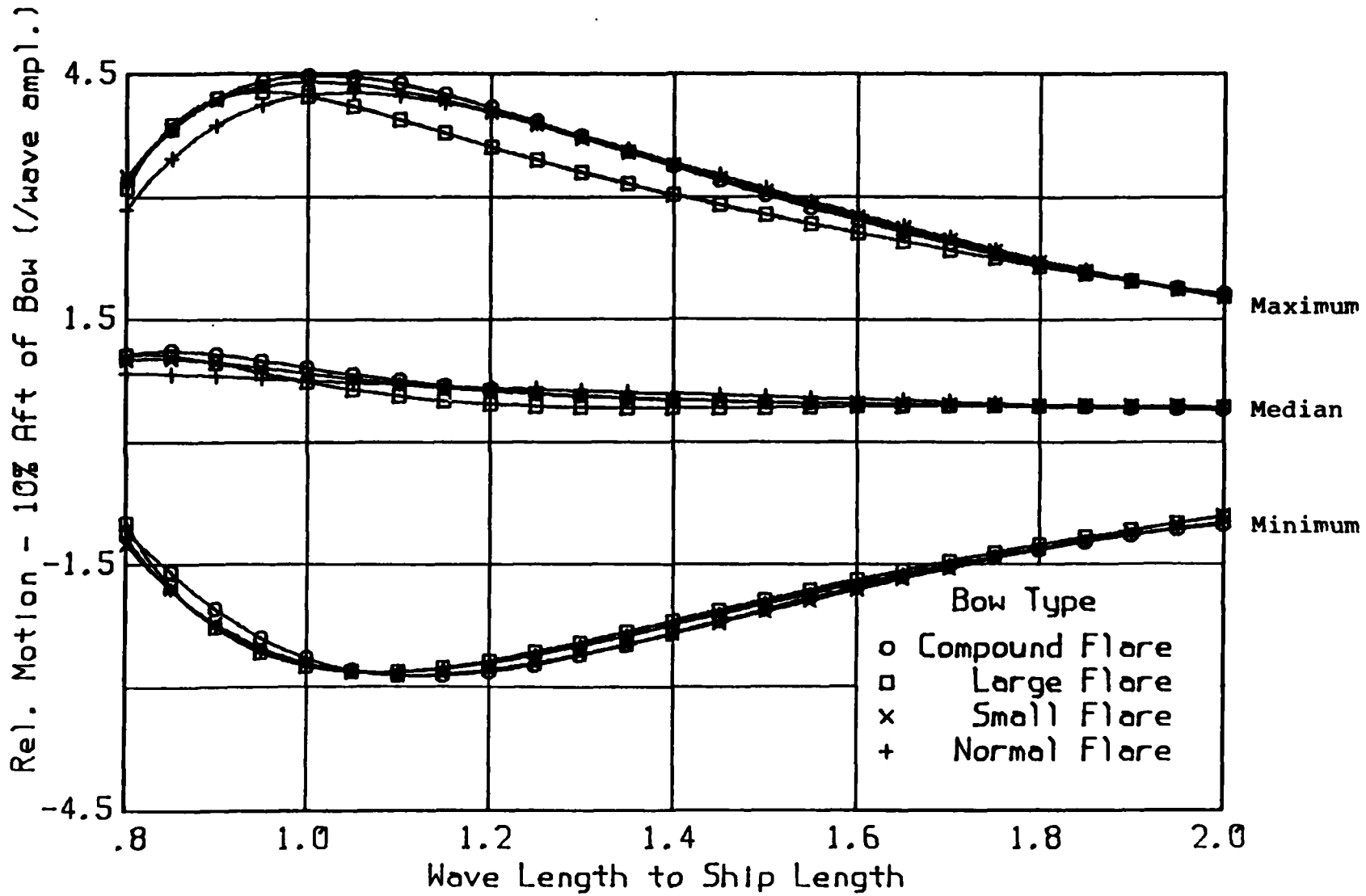

Figure 23. Relative Motion Statistics in 1:40 Head Seas - 10% Aft of Bow.

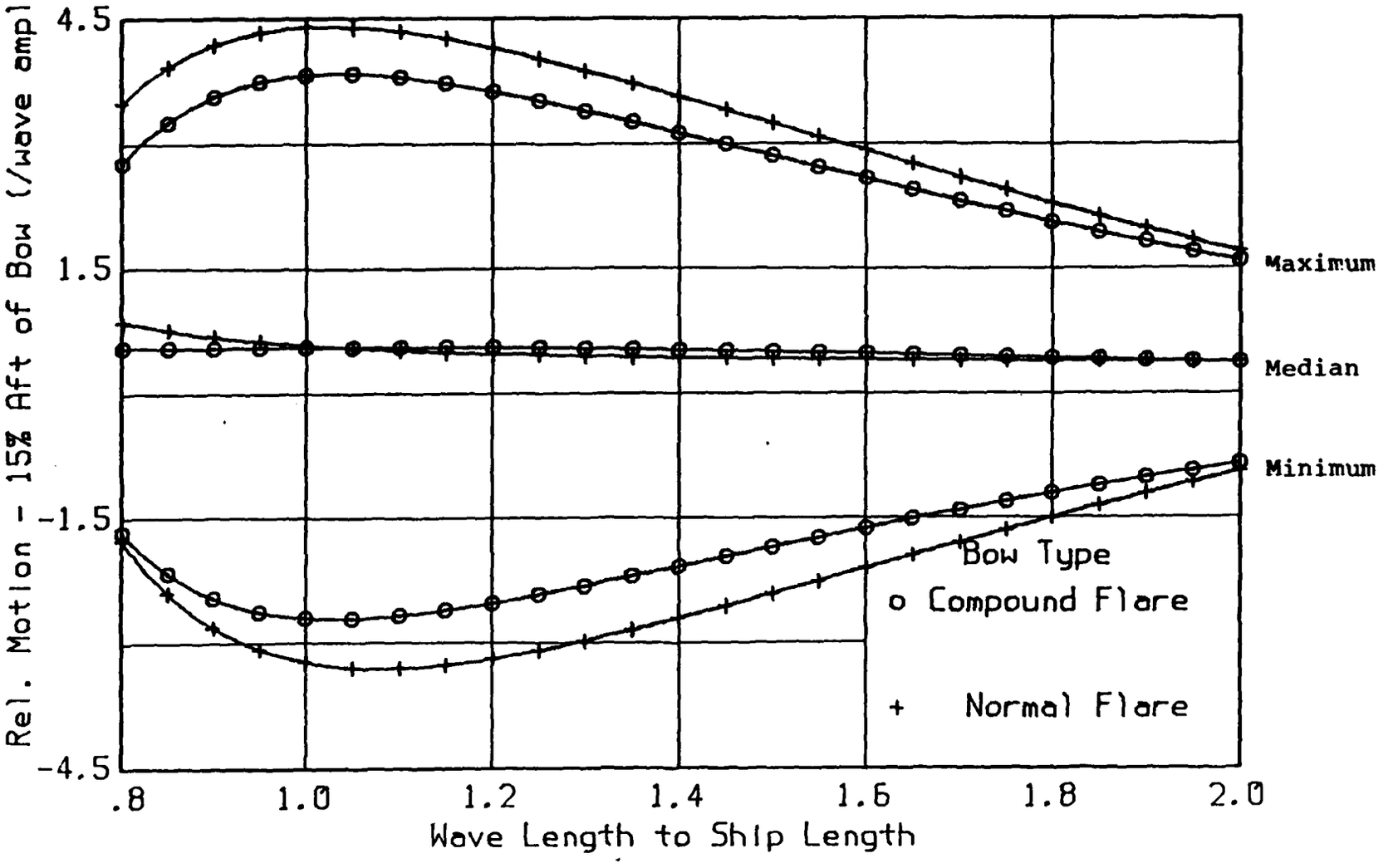

Figure 24. Relative Motion Statistics in 1:40 Head Seas - 15% Aft of Bow.

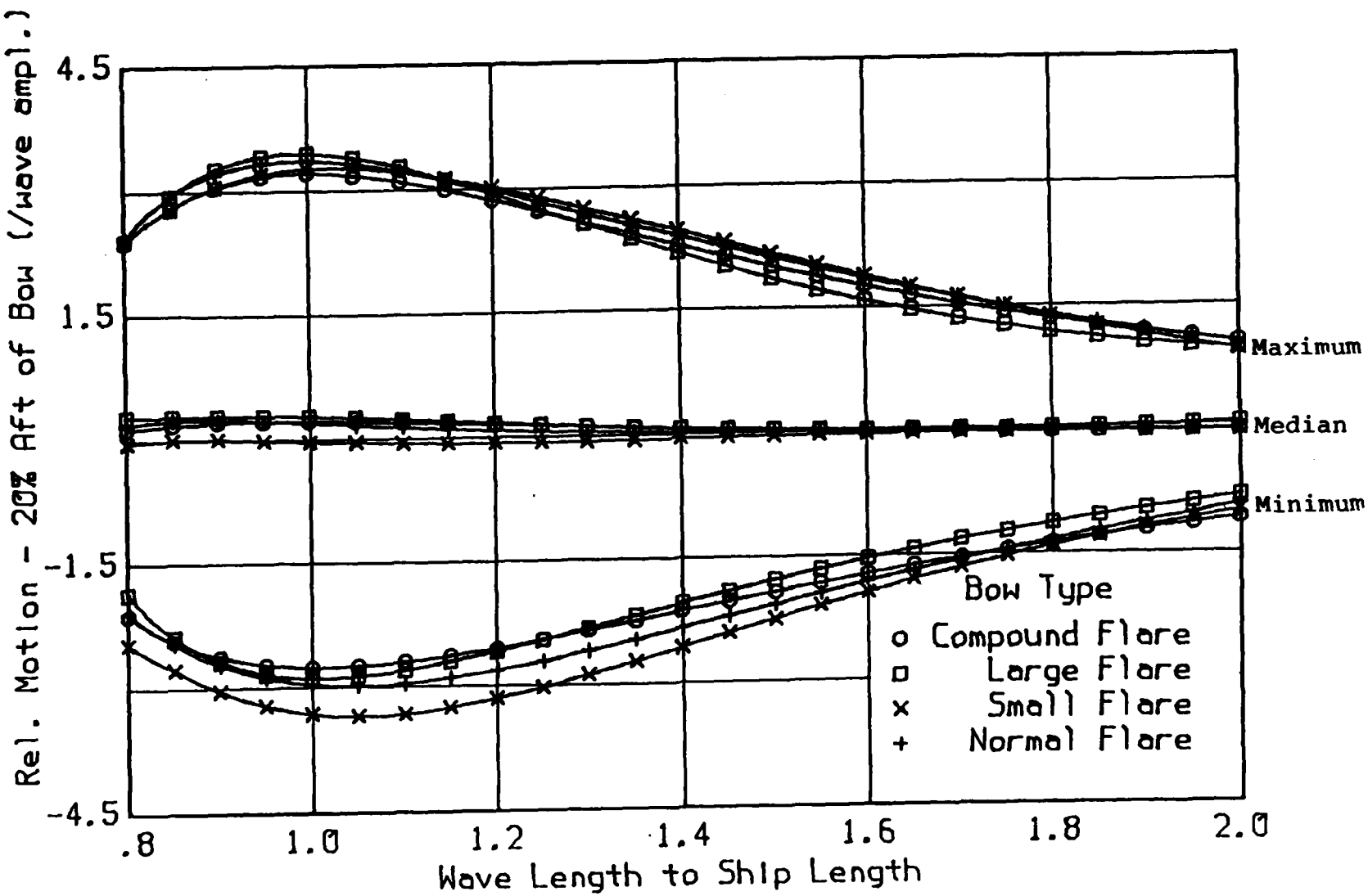

Figure 25. Relative Motion Statistics in 1:40 Head Seas - 20% Aft of Bow.

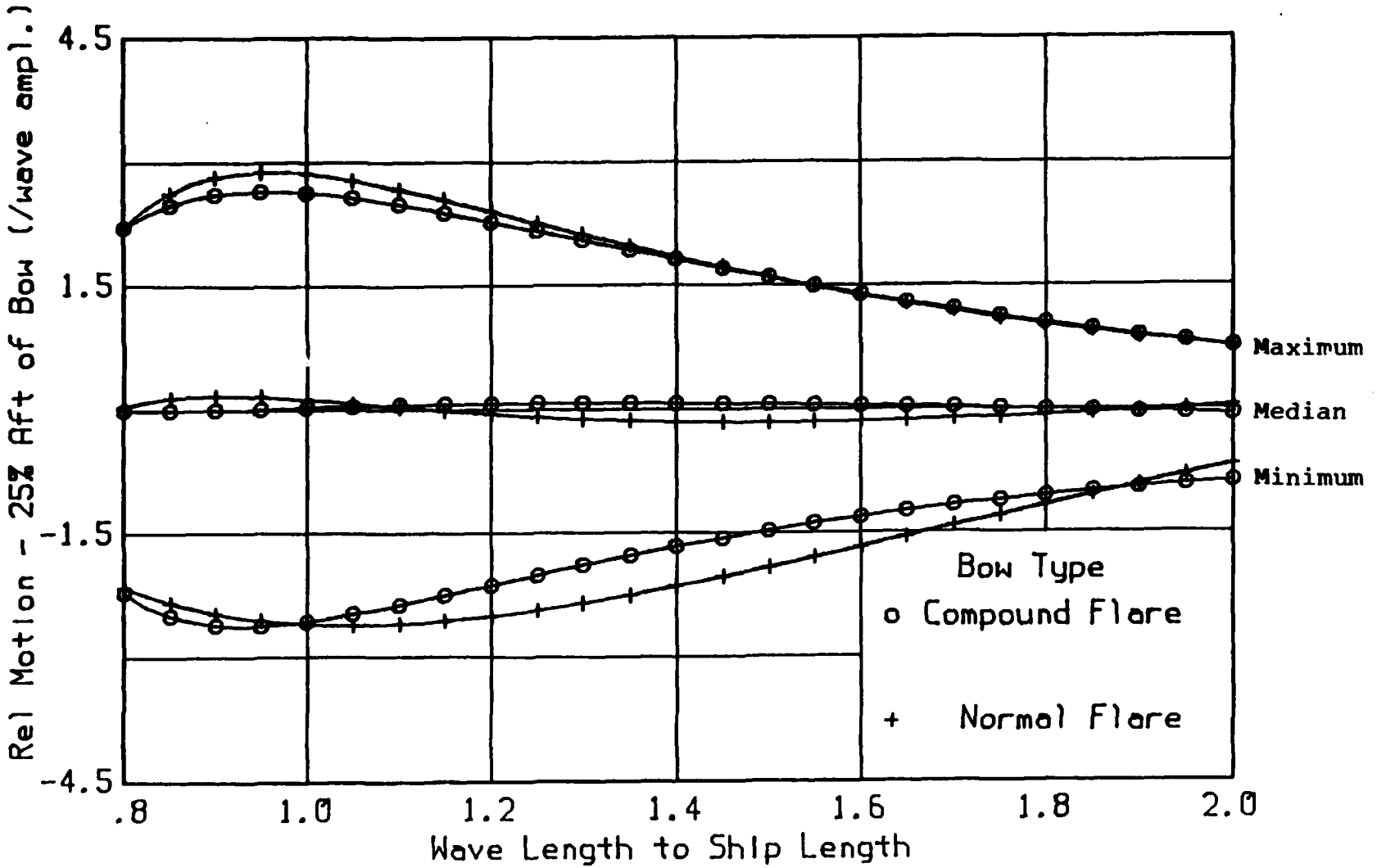

Figure 26. Relative Motion Statistics in 1:40 Head Seas - 25% Aft of Bow.

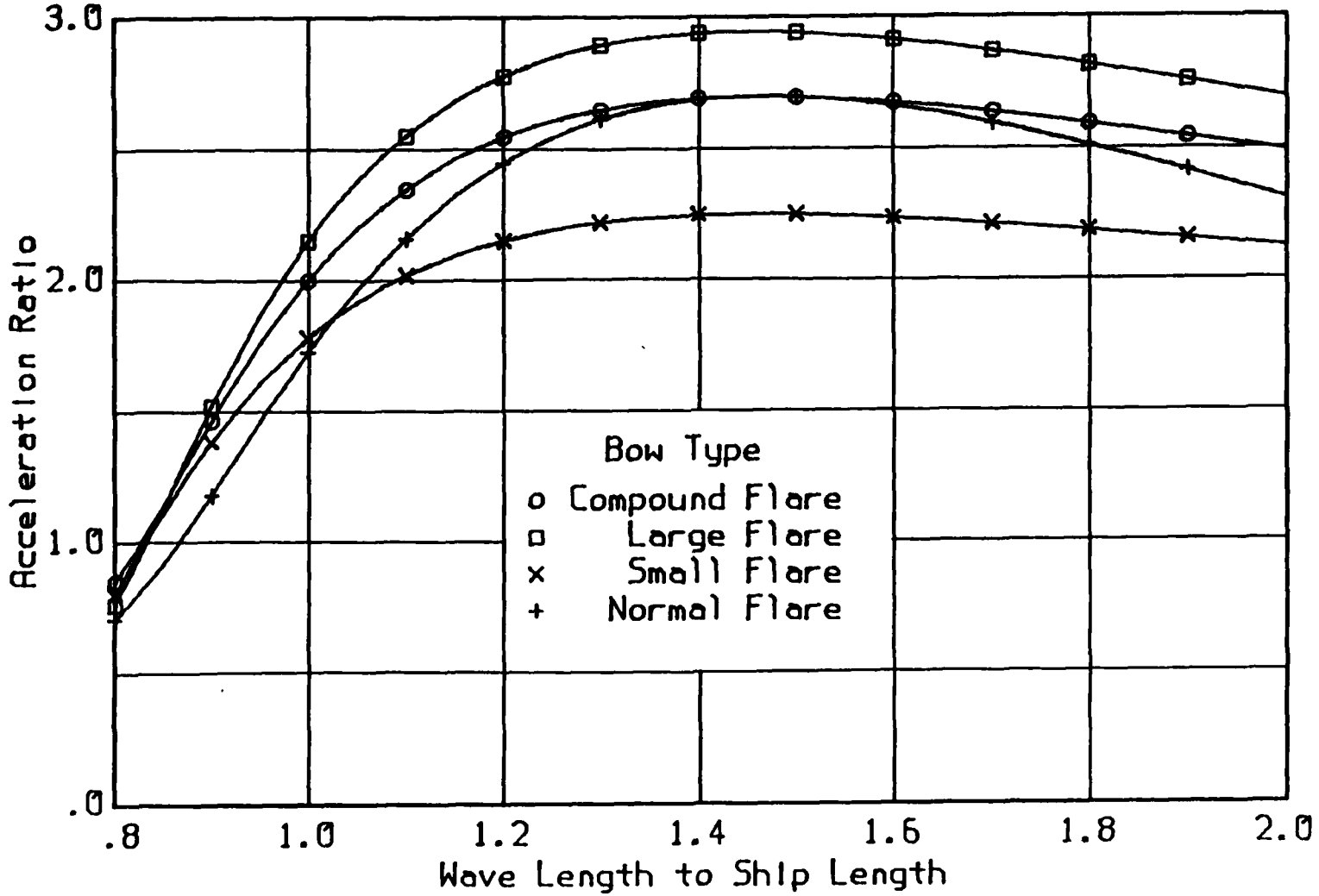

Figure 27. Acceleration Ratios for the Different Bows

Appendix

Every attempt was made to assure that the data was taken carefully. However, by the very nature experimentation, some scatter in the data was inevitable. In order to gain a clearer understanding of the trends afforded by these data, curves were fit to the original data points as described in the main body of the report. On the following pages the original data points and the corresponding fitted curves are shown so that the reader can assess the scatter and the closeness of fit acheived.

The following convention is adopted. The figure number given is of the form Axx.y, where the A refers to this appendix, xx corresponds to the figure in the main report in which the fitted curve is shown, and y is a letter from a to d which refers to the type of bow, following the table on page 3.

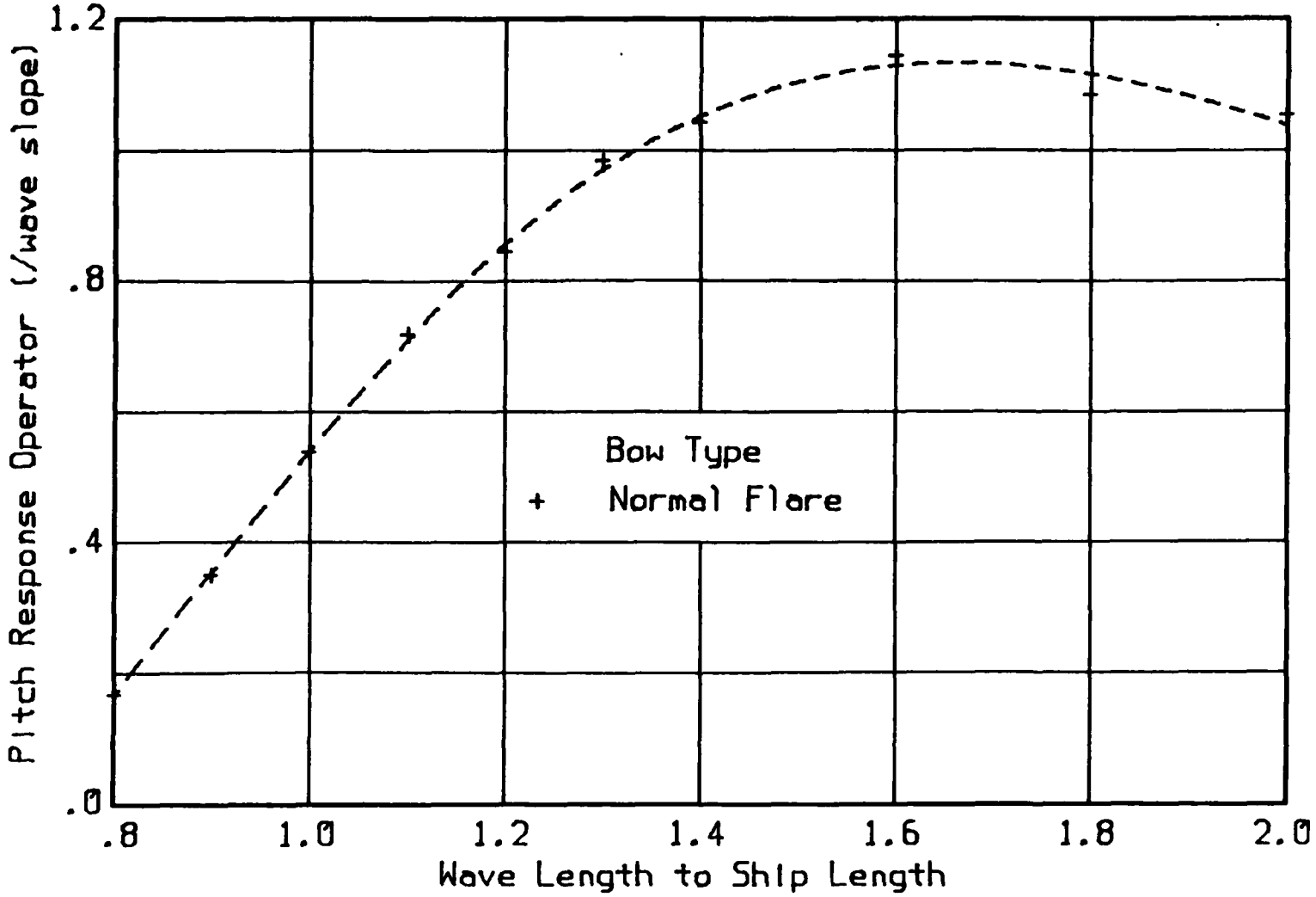

Figure A13a. Pitch Transfer Function in 1:40 Regular Head Seas

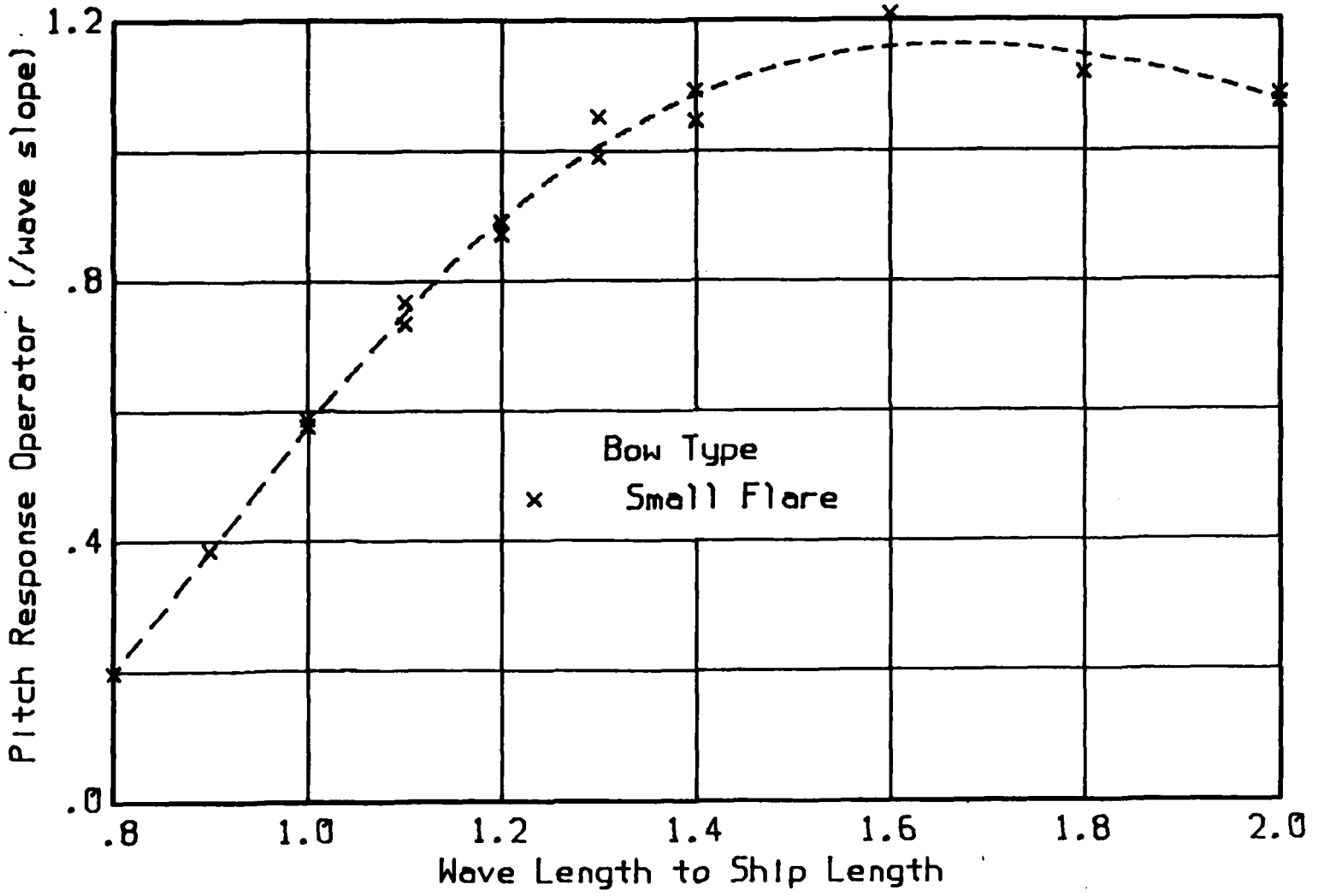

Figure A13b. Pitch Transfer Function in 1:40 Regular Head Seas

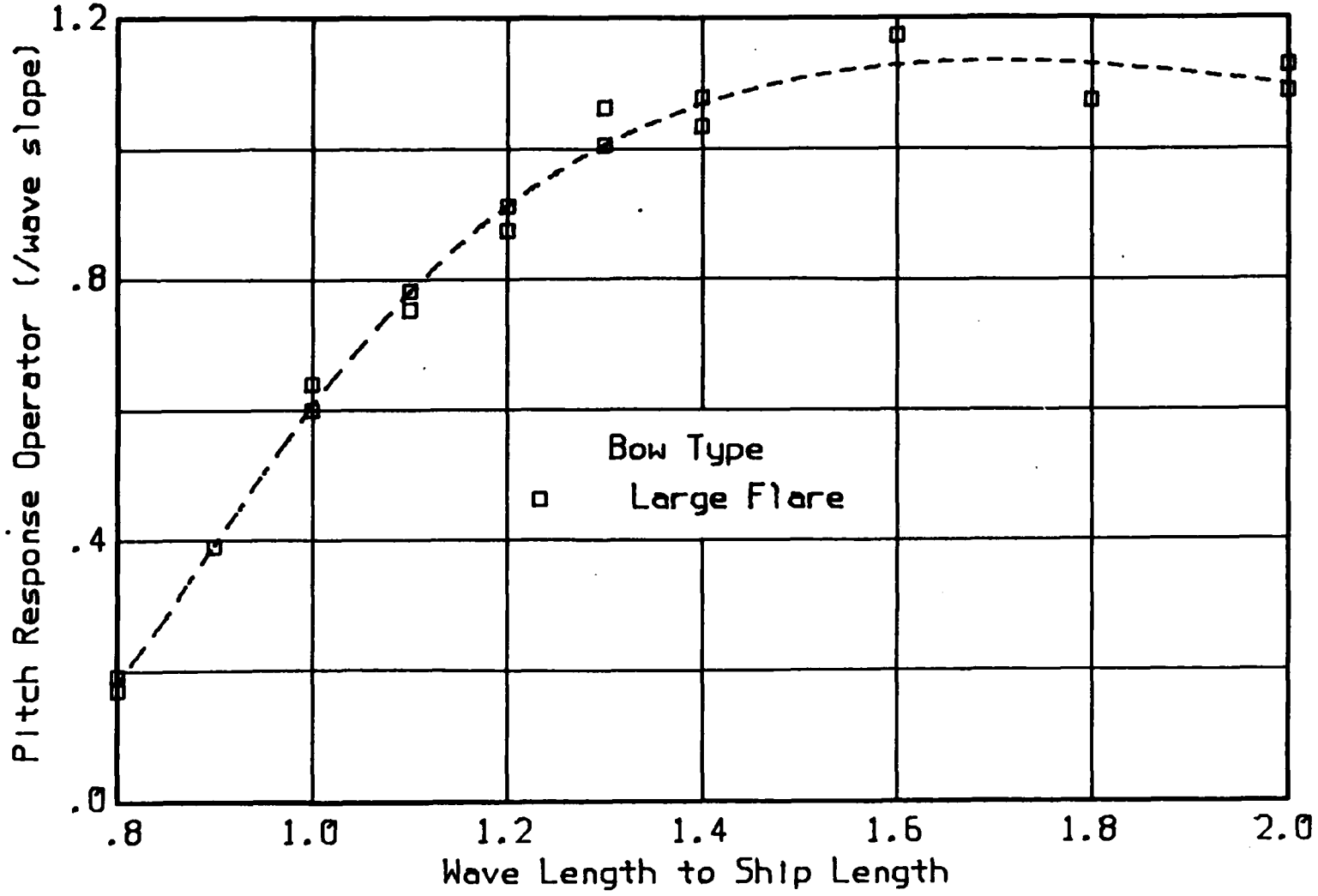

Figure A13c. Pitch Transfer Function in 1:40 Regular Head Seas

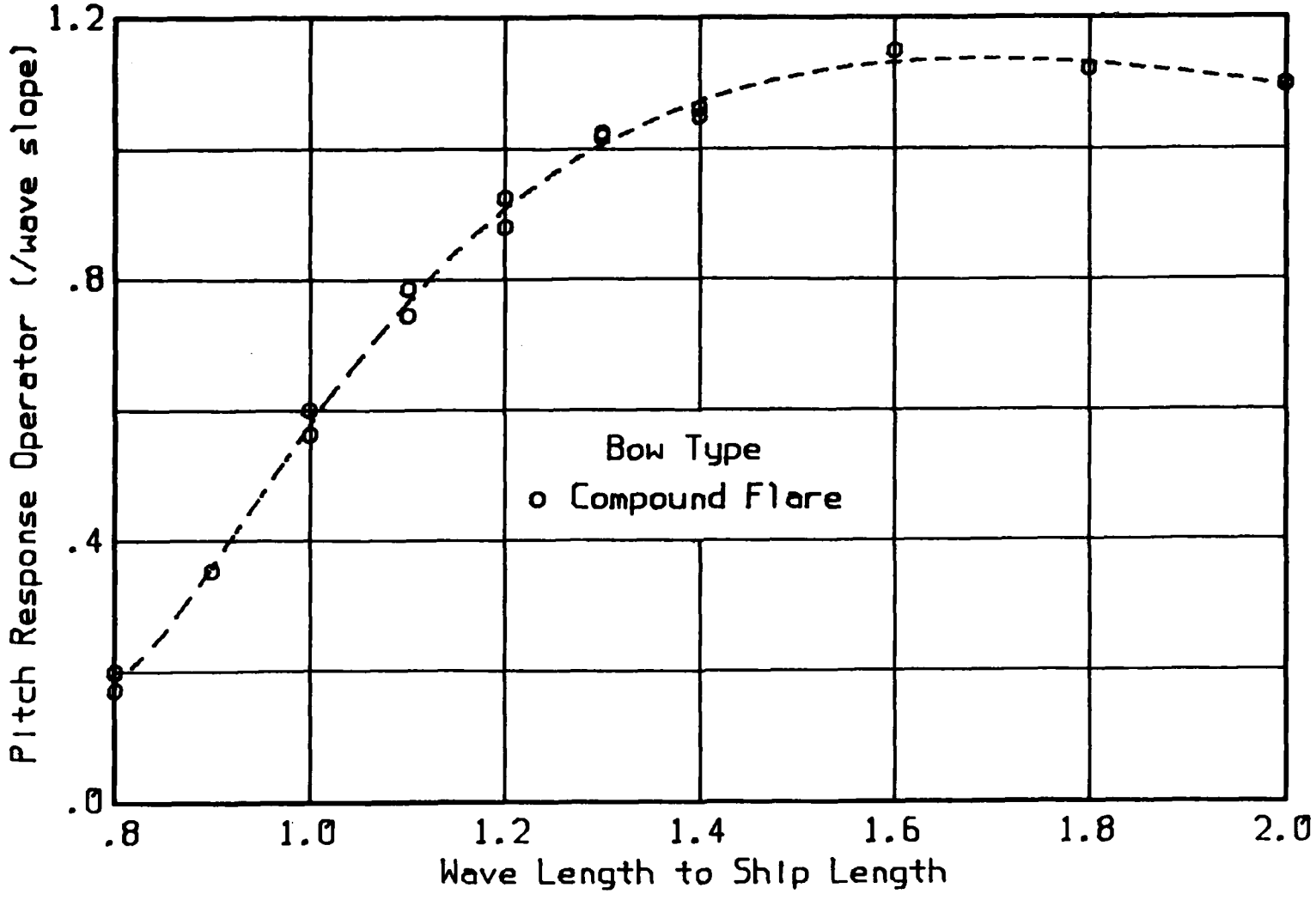

Figure A13d. Pitch Transfer Function in 1:40 Regular Head Seas

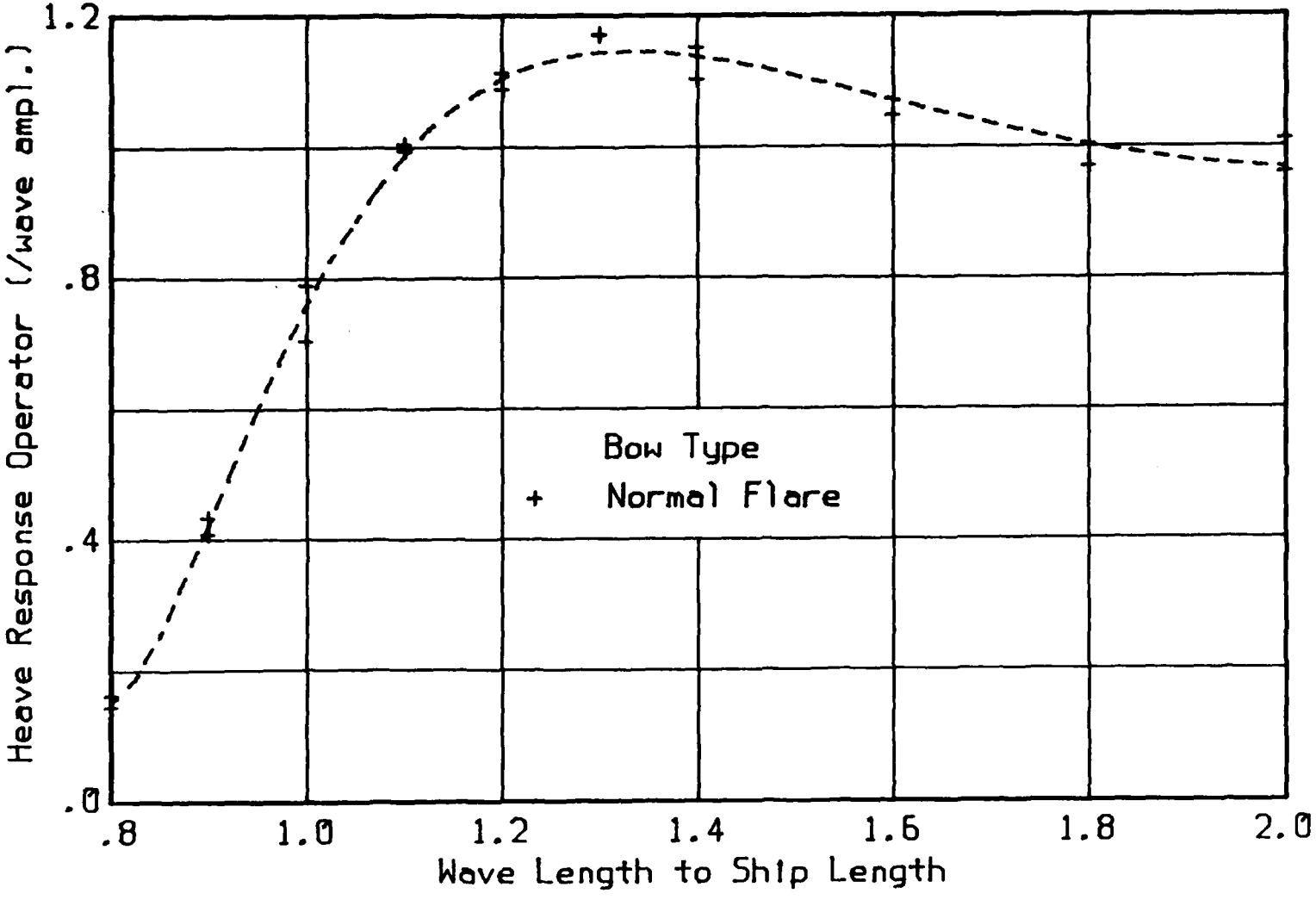

Figure A14a. Heave Transfer Function in 1:40 Regular Head Seas

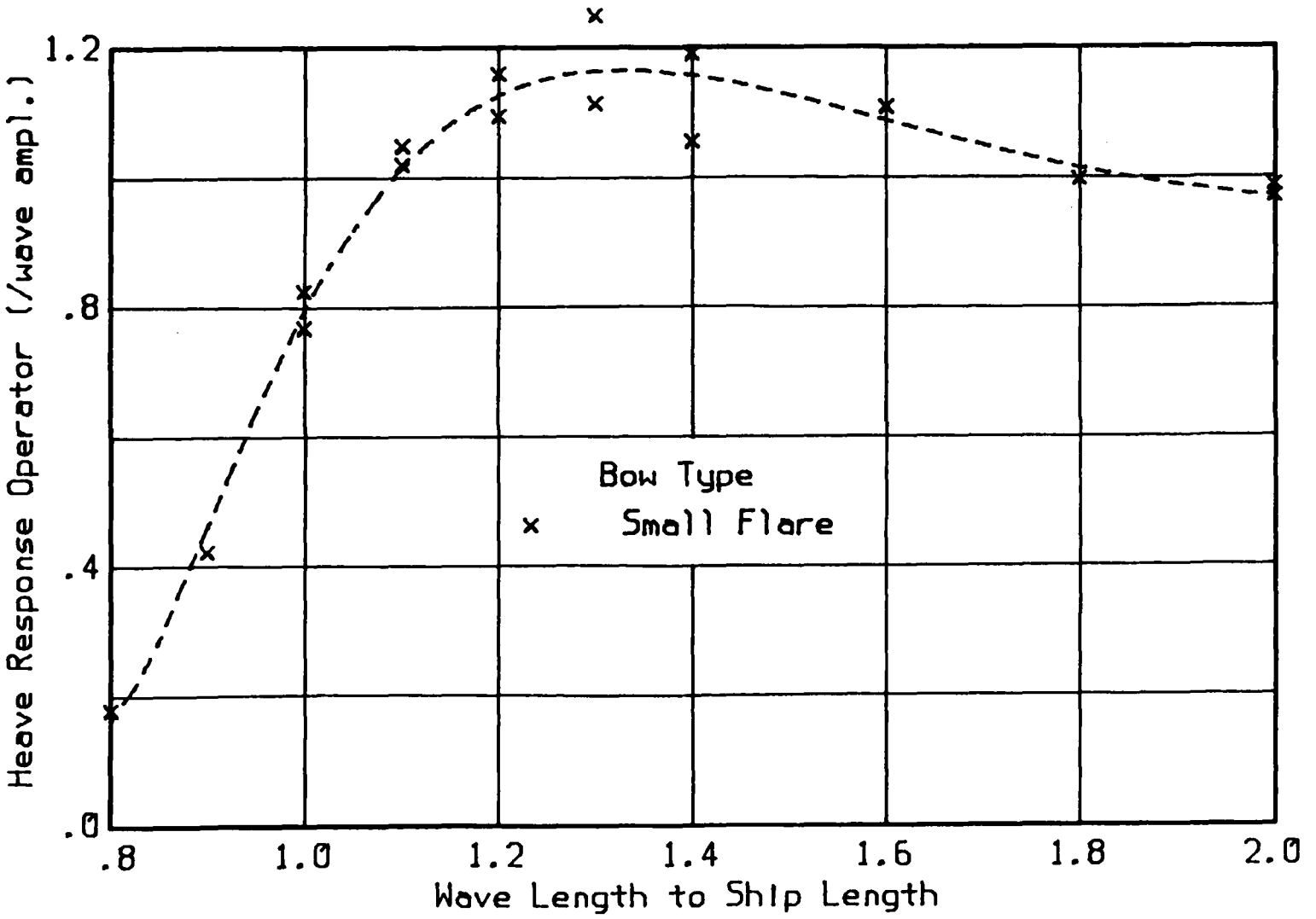

Figure A14b. Heave Transfer Function in 1:40 Regular Head Seas

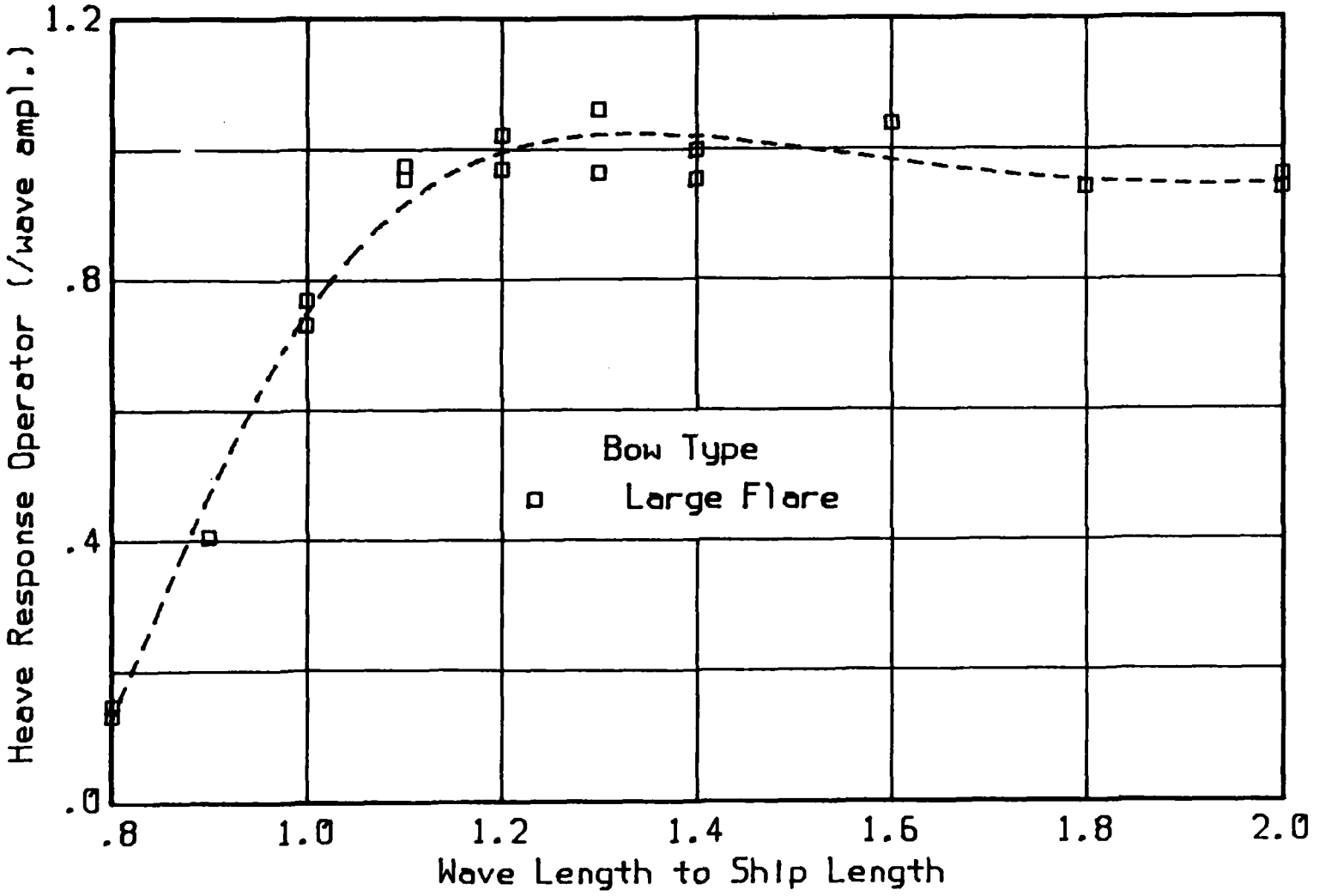

Figure A14c. Heave Transfer Function in 1:40 Regular Head Seas

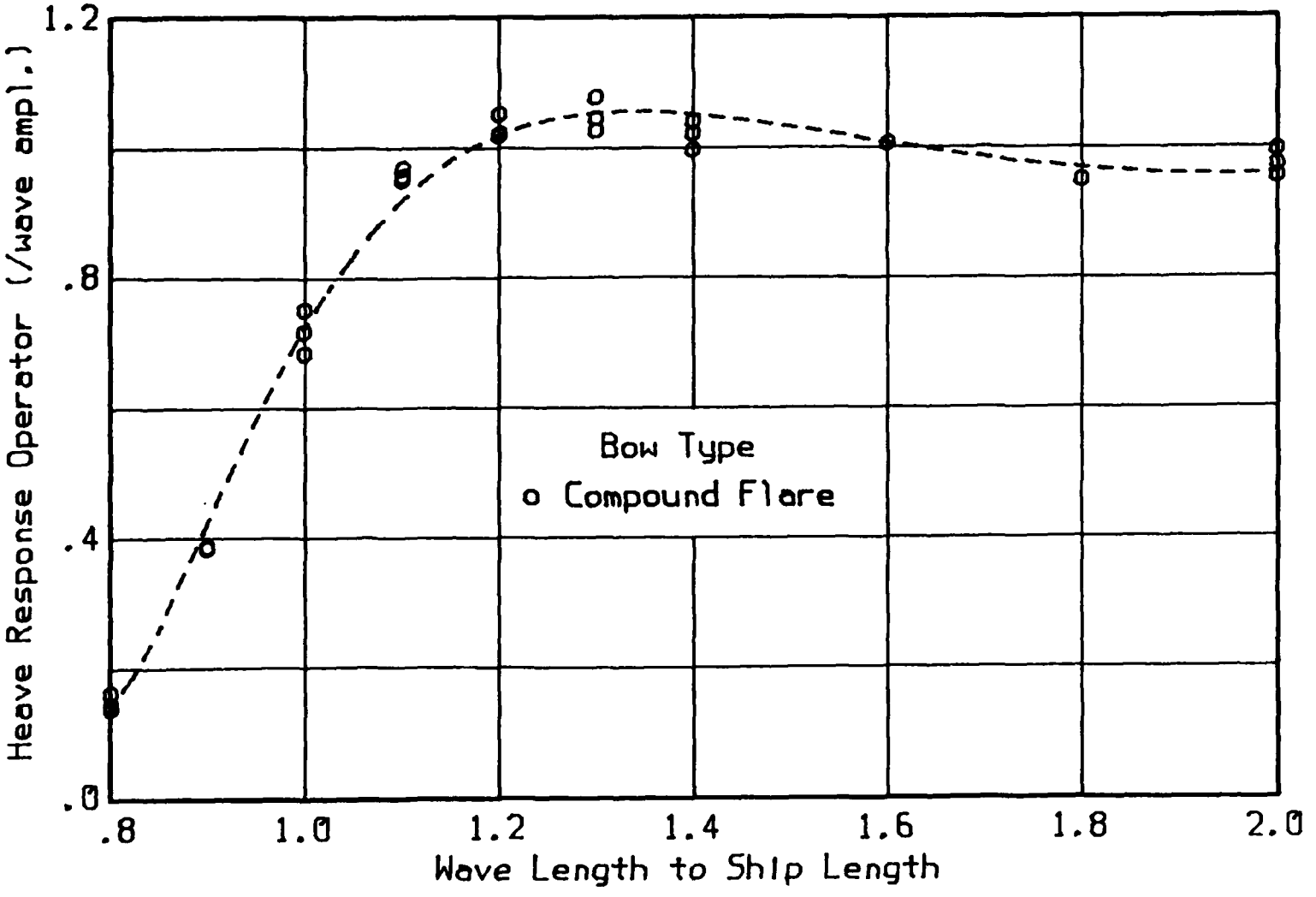

Figure A14d. Heave Transfer Function in 1:40 Regular Head Seas

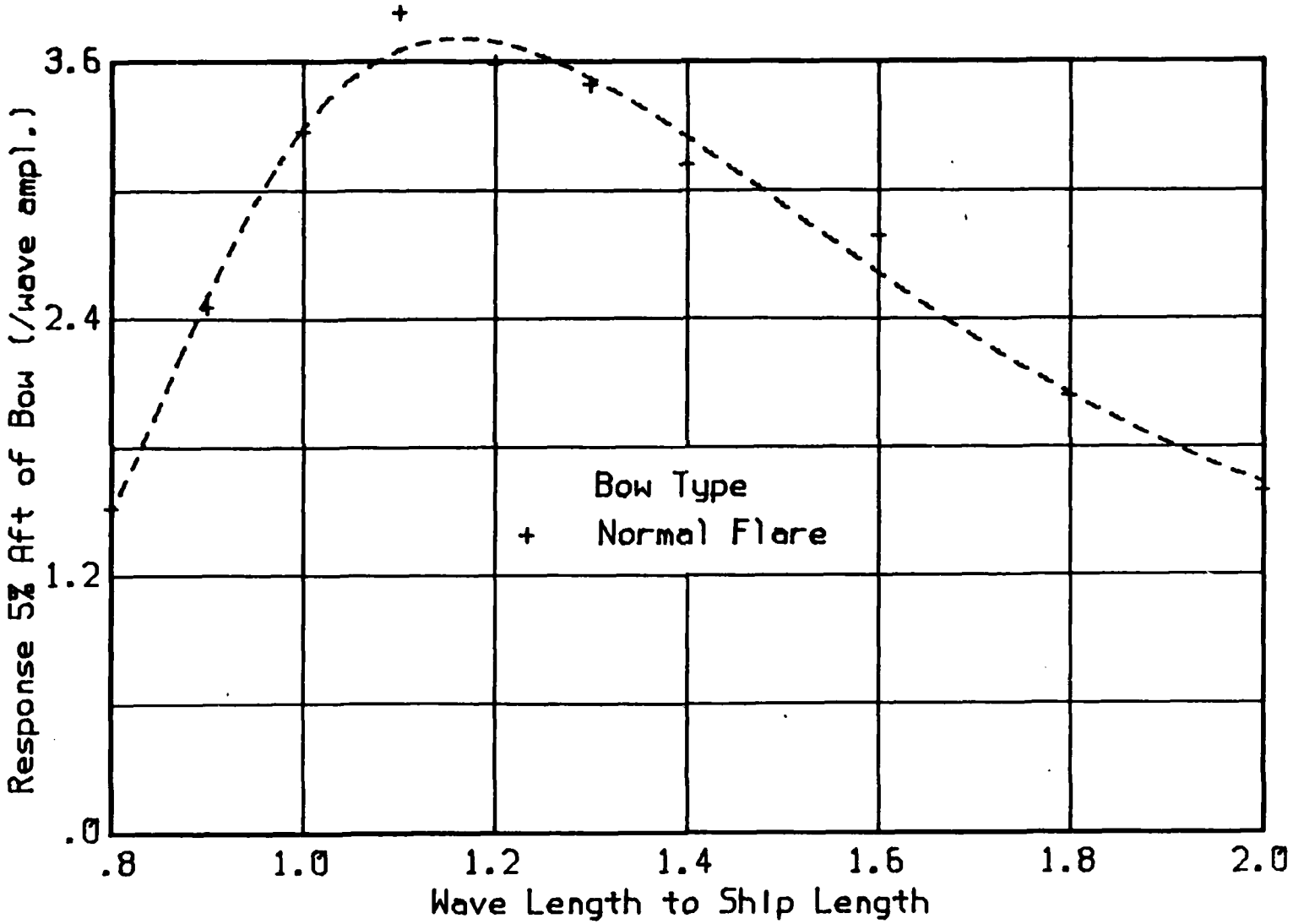

Figure A15a. Relative Wave Height Transfer Function in 1:40 Regular Head Seas - 5% Aft of Bow

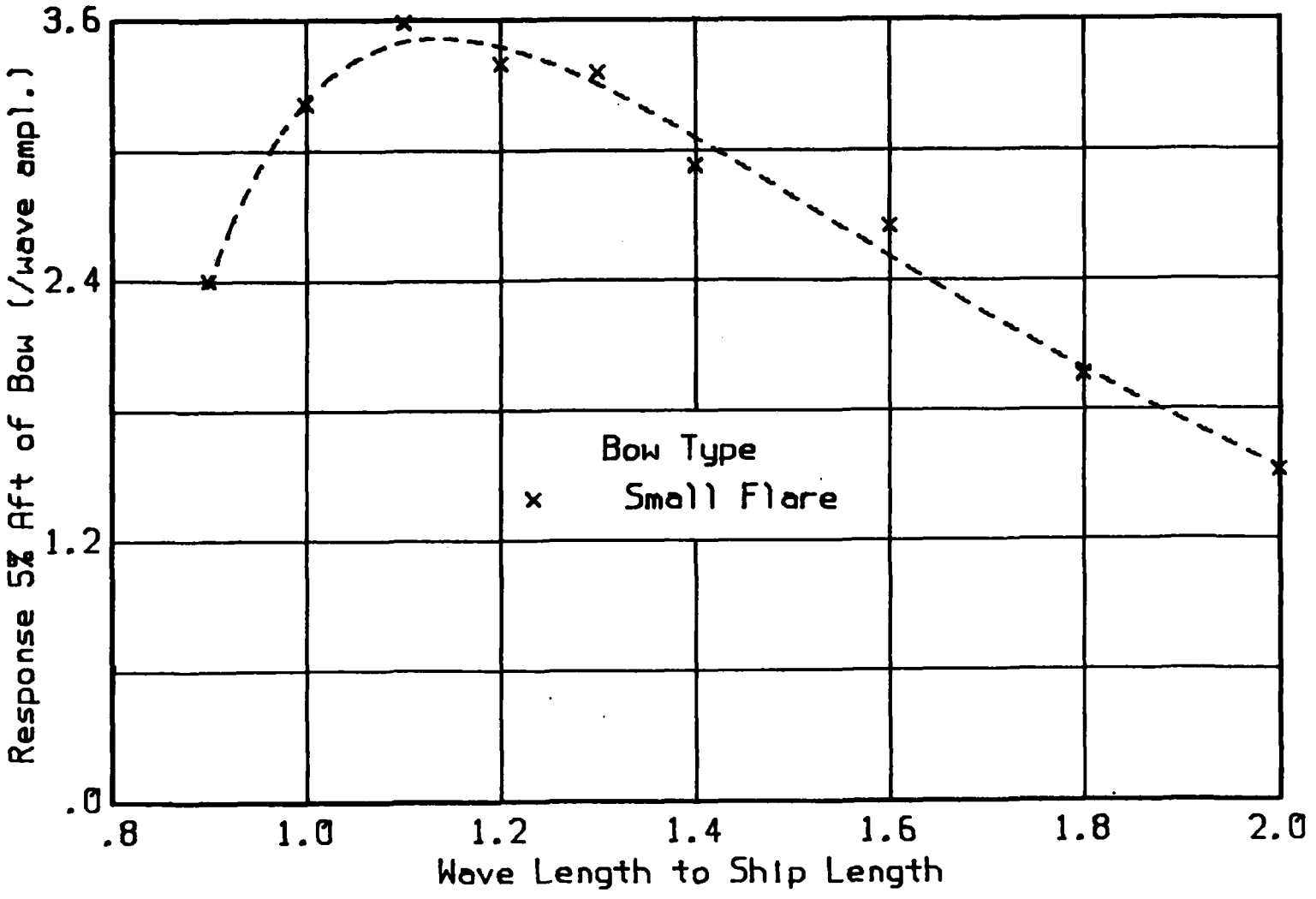

Figure A15b. Relative Wave Height Transfer Function in 1:40 Regular Head Seas - 5% Aft of Bow

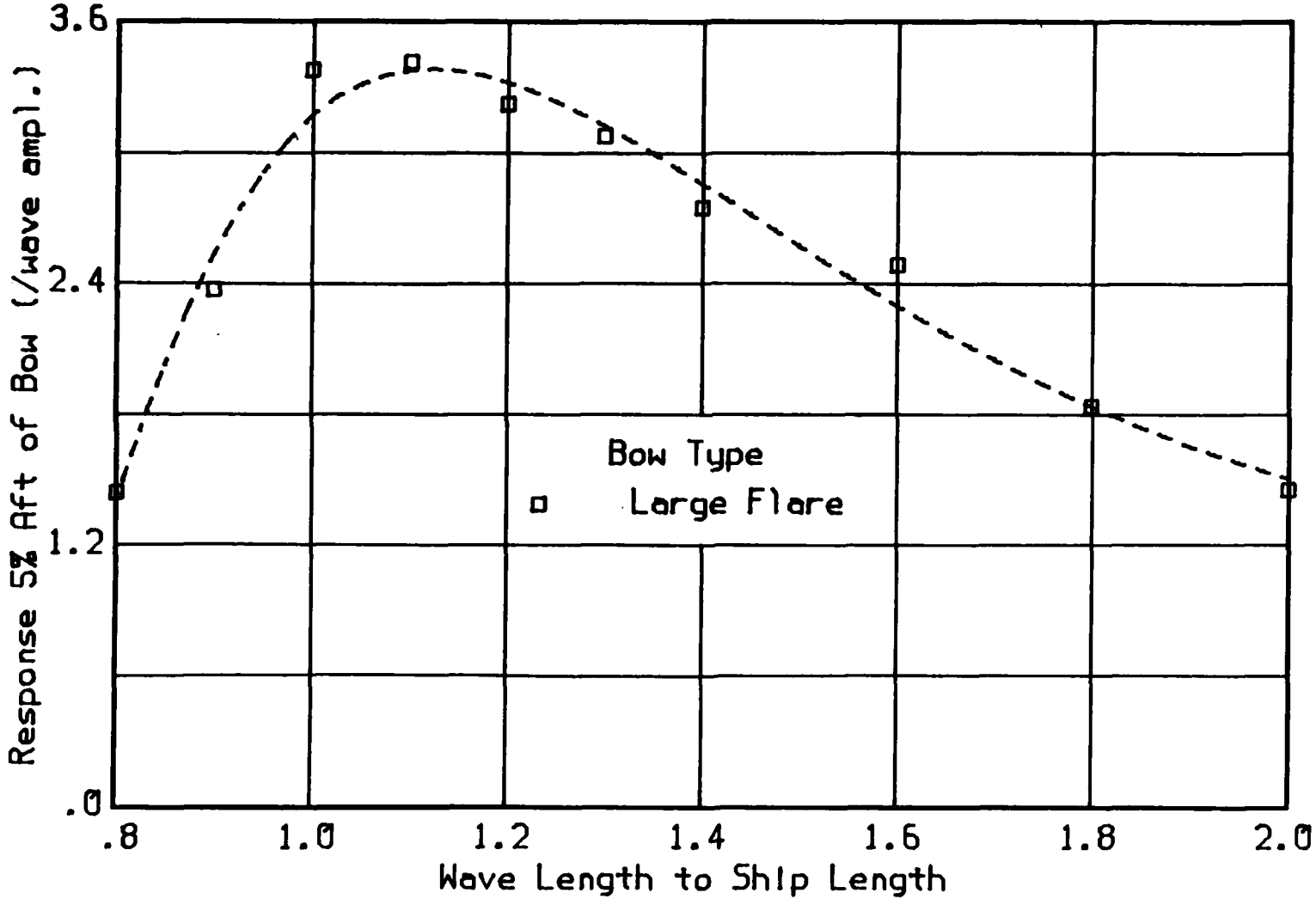

Figure A15c. Relative Wave Height Transfer Function in 1:40 Regular Head Seas - 5% Aft of Bow

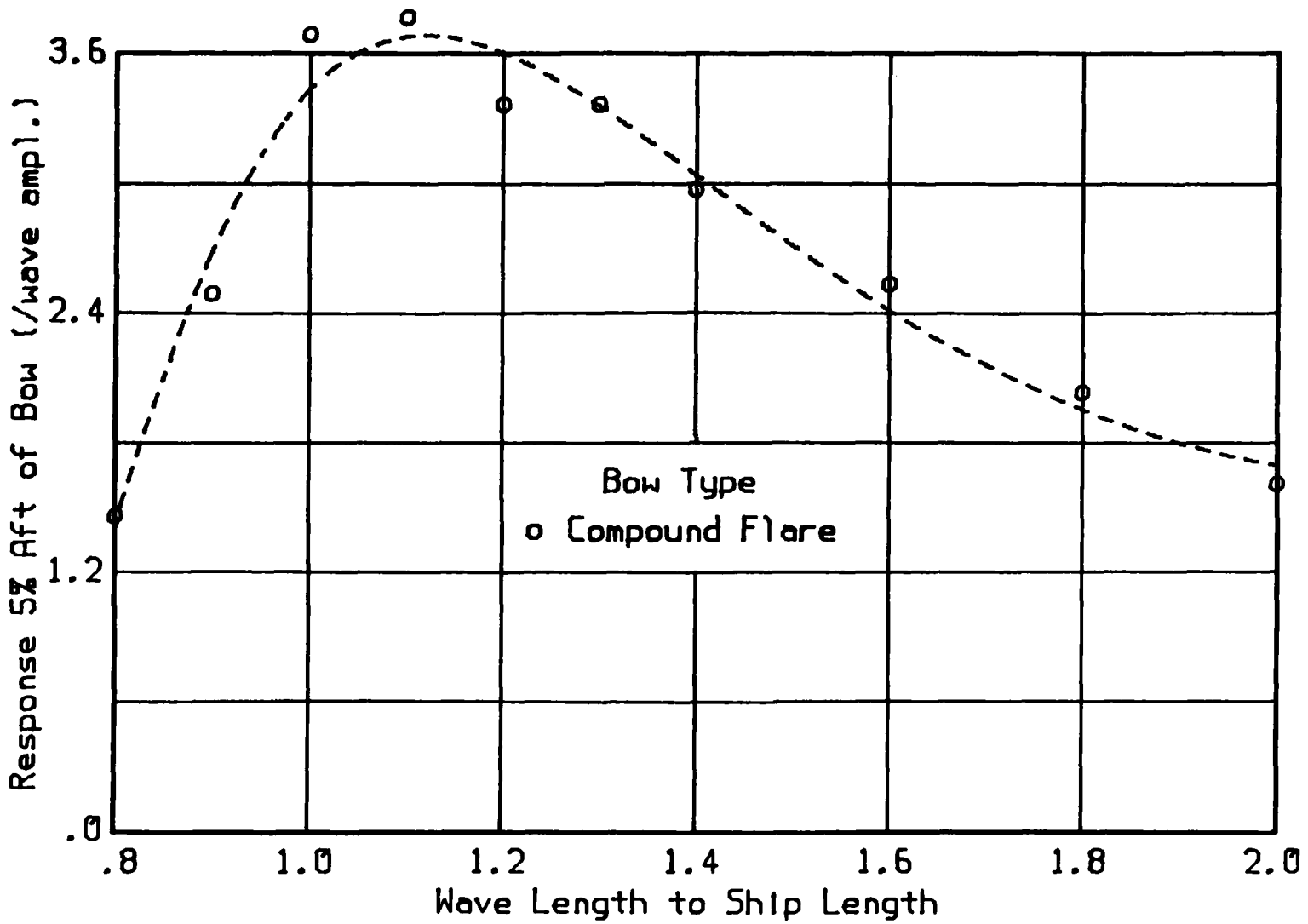

Figure A15d. Relative Wave Height Transfer Function in 1:40 Regular Head Seas - 5% Aft of Bow

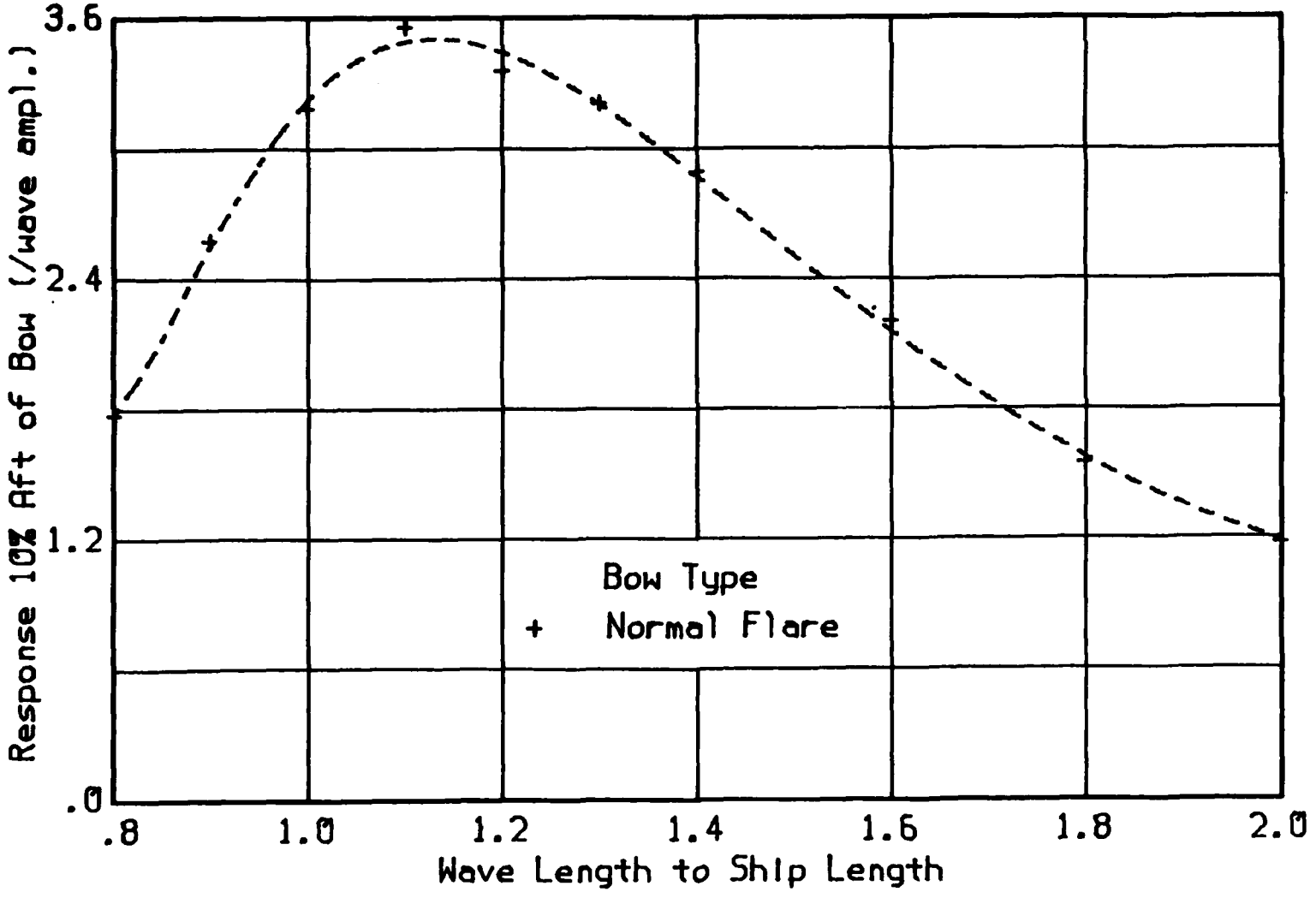

Figure A16a. Relative Wave Height Transfer Function in 1:40 Regular Head Seas - 10% Aft of Bow

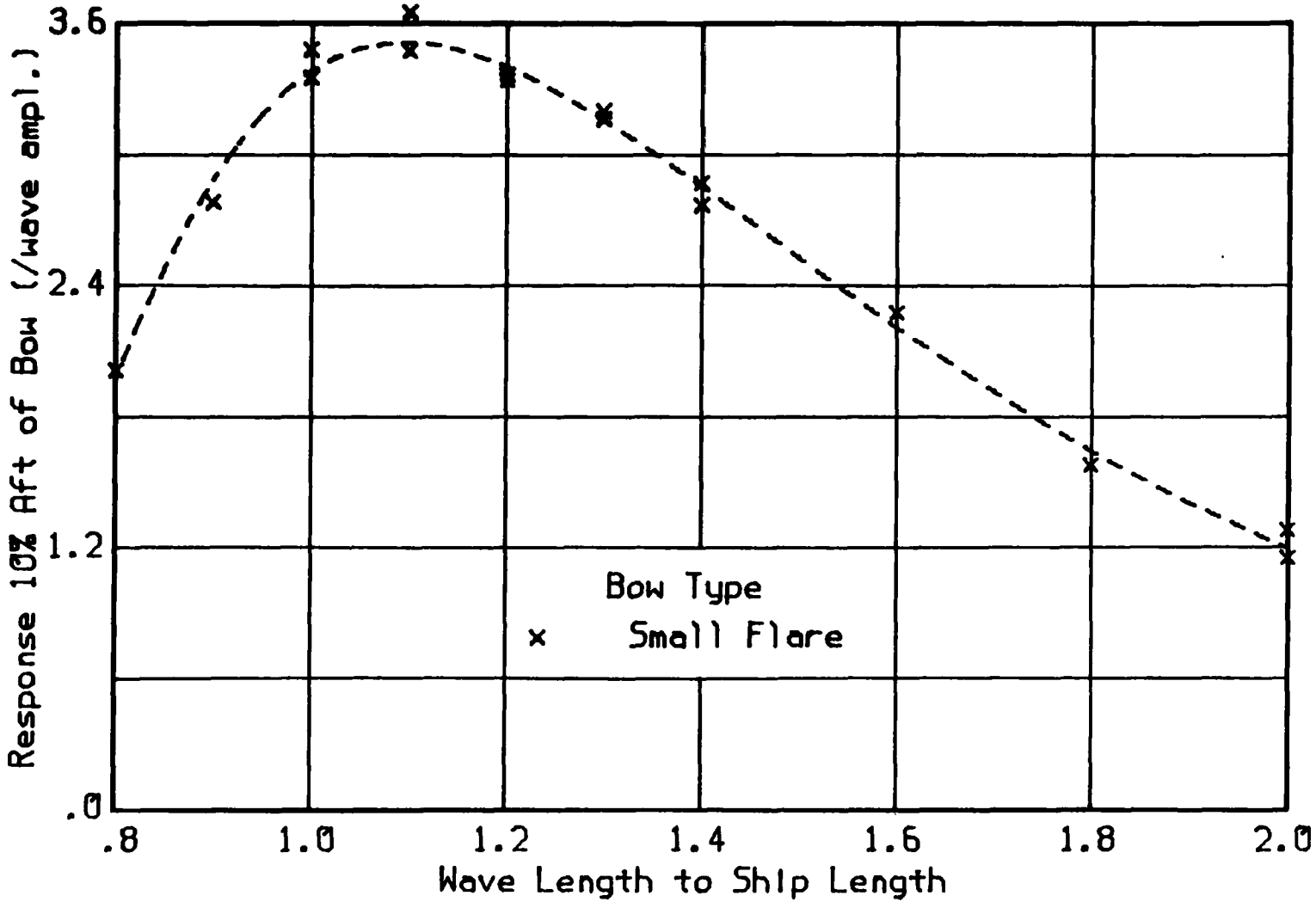

Figure A16b. Relative Wave Height Transfer Function in 1:40 Regular Head Seas - 10% Aft of Bow

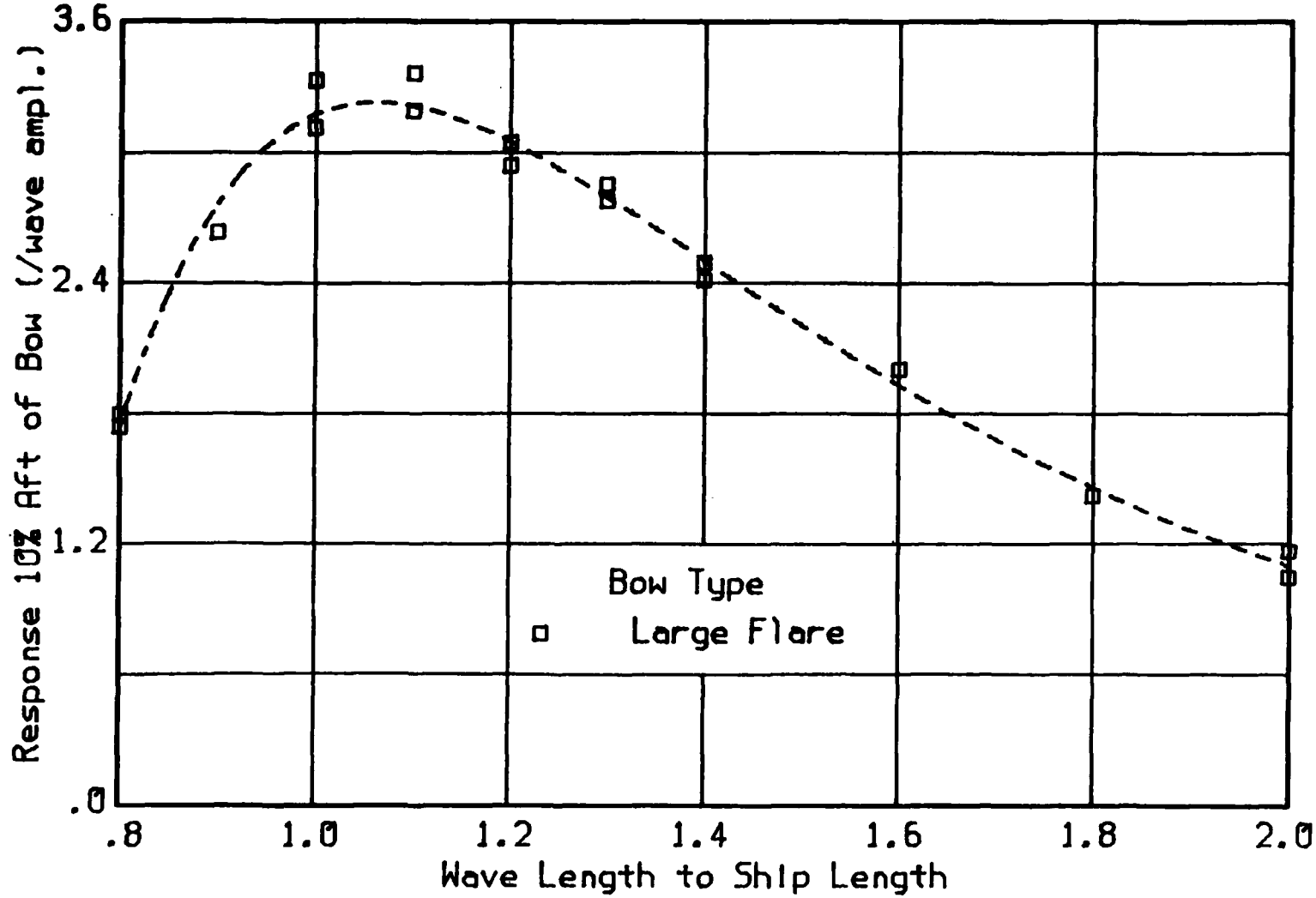

Figure A16c. Relative Wave Height Transfer Function in 1:40 Regular Head Seas - 10% Aft of Bow

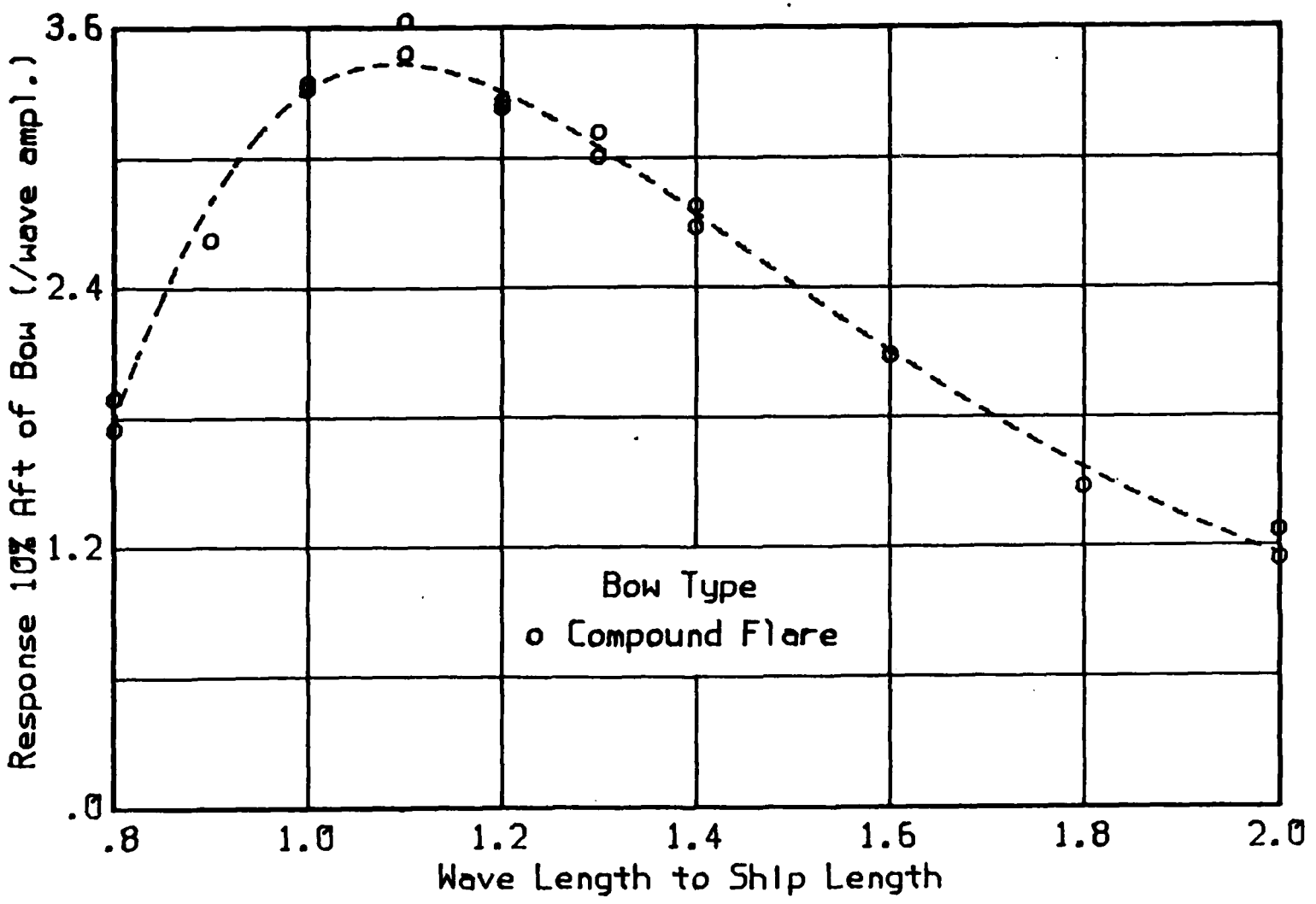

Figure A16d. Relative Wave Height Transfer Function in 1:40 Regular Head Seas - 10% Aft of Bow

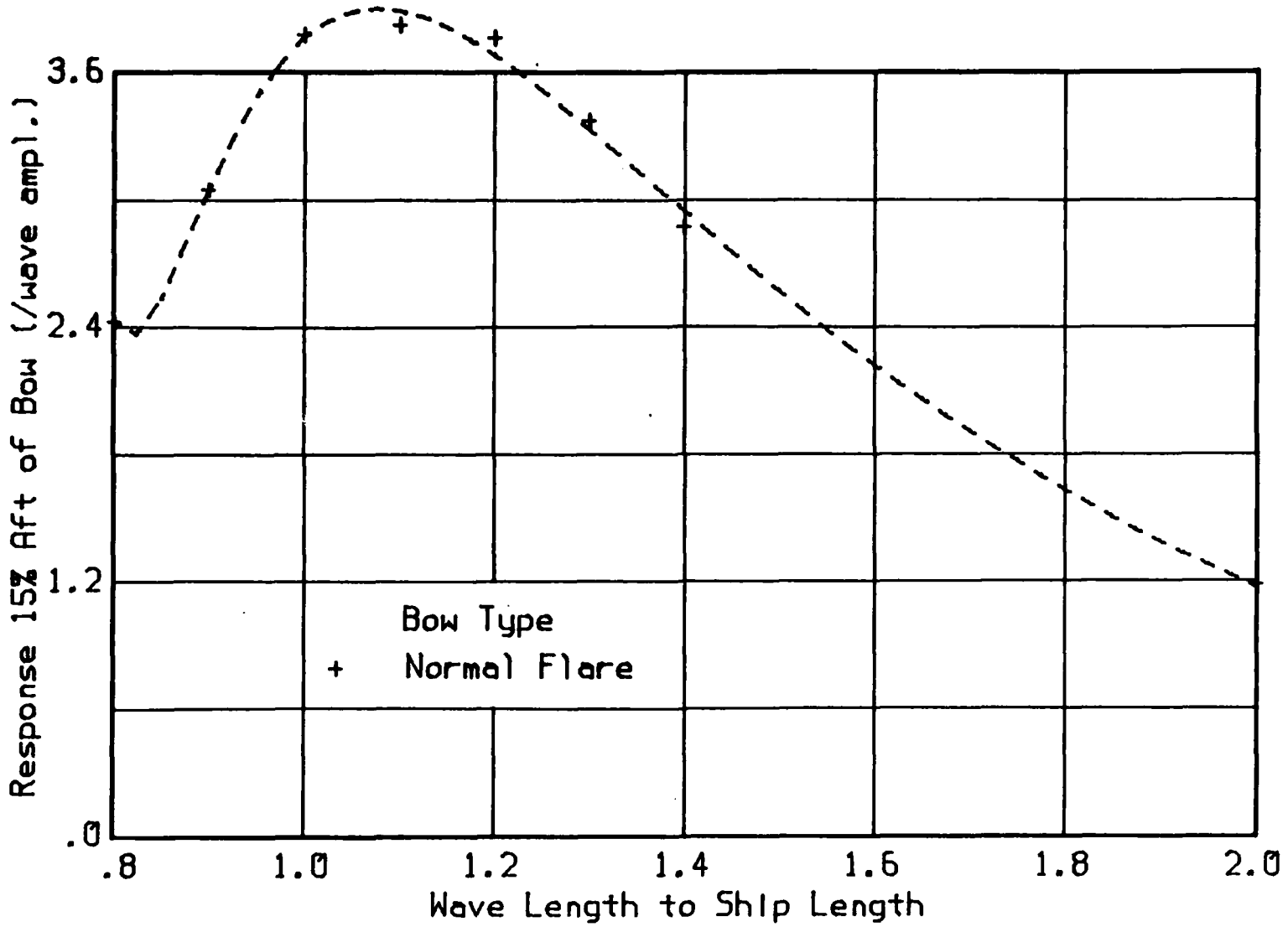

Figure A17a. Relative Wave Height Transfer Function in 1:40 Regular Head Seas - 15% Aft of Bow

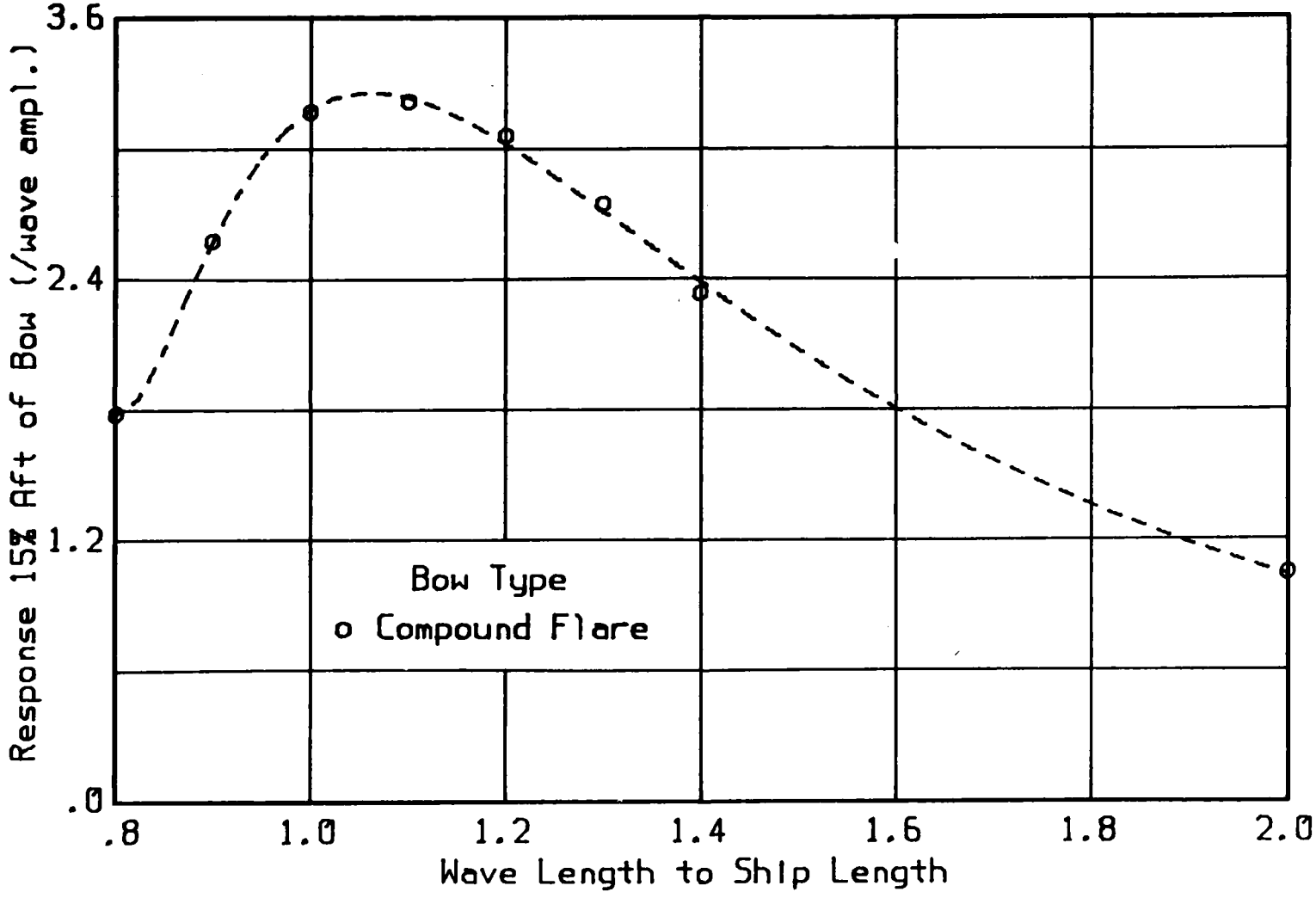

Figure A17d. Relative Wave Height Transfer Function in 1:40 Regular Head Seas - 15% Aft of Bow

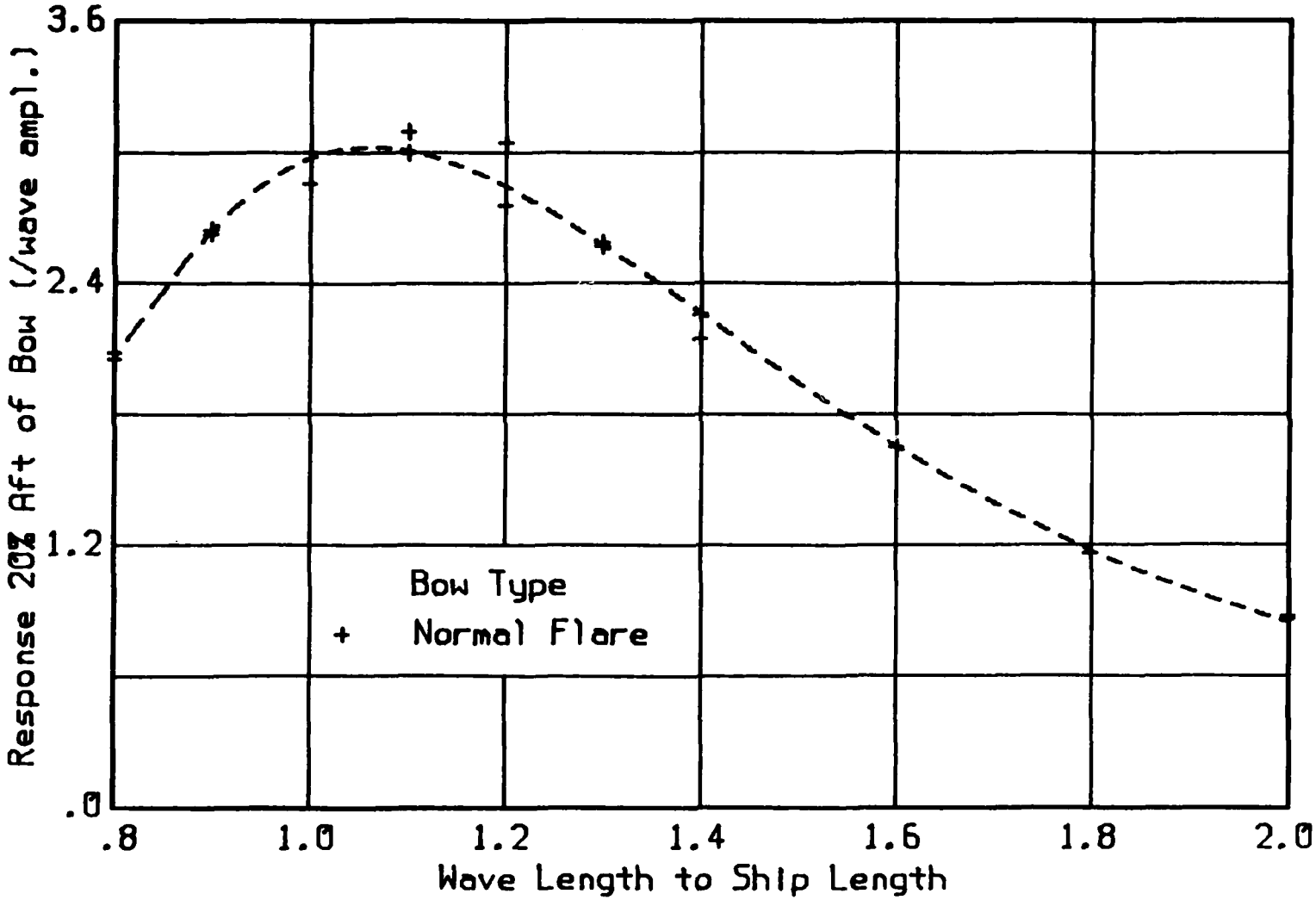

Figure A18a. Relative Wave Height Transfer Function in 1:40 Regular Head Seas - 20% Aft of Bow

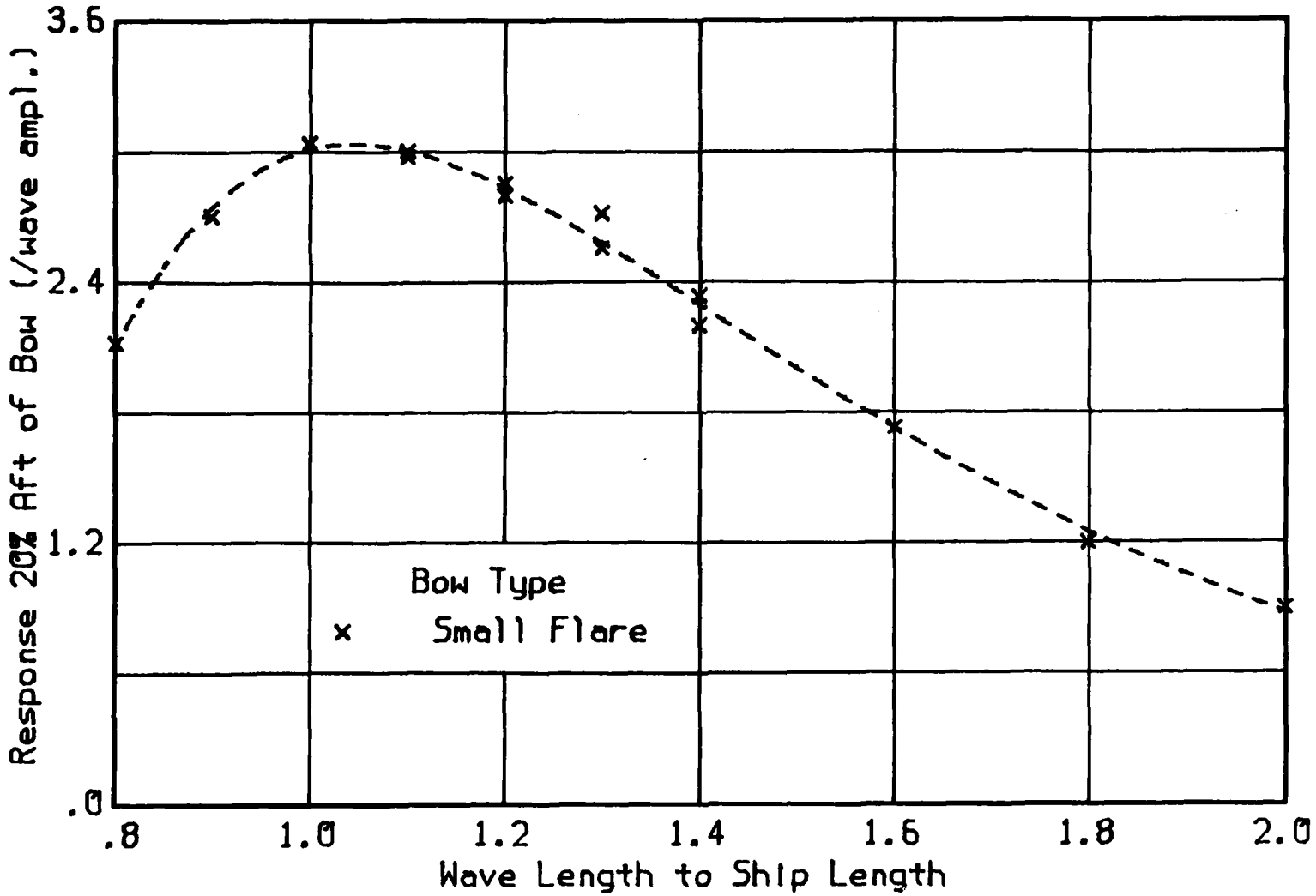

Figure A18b. Relative Wave Height Transfer Function in 1:40 Regular Head Seas - 20% Aft of Bow

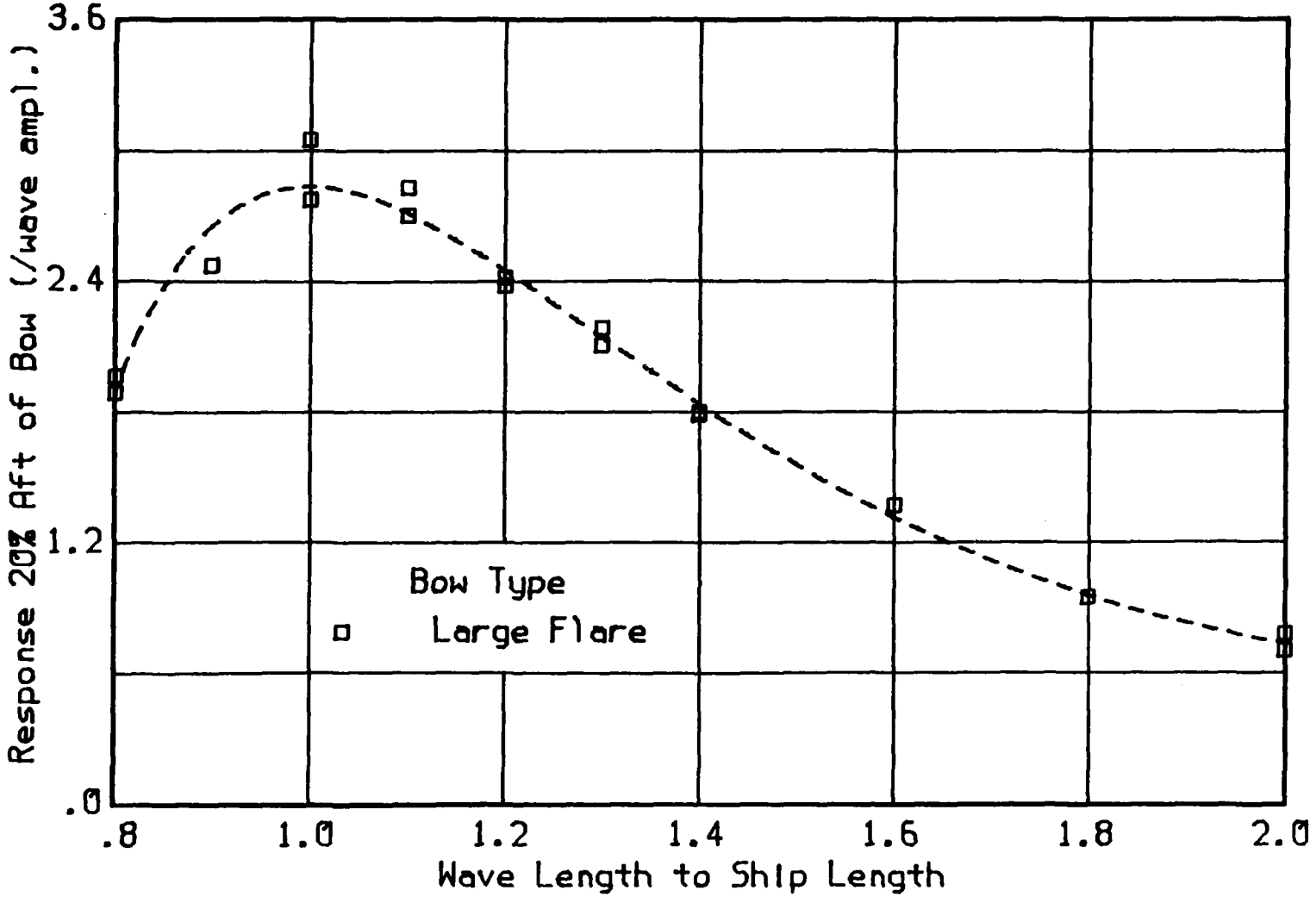

Figure A18c. Relative Wave Height Transfer Function in 1:40 Regular Head Seas - 20% Aft of Bow

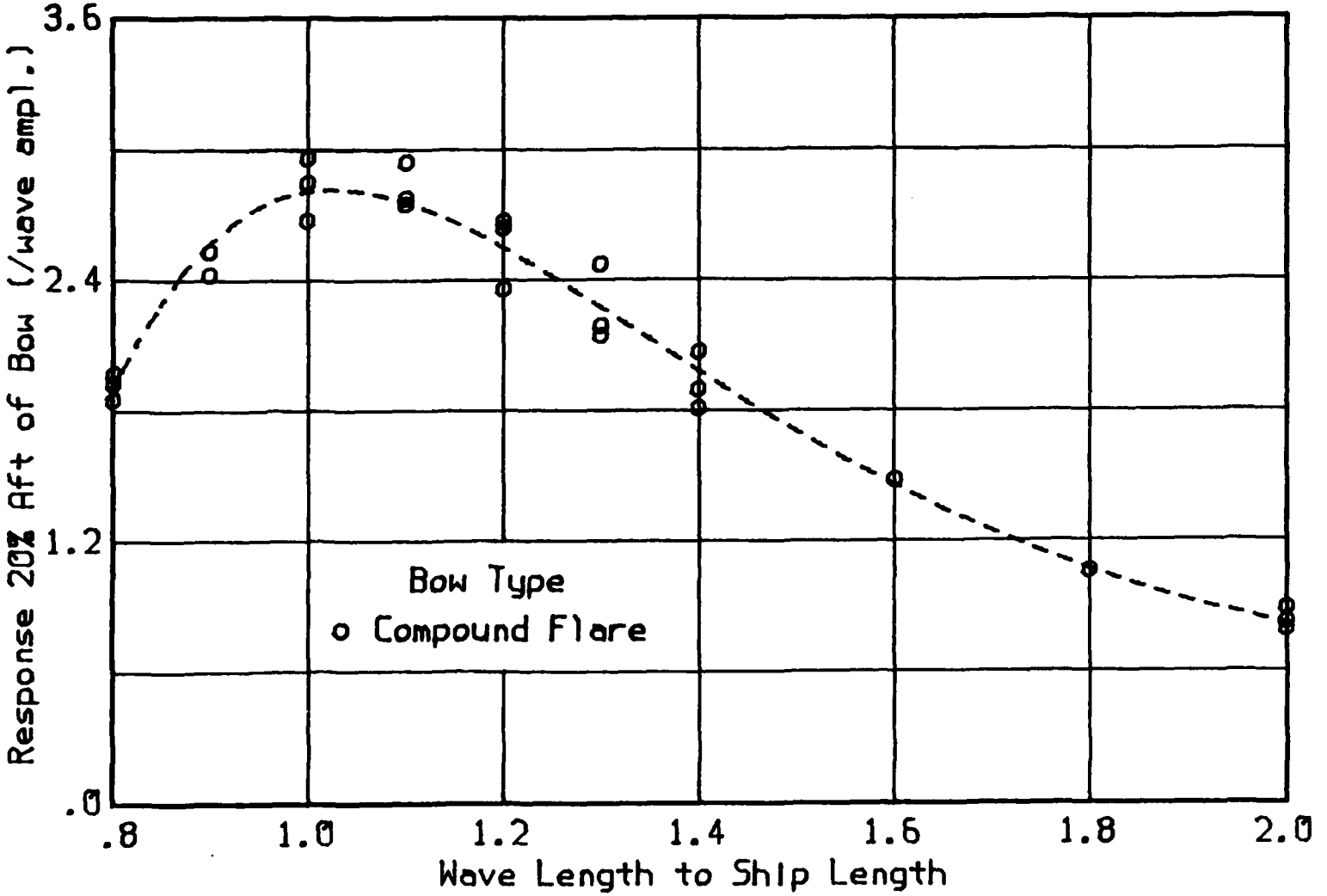

Figure A18d. Relative Wave Height Transfer Function in 1:40 Regular Head Seas - 20% Aft of Bow

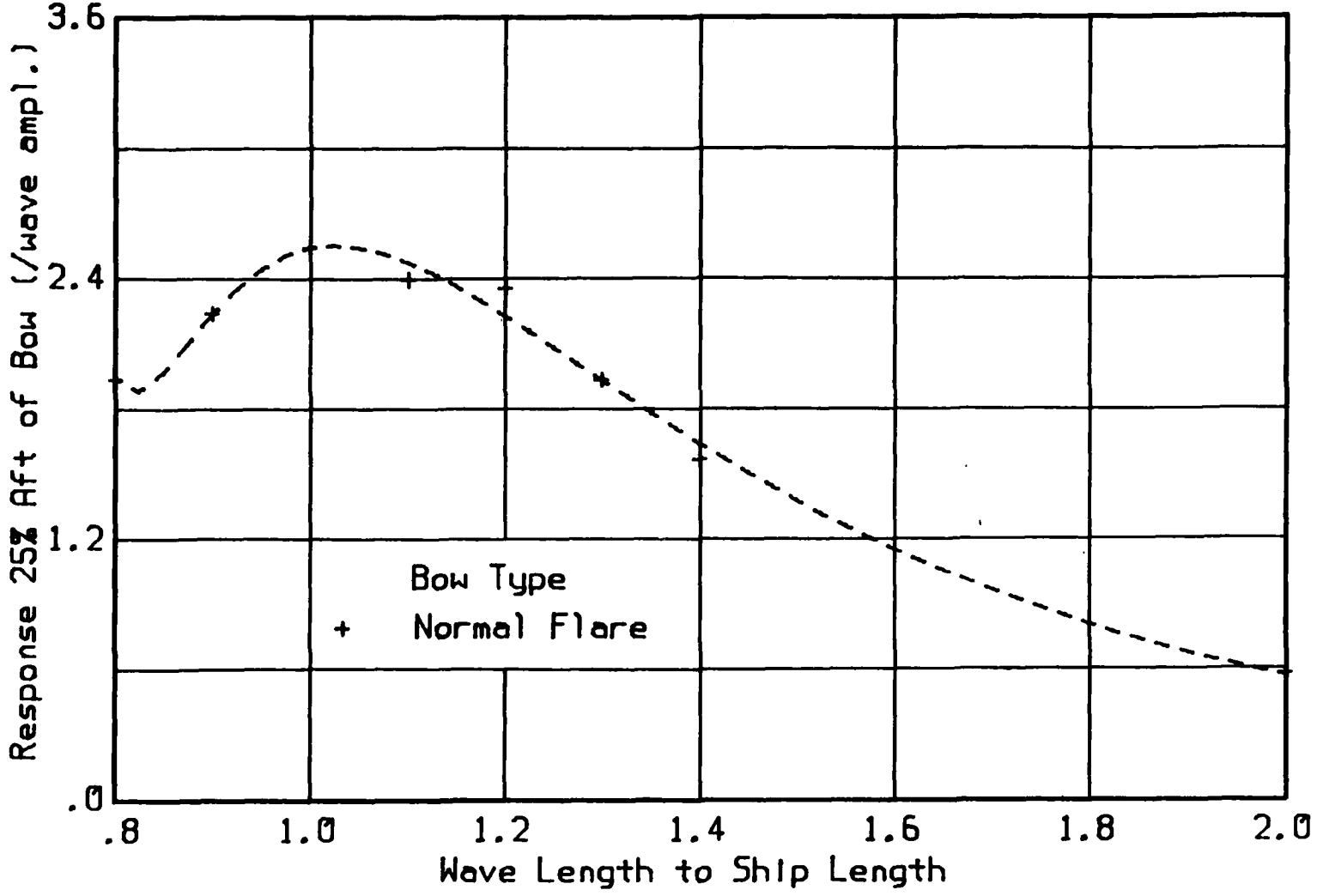

Figure A19a. Relative Wave Height Transfer Function in 1:40 Regular Head Seas - 25% Aft of Bow

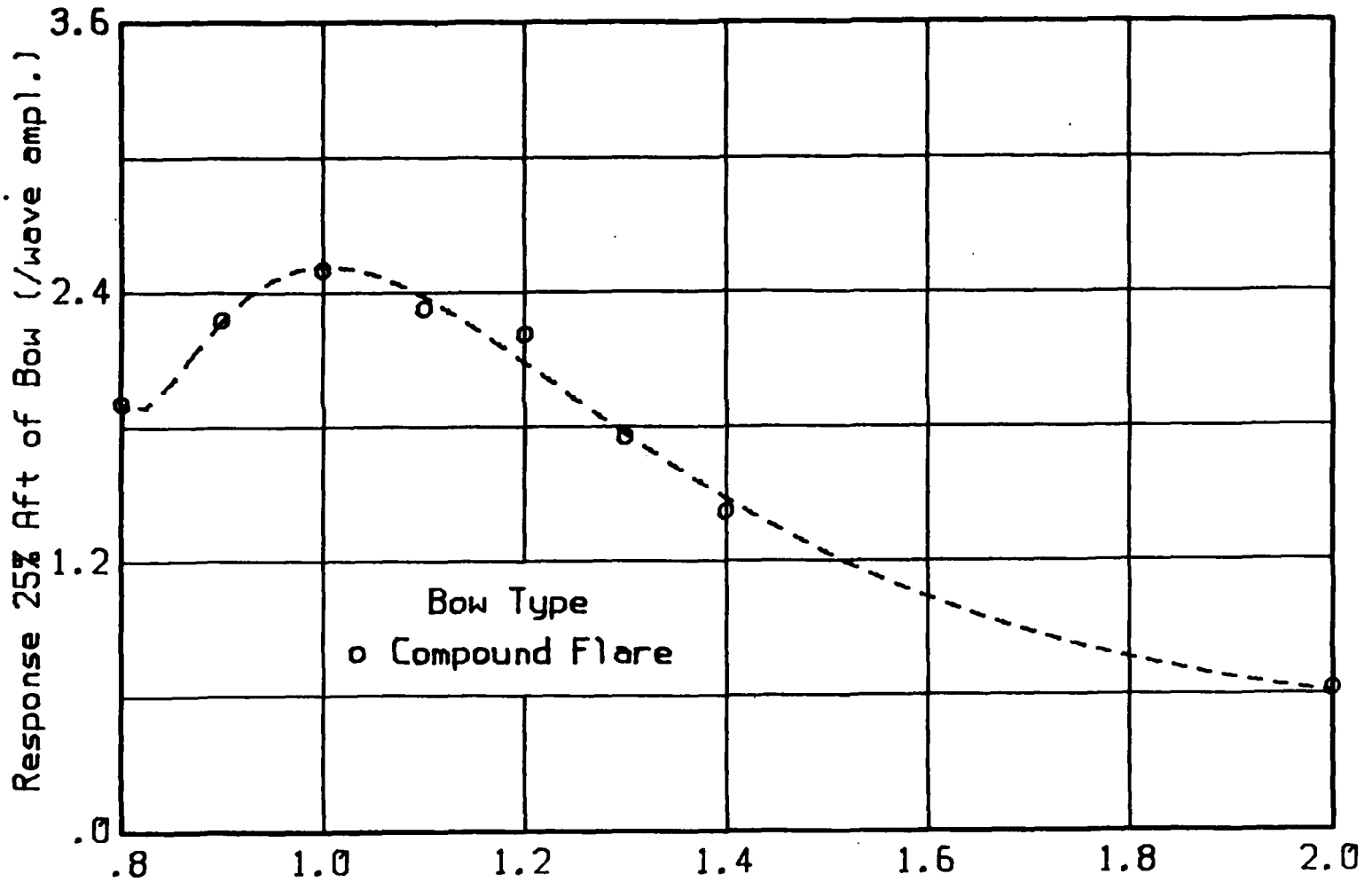

Figure A19d. Relative Wave Height Transfer Function in 1:40 Regular Head Seas - 25% Aft of Bow

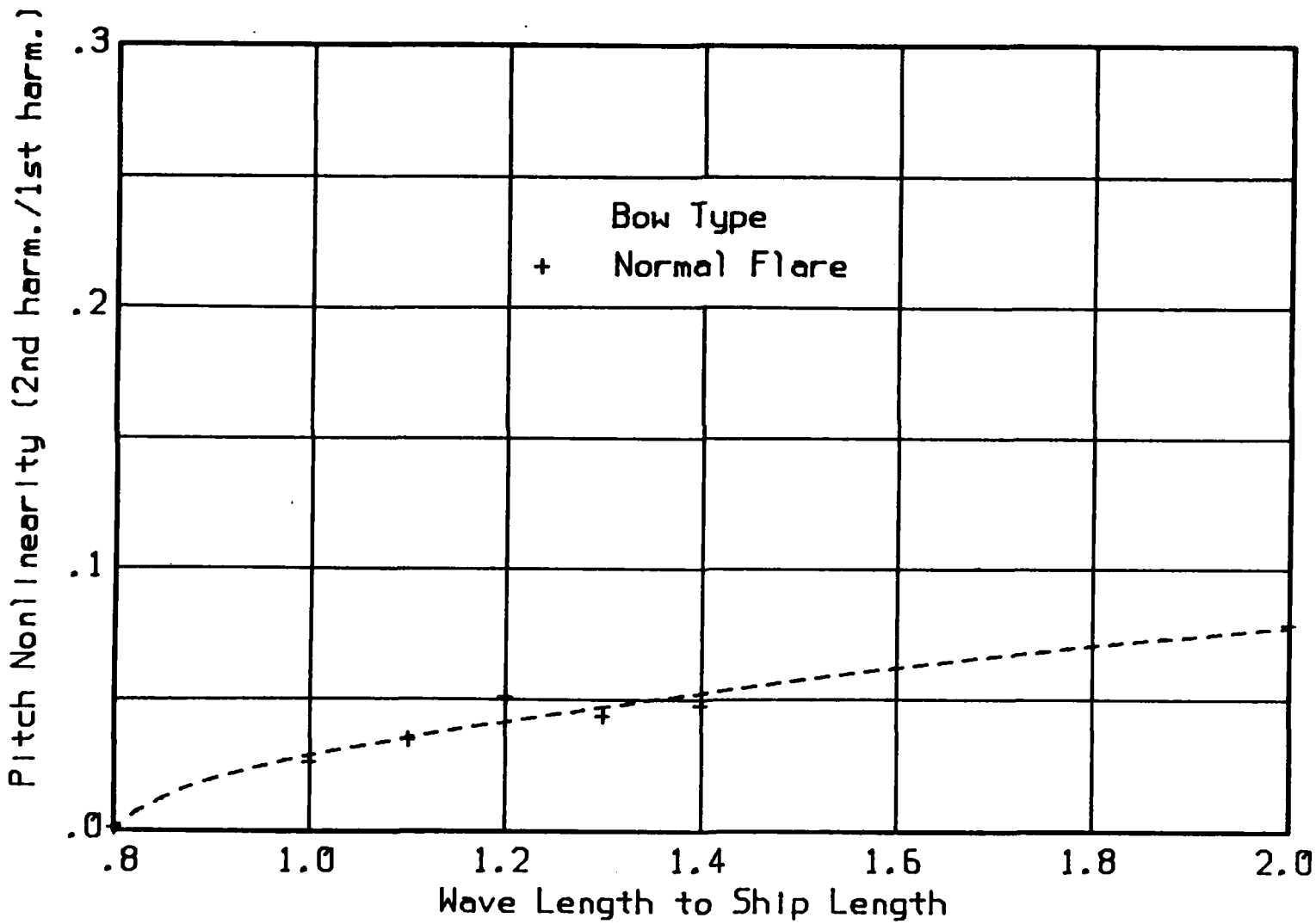

Figure A20a. Pitch Motion Nonlinearity Factor

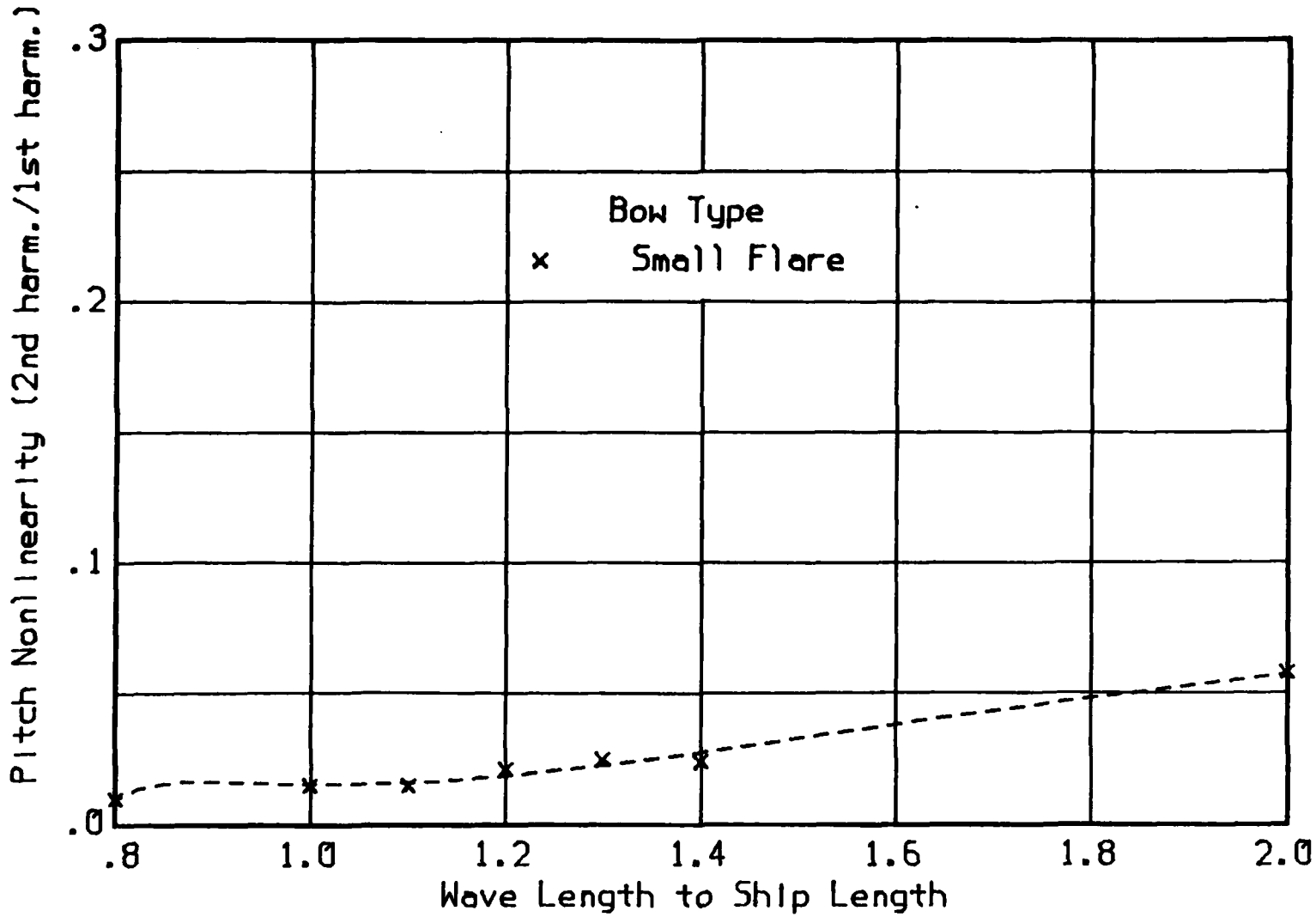

Figure A20b. Pitch Motion Nonlinearity Factor

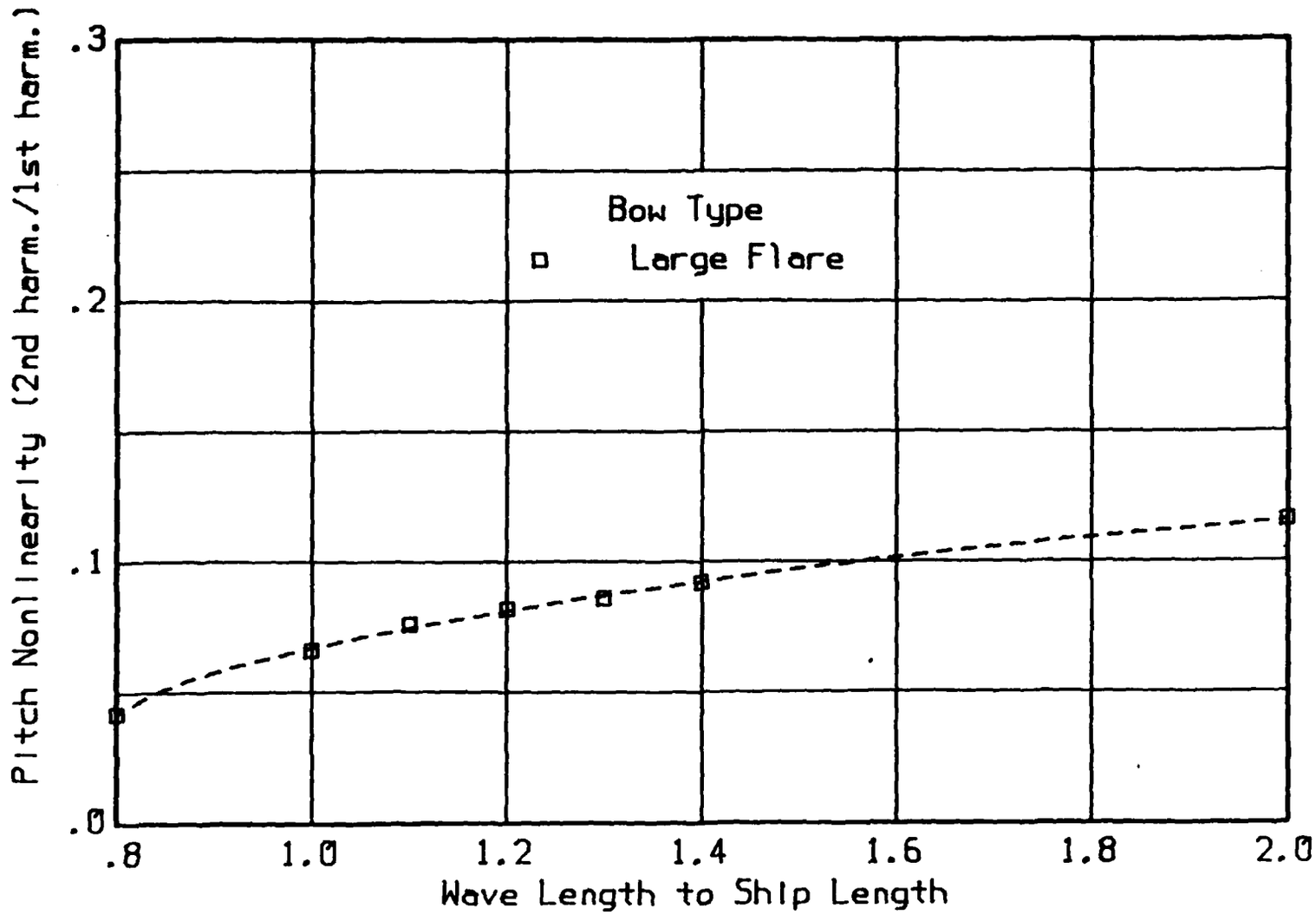

Figure A20c. Pitch Motion Nonlinearity Factor

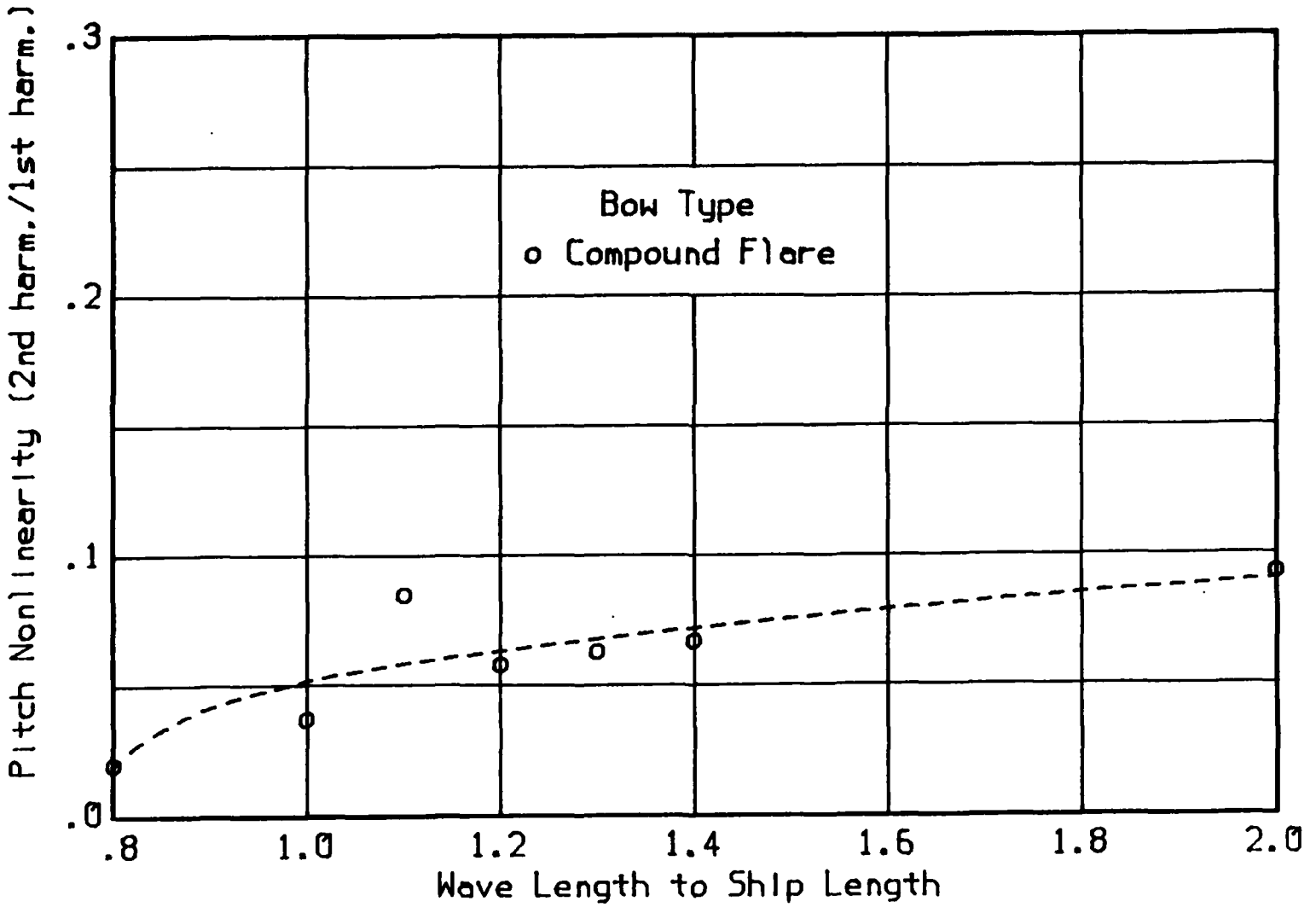

Figure A20d. Pitch Motion Nonlinearity Factor

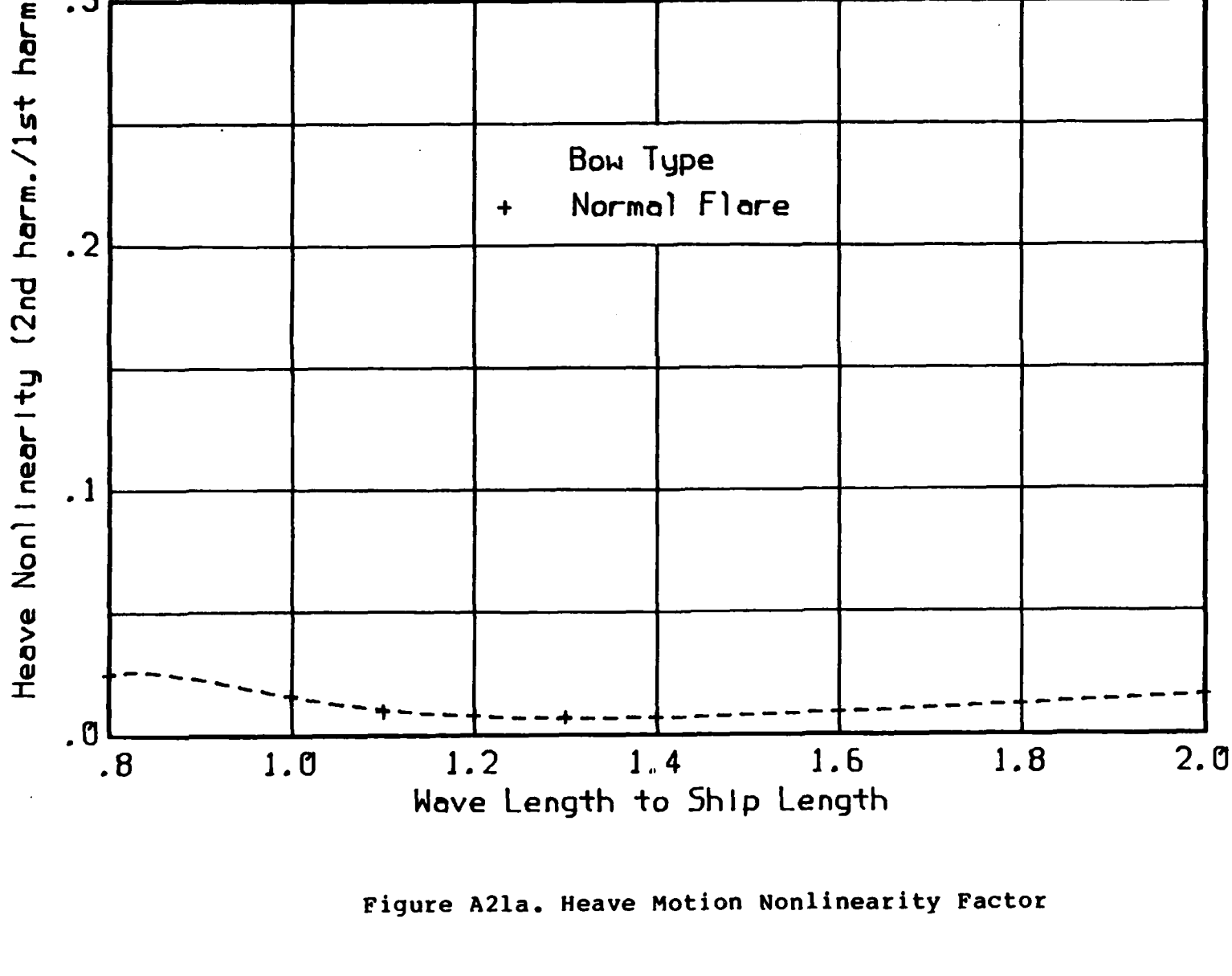

Figure A21a. Heave Motion Nonlinearity Factor

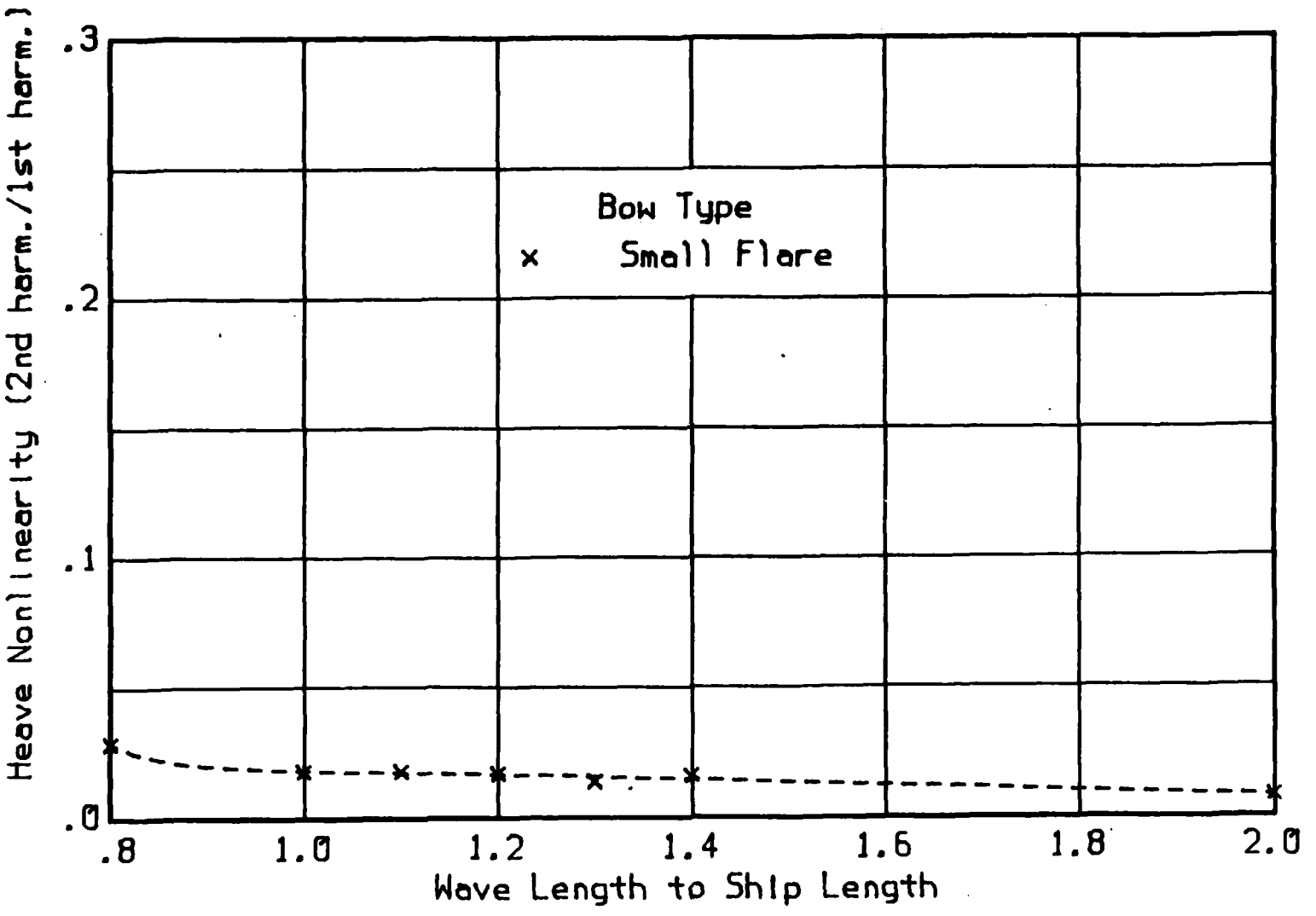

Figure A21b. Heave Motion Nonlinearity Factor

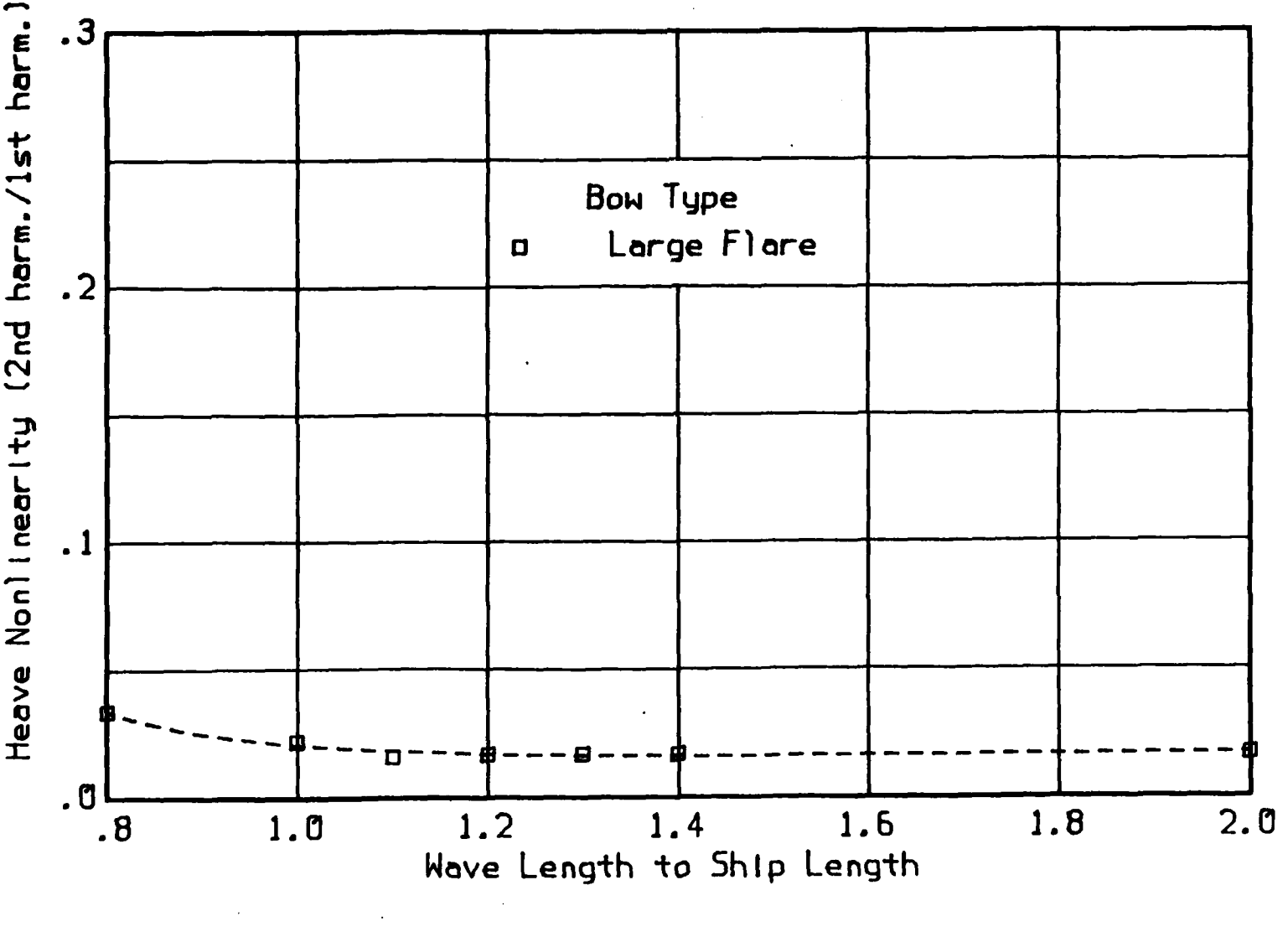

Figure A21c. Heave Motion Nonlinearity Factor

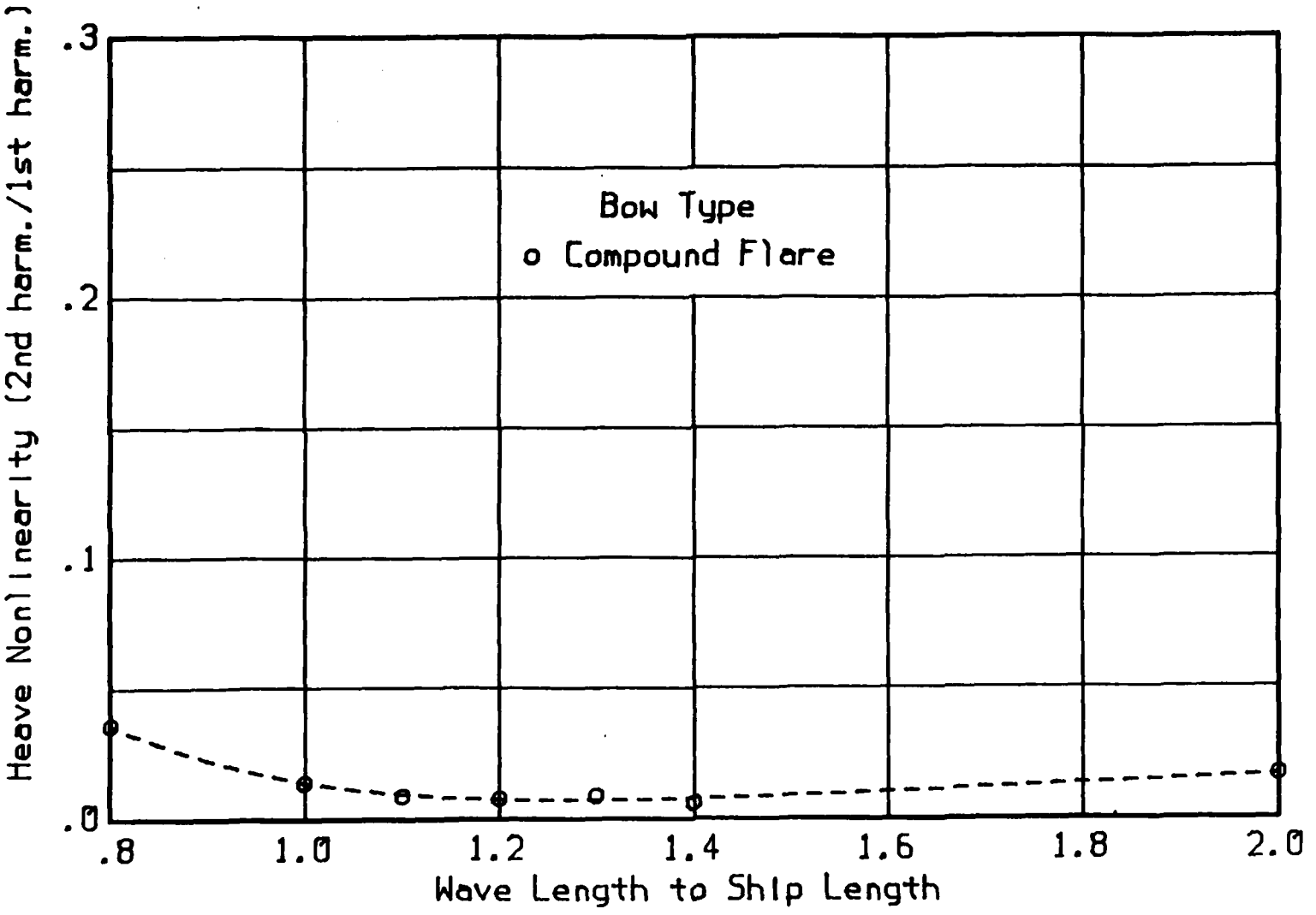

Figure A21d. Heave Motion Nonlinearity Factor

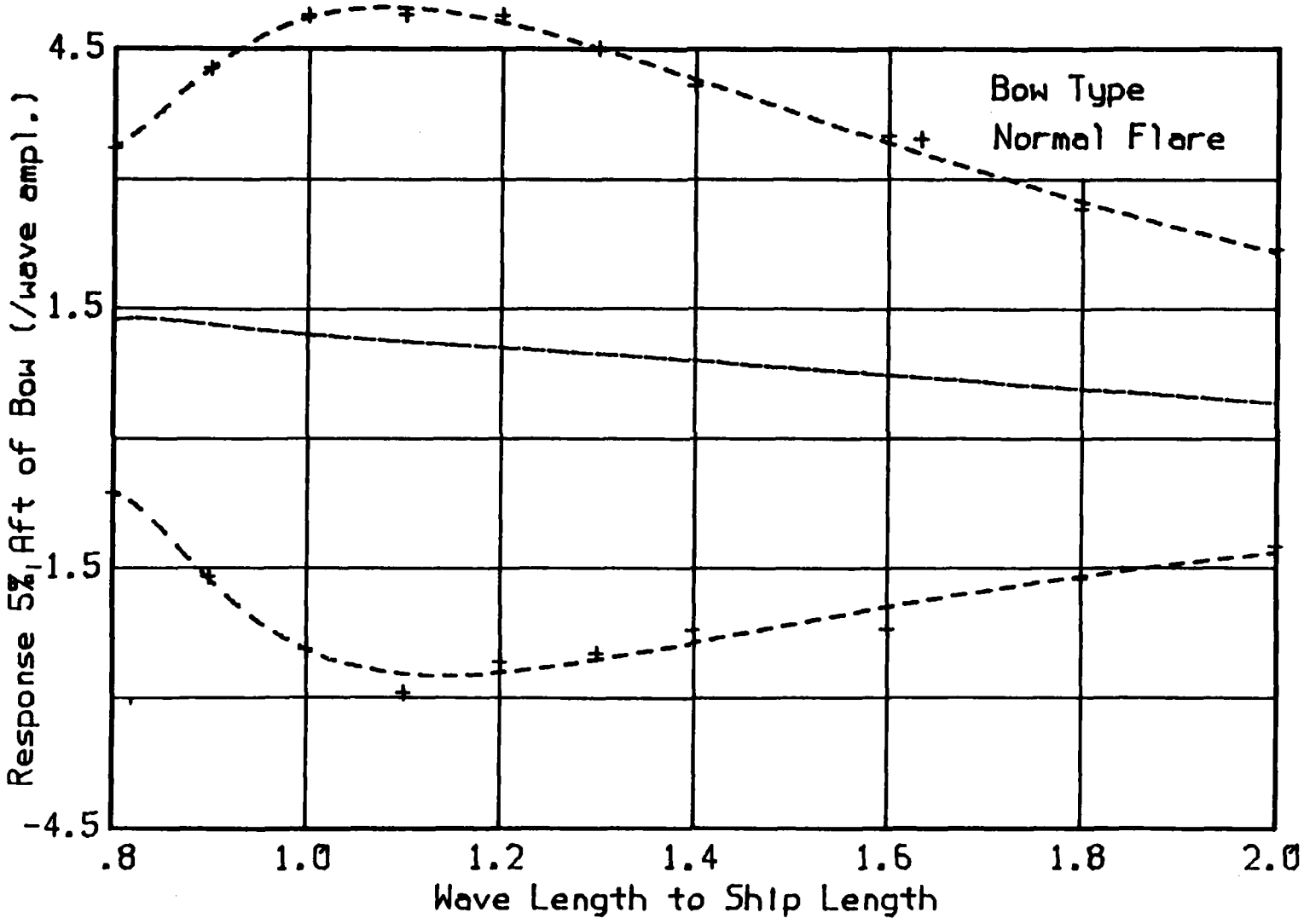

Figure A22a. Relative Motion Statistics in
1:40 Head Seas - 5% Aft of Bow

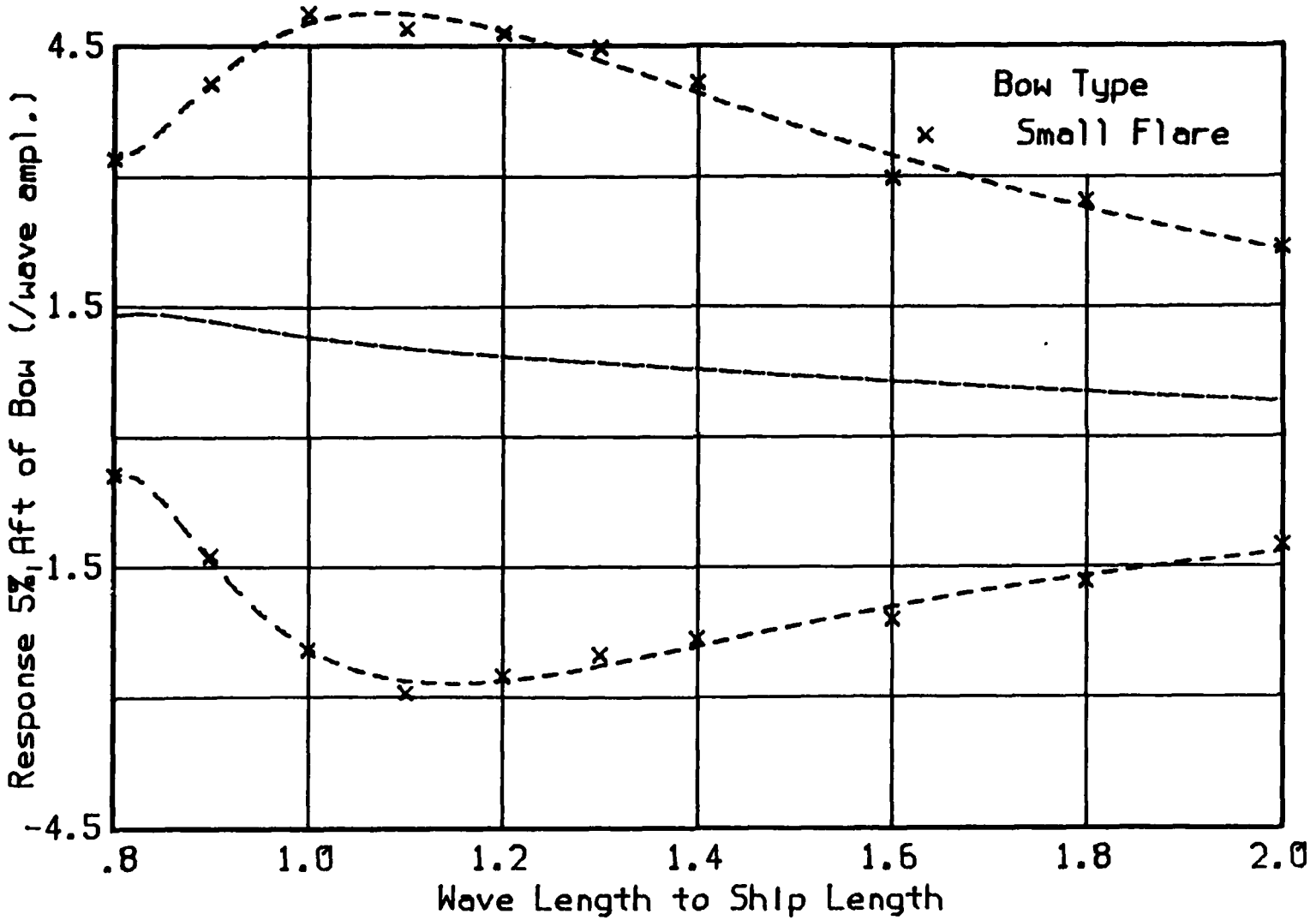

Figure A22b. Relative Motion Statistics in
1:40 Head Seas - 5% Aft of Bow

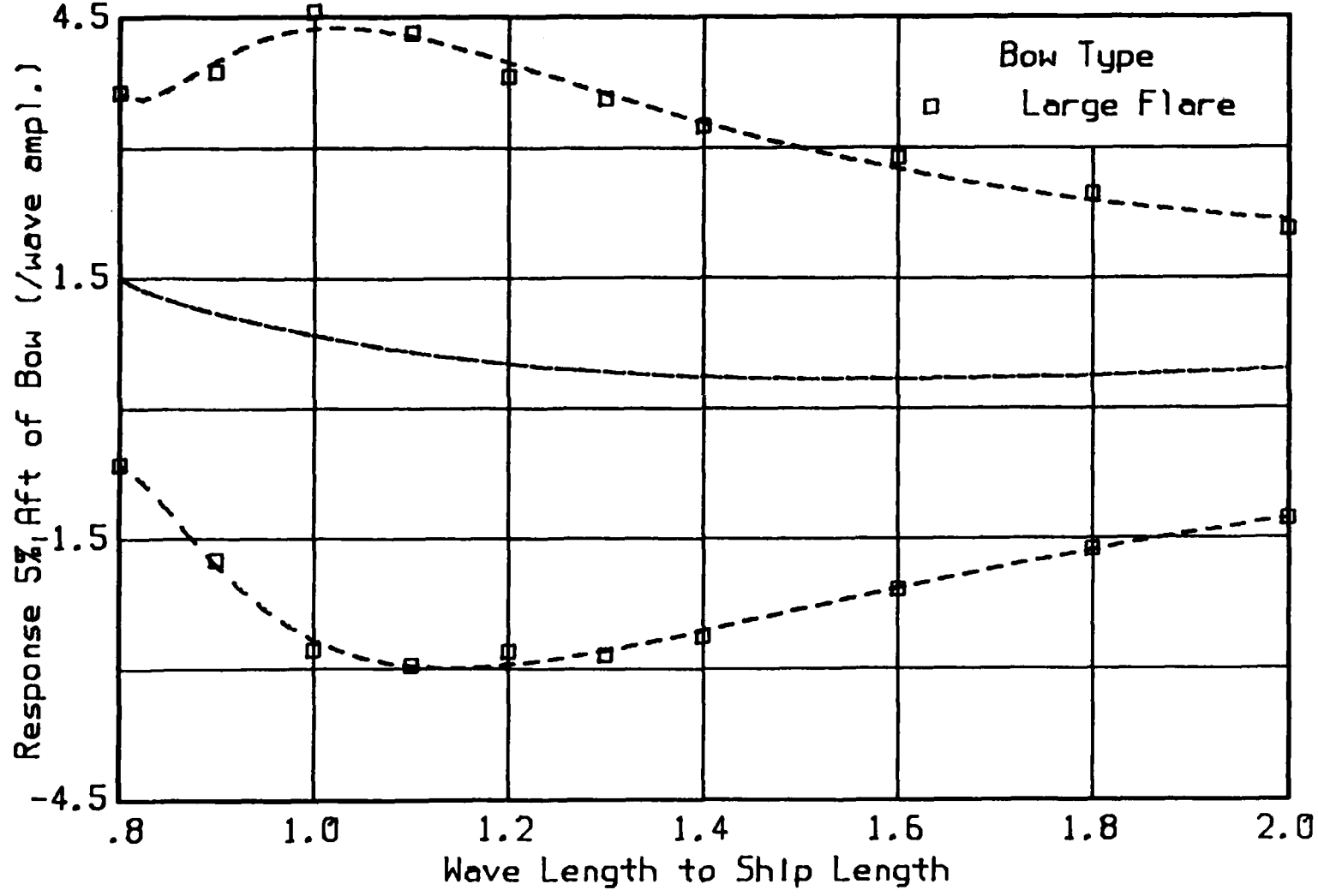

Figure A22c. Relative Motion Statistics in 1:40 Head Seas - 5% Aft of Bow

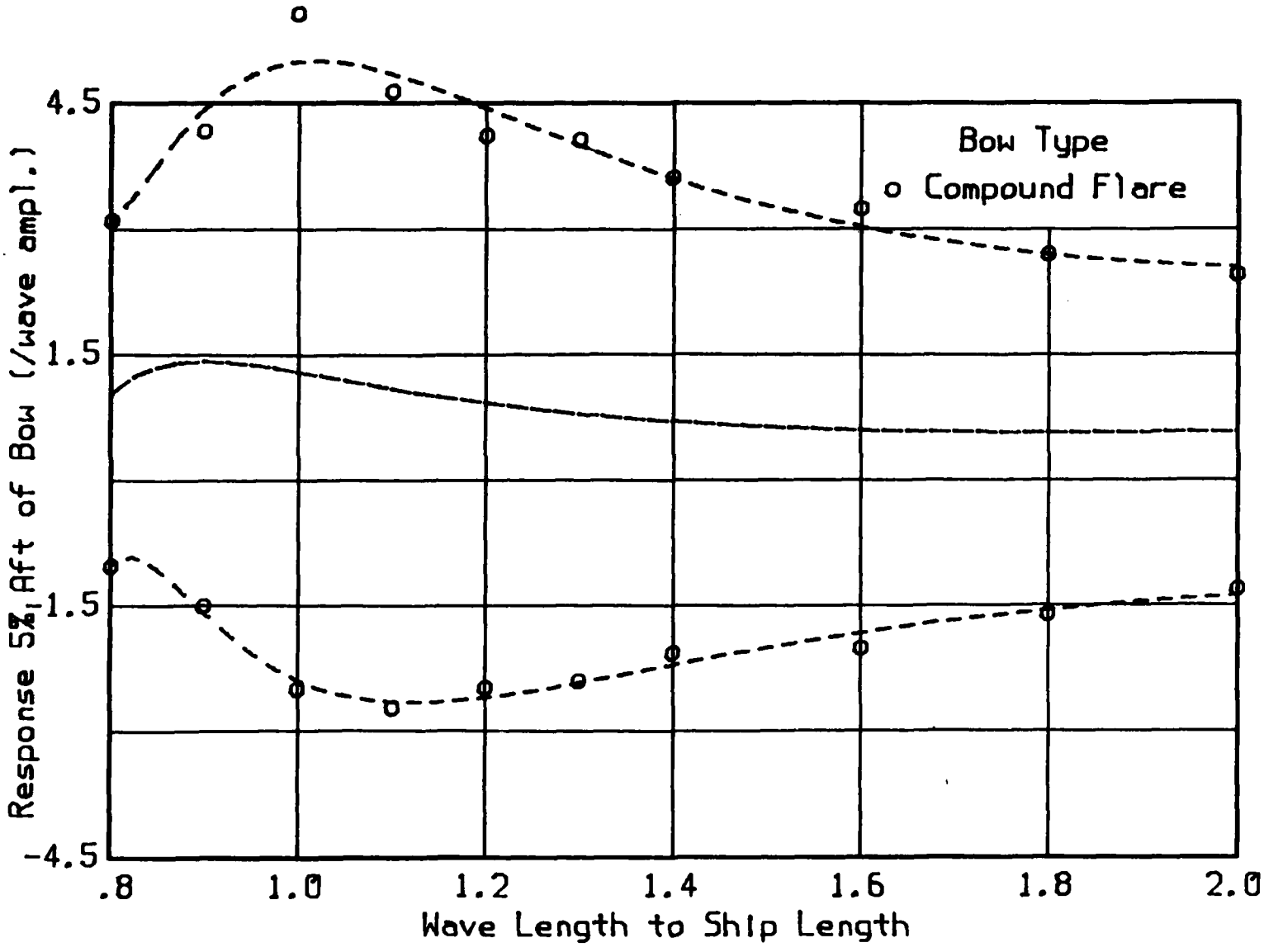

Figure A22d. Relative Motion Statistics in
1:40 Head Seas - 5% Aft of Bow

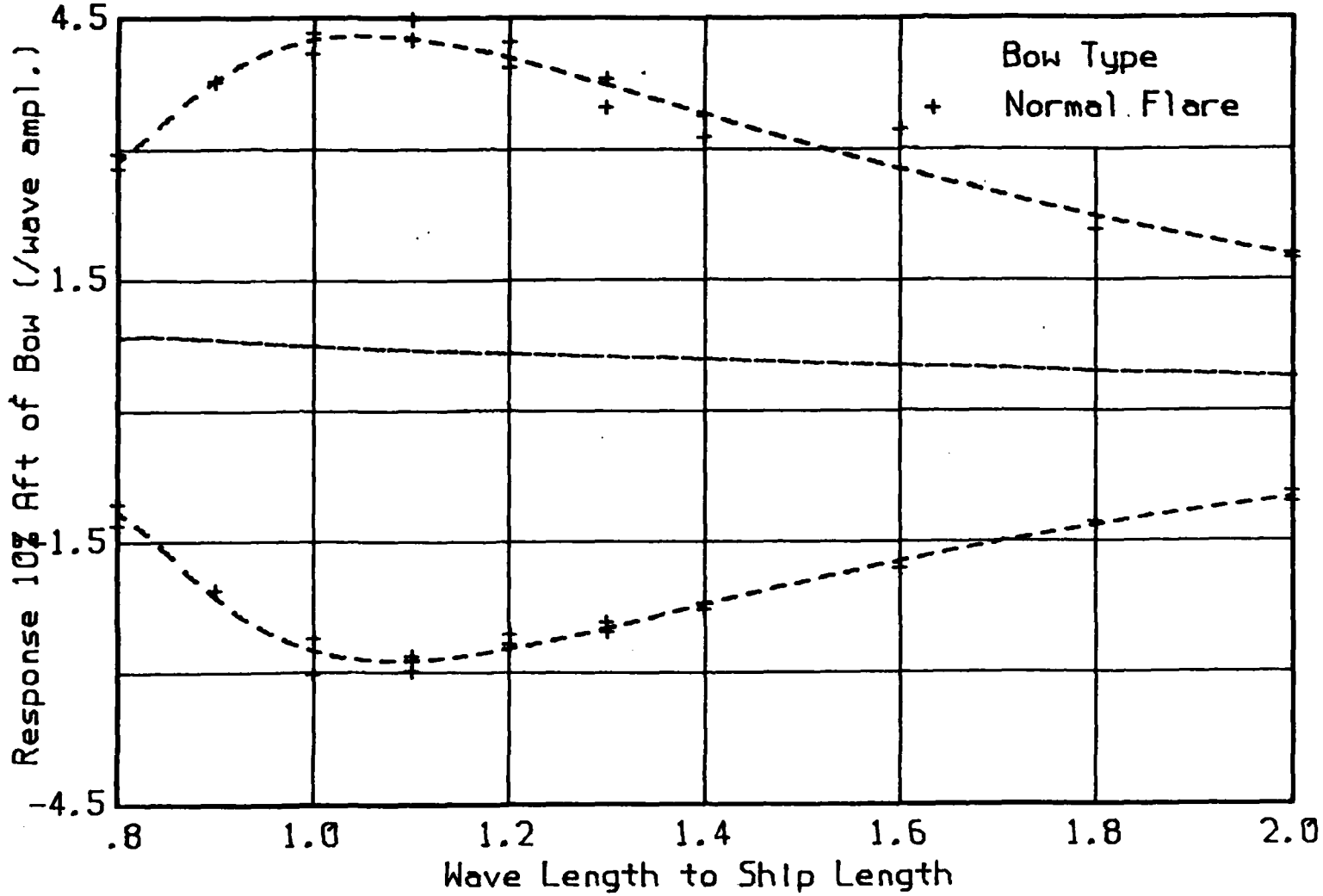

Figure A23a. Relative Motion Statistics in 1:40 Head Seas - 10% Aft of Bow

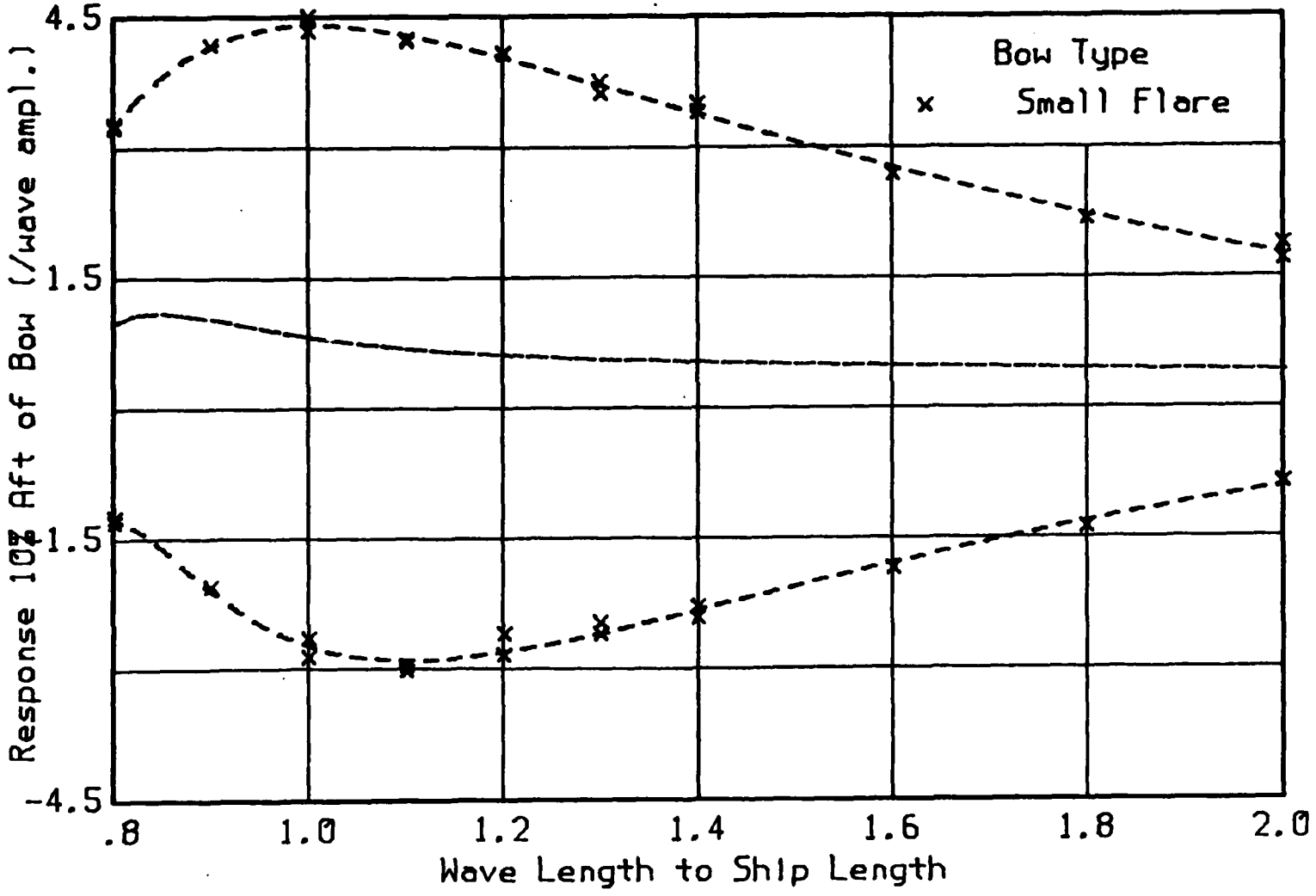

Figure A23b. Relative Motion Statistics in
1:40 Head Seas - 10% Aft of Bow

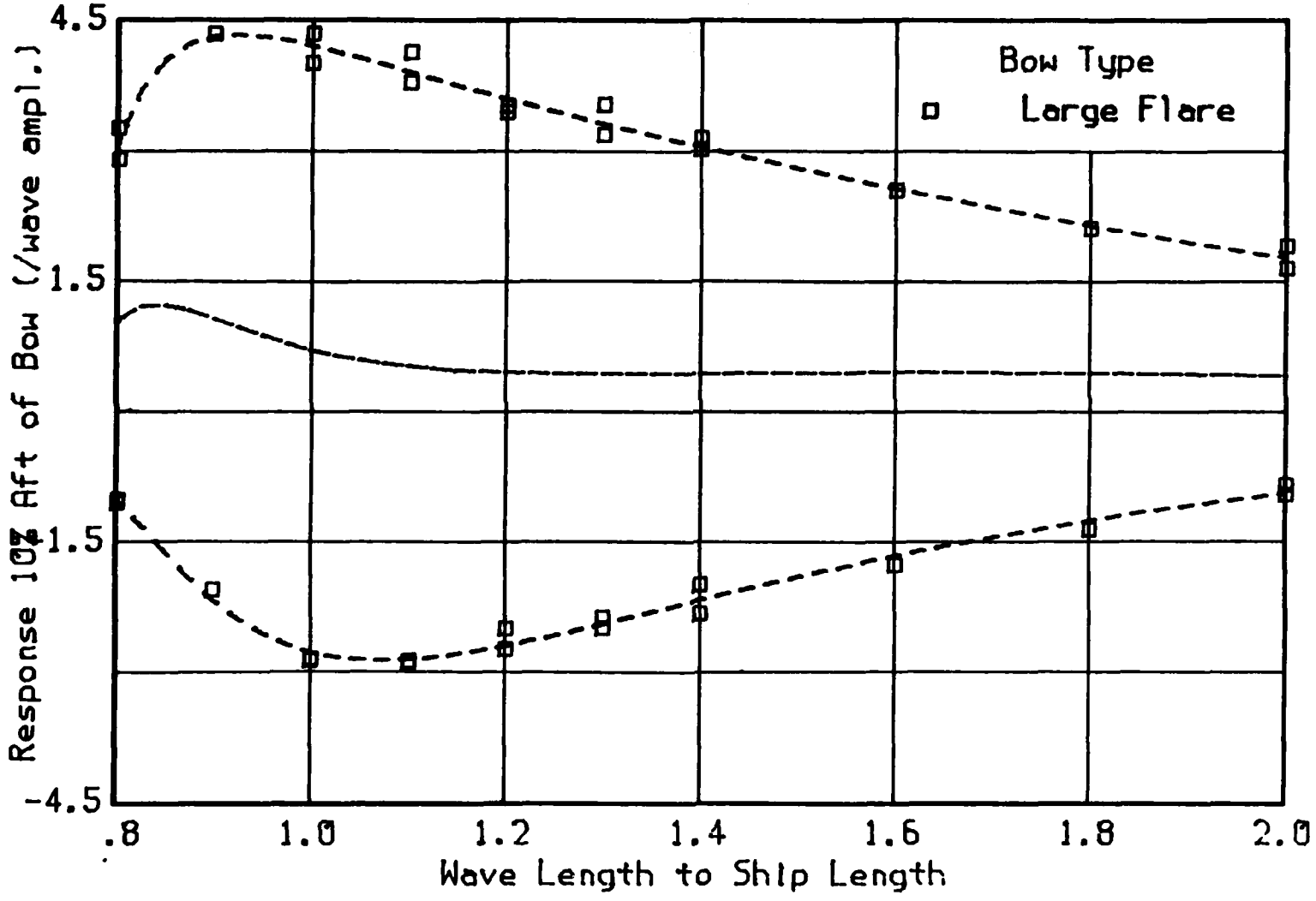

Figure A23c. Relative Motion Statistics in 1:40 Head Seas - 10% Aft of Bow

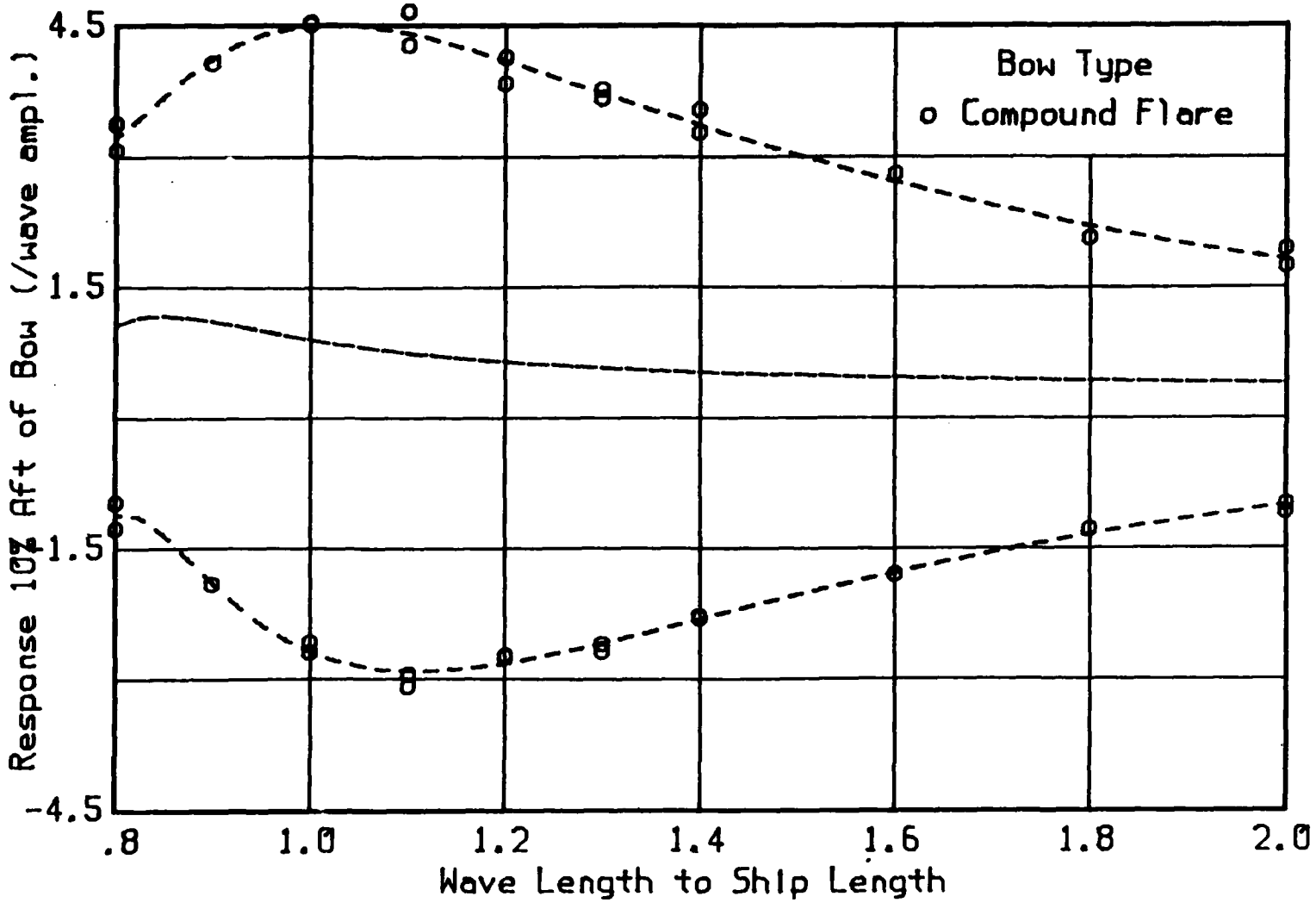

Figure A23d. Relative Motion Statistics in 1:40 Head Seas - 10% Aft of Bow

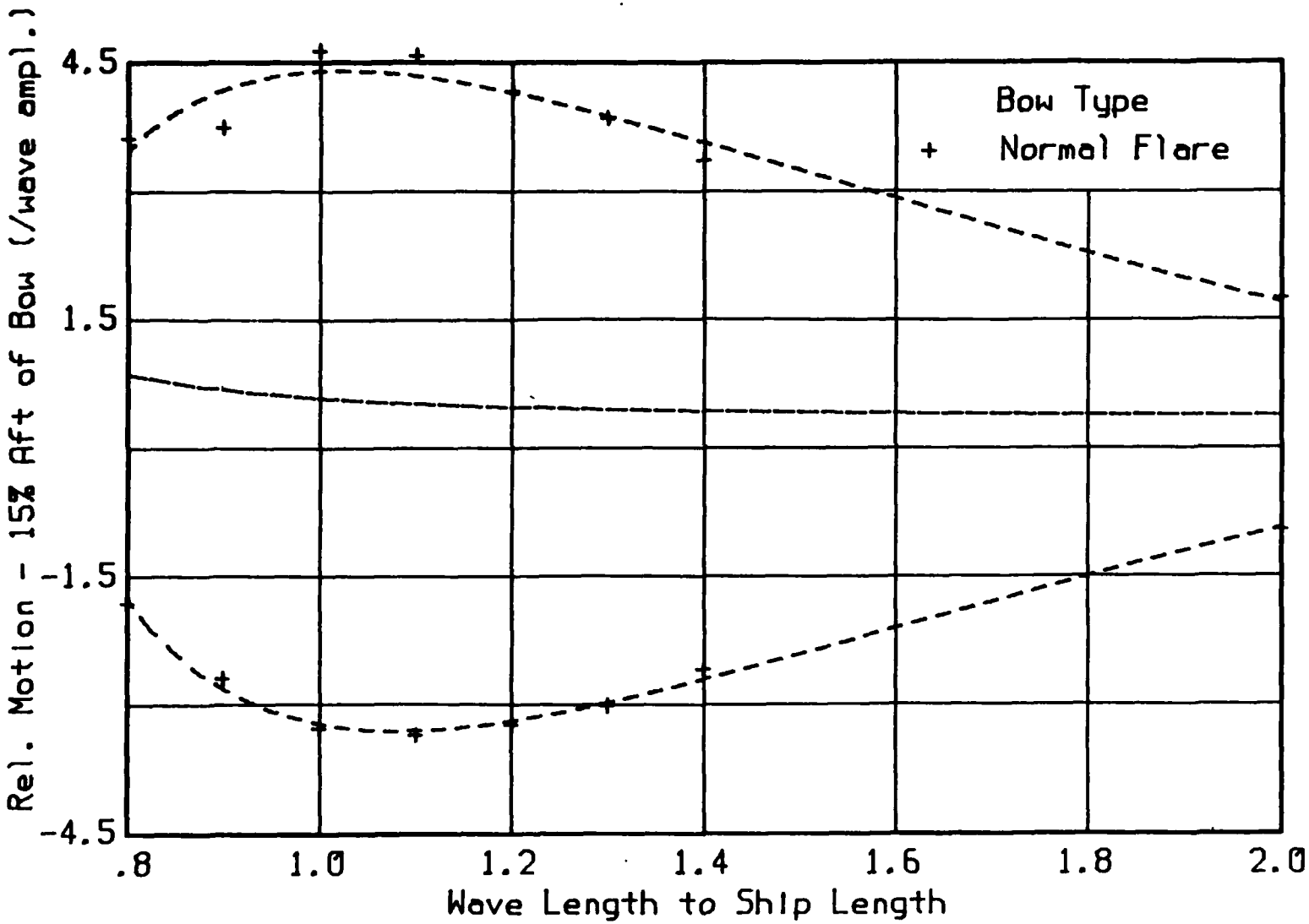

Figure A24a. Relative Motion Statistics in 1:40 Head Seas - 15% Aft of Bow

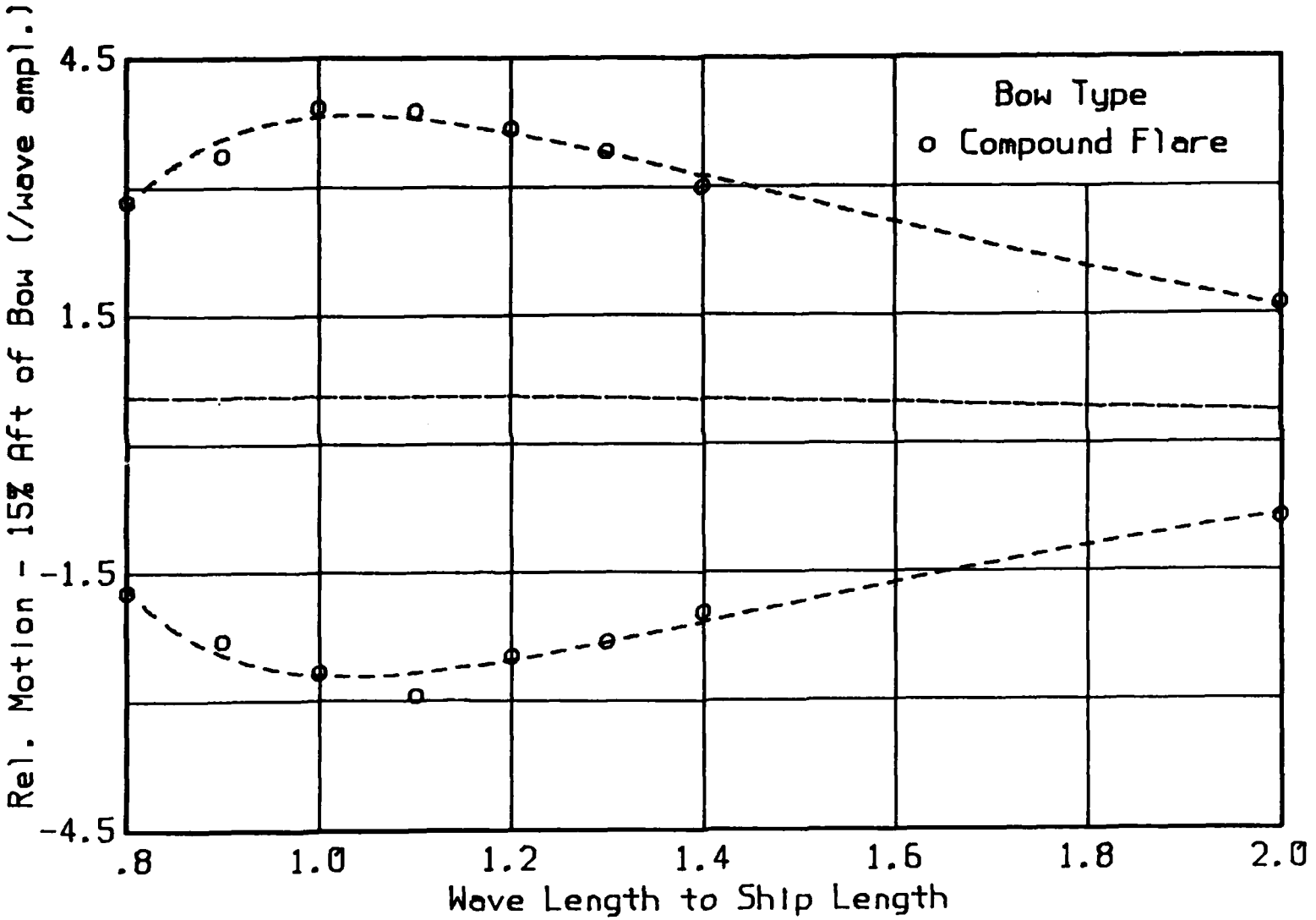

Figure A24d. Relative Motion Statistics in
1:40 Head Seas - 15% Aft of Bow

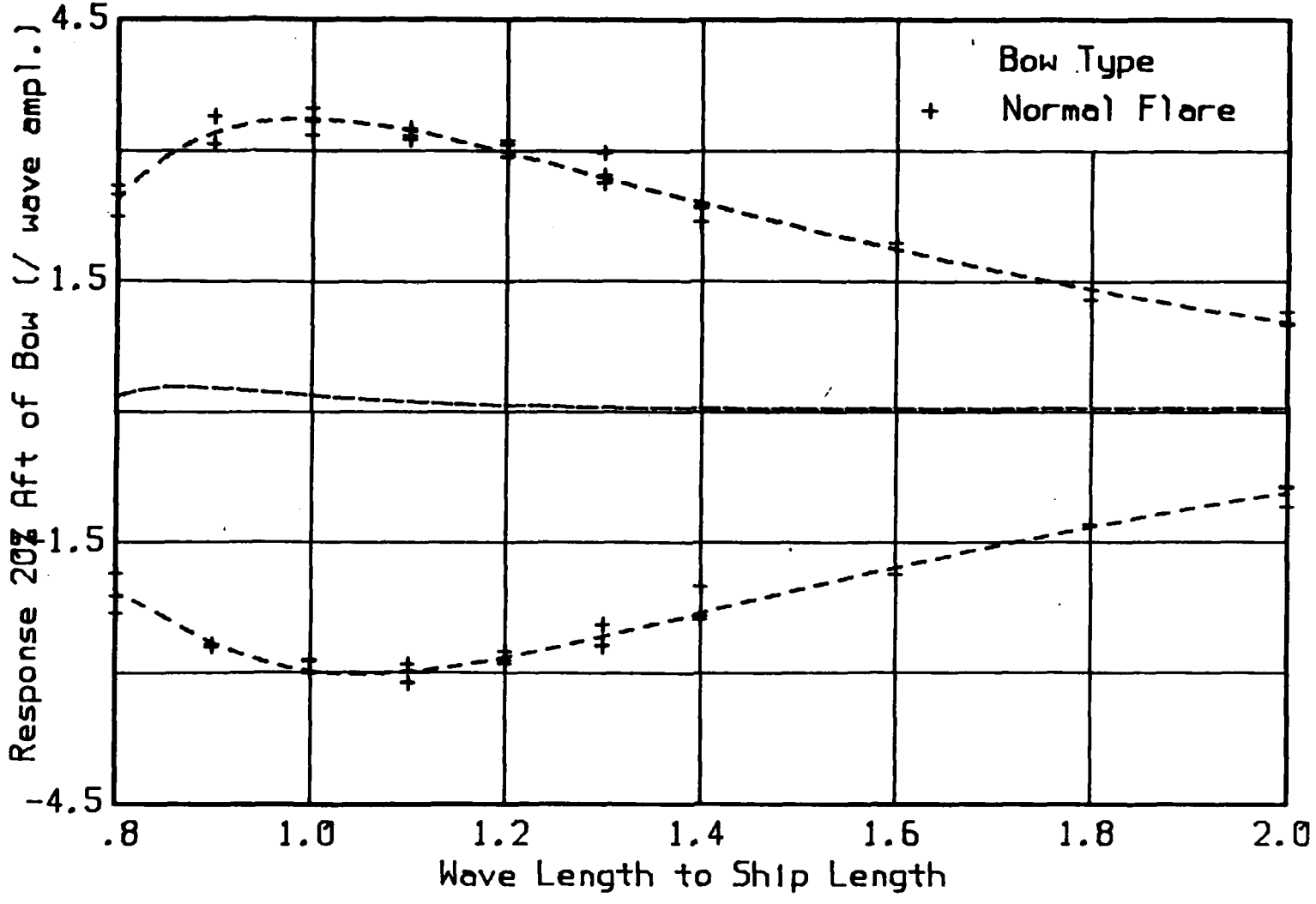

Figure A25a. Relative Motion Statistics in
1:40 Head Seas - 20% Aft of Bow

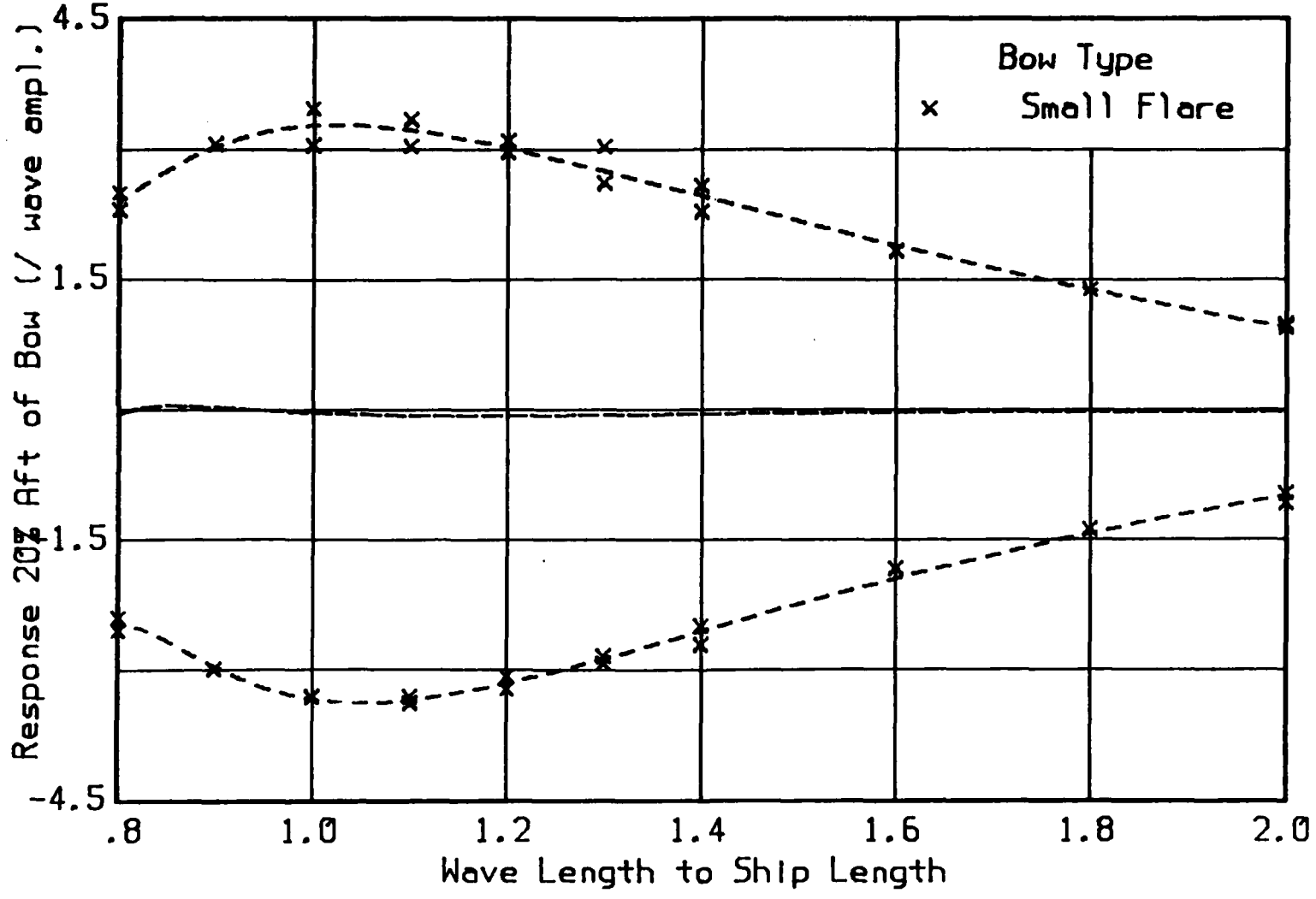

Figure A25b. Relative Motion Statistics in
1:40 Head Seas - 20% Aft of Bow

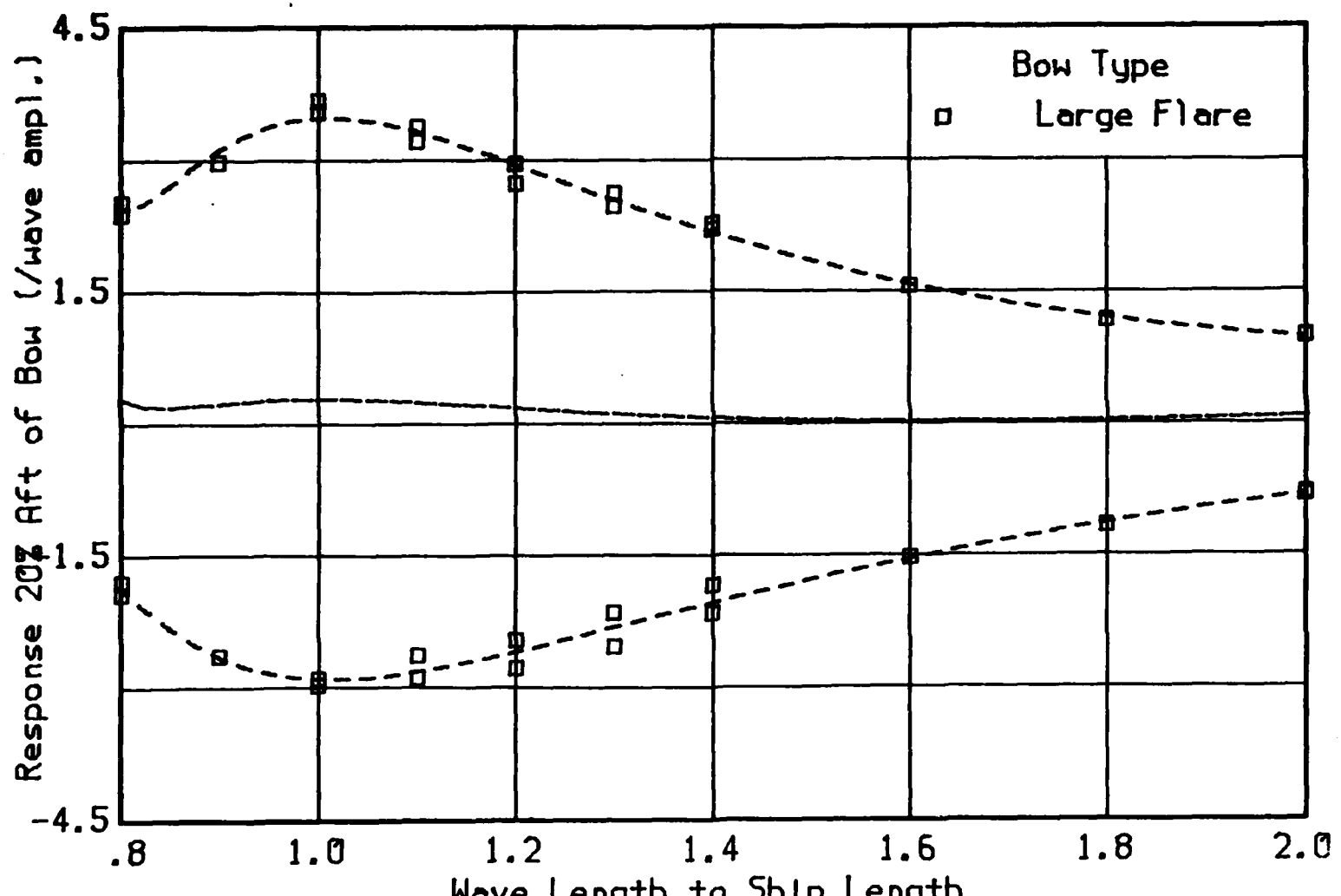

Figure A25c. Relative Motion Statistics in
1:40 Head Seas - 20% Aft of Bow

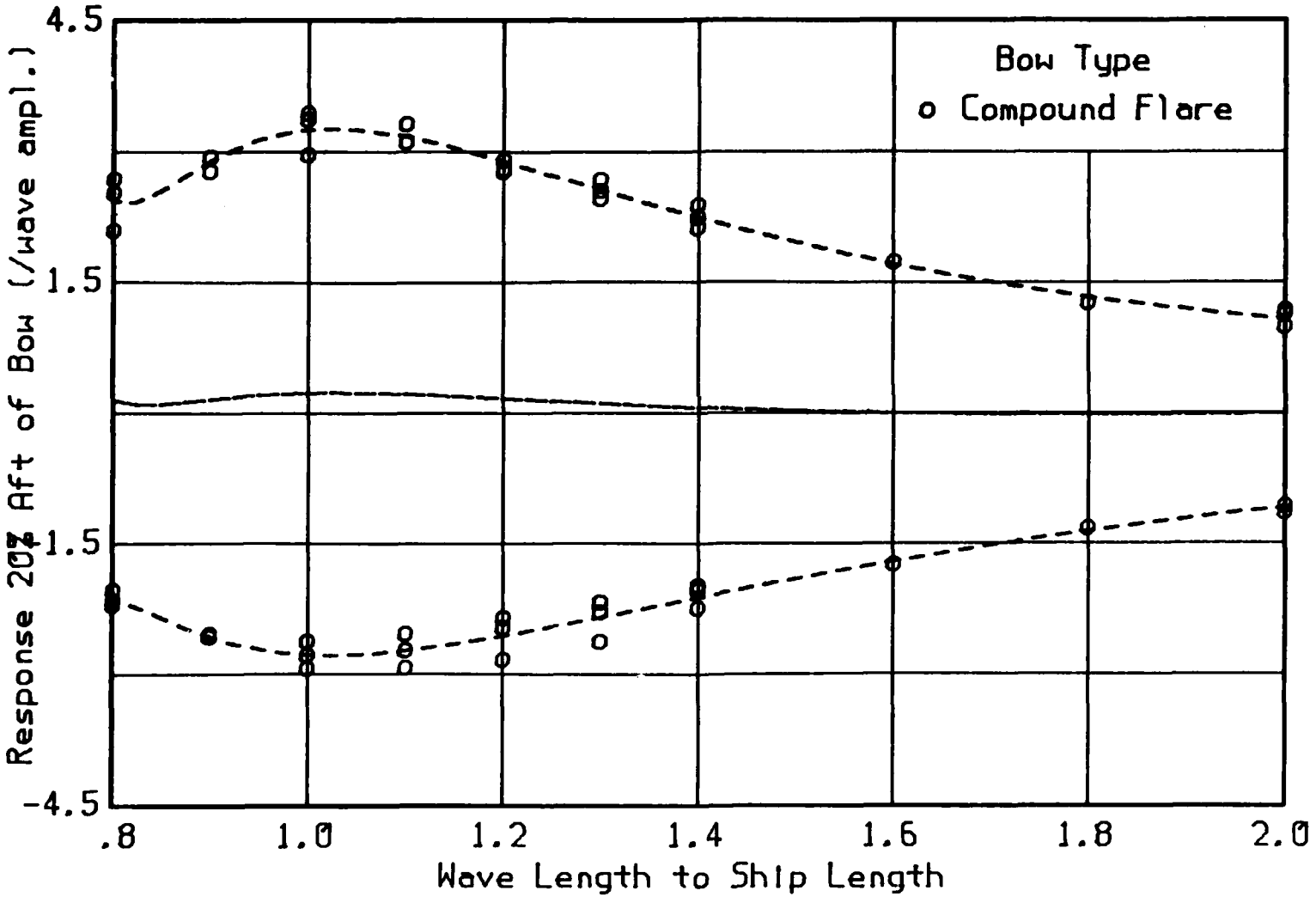

Figure A25d. Relative Motion Statistics in
1:40 Head Seas - 20% Aft of Bow

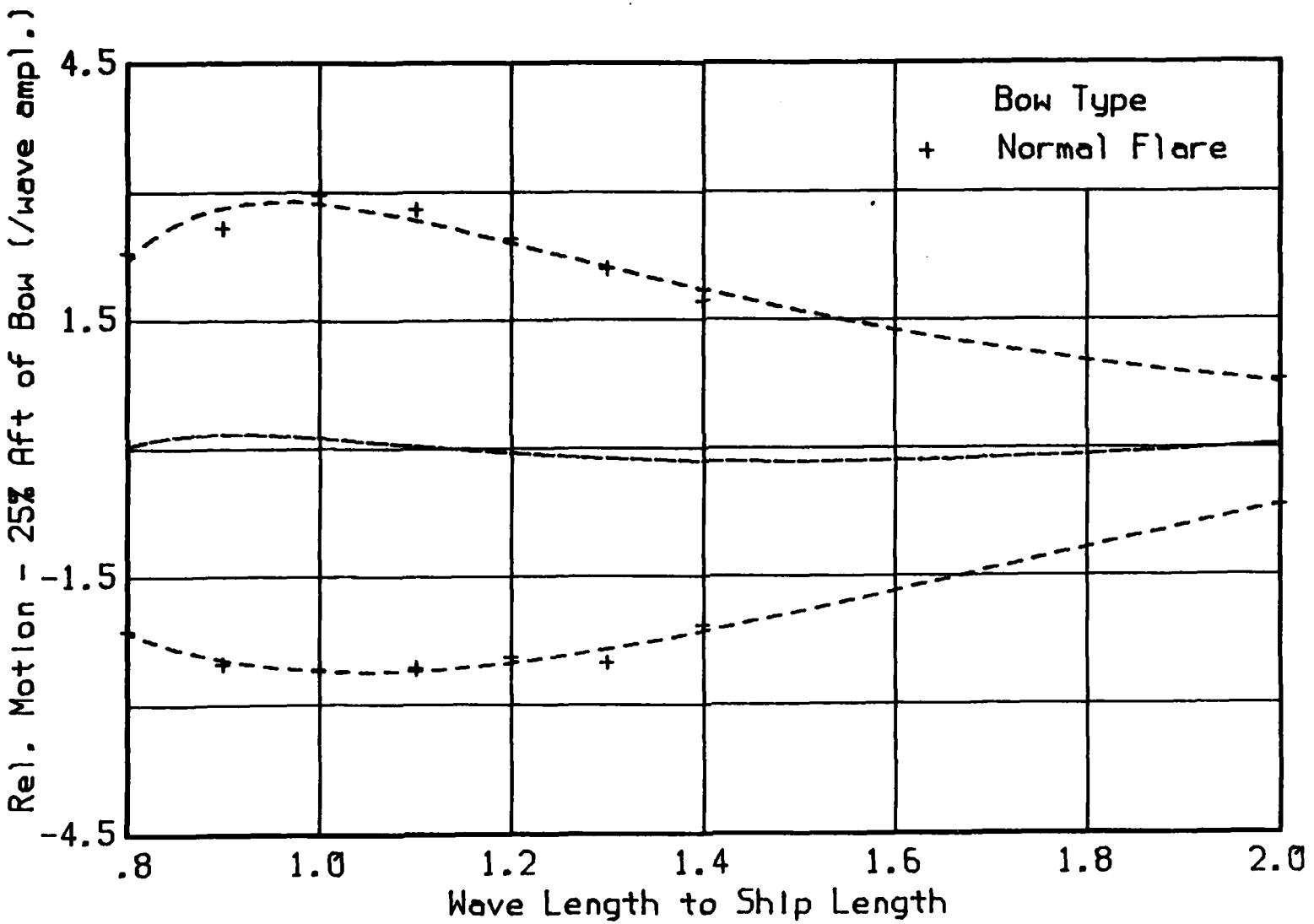

Figure A26a. Relative Motion Statistics in 1:40 Head Seas - 25% Aft of Bow

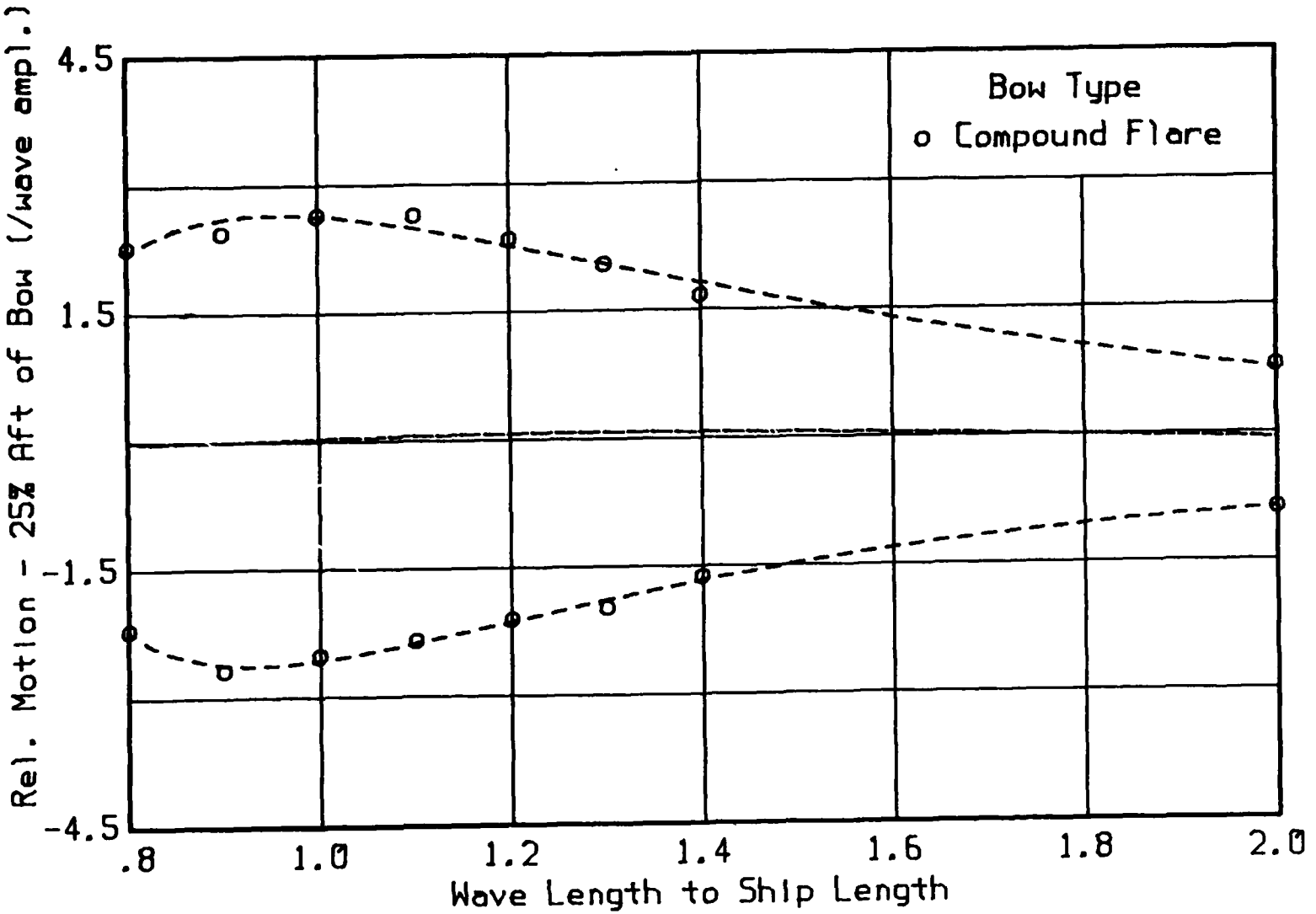

Figure A26d. Relative Motion Statistics in 1:40 Head Seas - 25% Aft of Bow

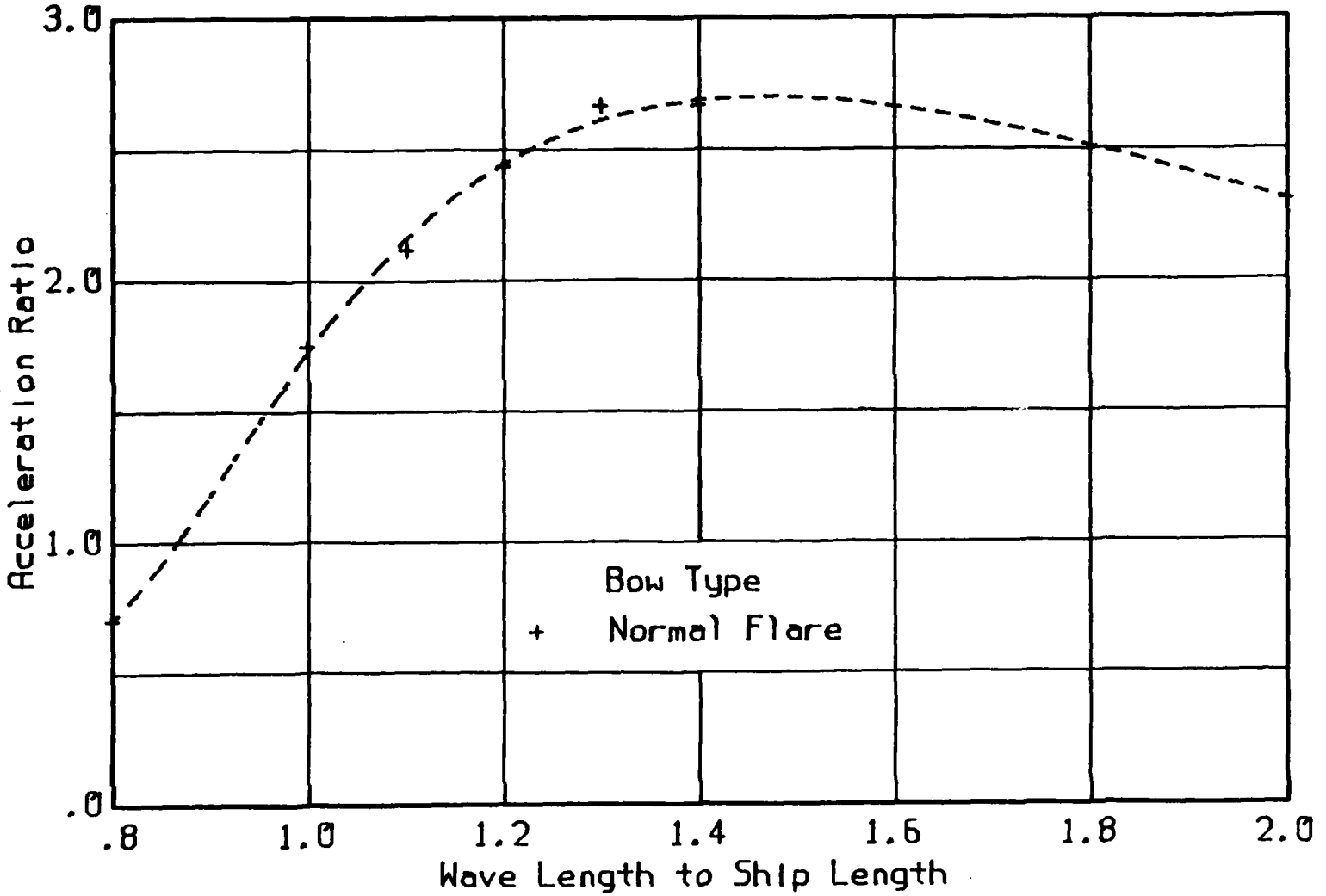

Figure A27a. Acceleration Ratio

AD-A137 409 AN EXPERIMENTAL STUDY ON THE EFFECT OF BOW SHAPE ON THE SEAWORTHINESS OF A SHIP(U) CALIFORNIA UNIV BERKELEY DEPT OF NAVAL ARCHITECTURE W C WEBSTER ET AL. SEP 83 2/2

UNCLASSIFIED N00014-80-C-0226 F/G 13/10 NL

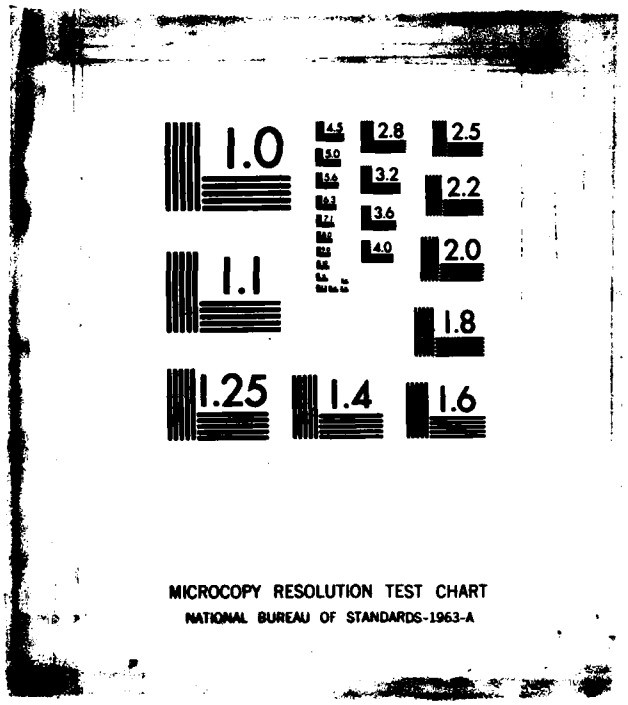
1.0
2.8
2.5
3.2
2.2
3.6
4.0
2.0
1.1
1.8
1.25
1.4
1.6
MICROCOPY RESOLUTION TEST CHART
NATIONAL BUREAU OF STANDARDS-1963-A

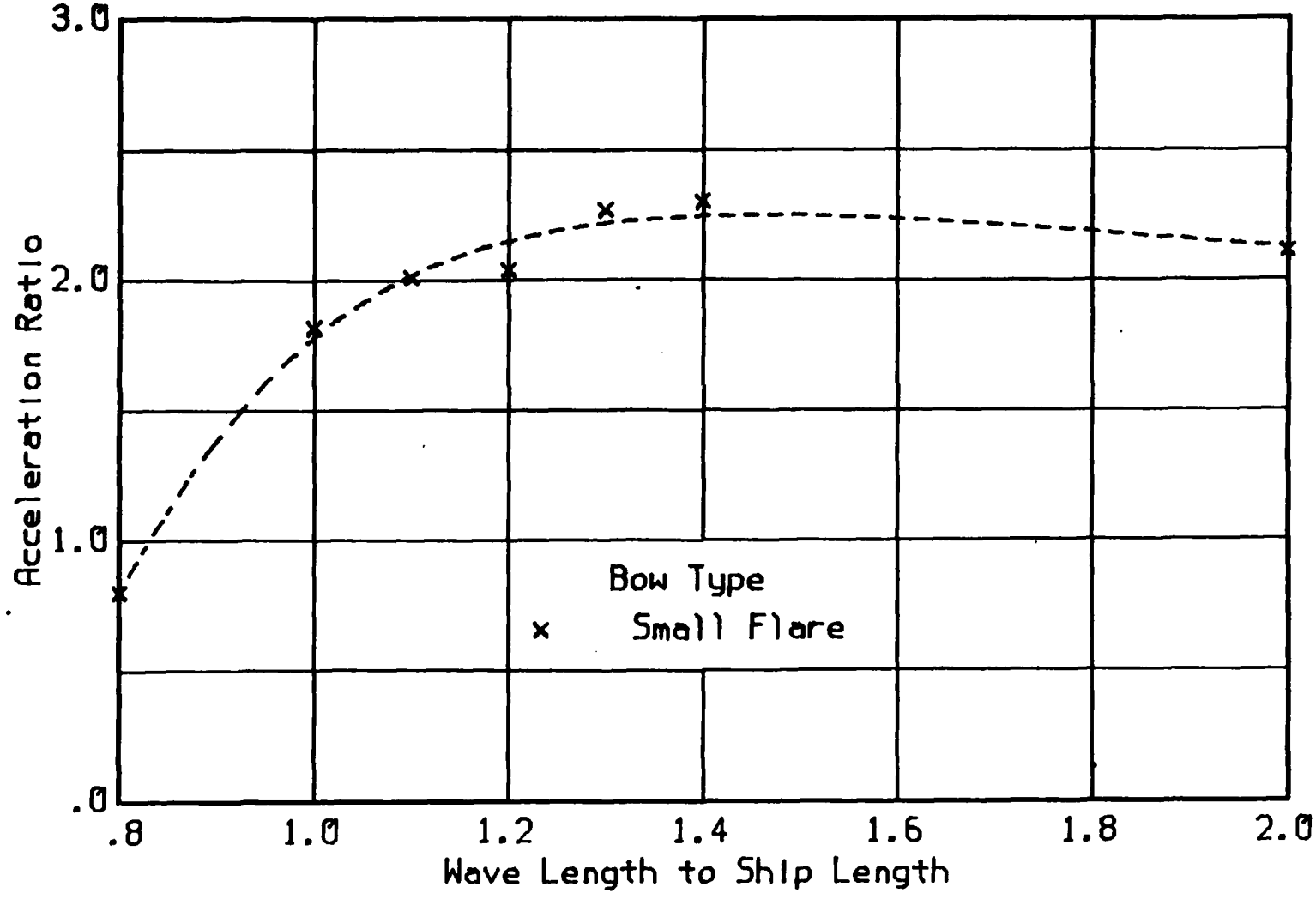

Figure A27b. Acceleration Ratio

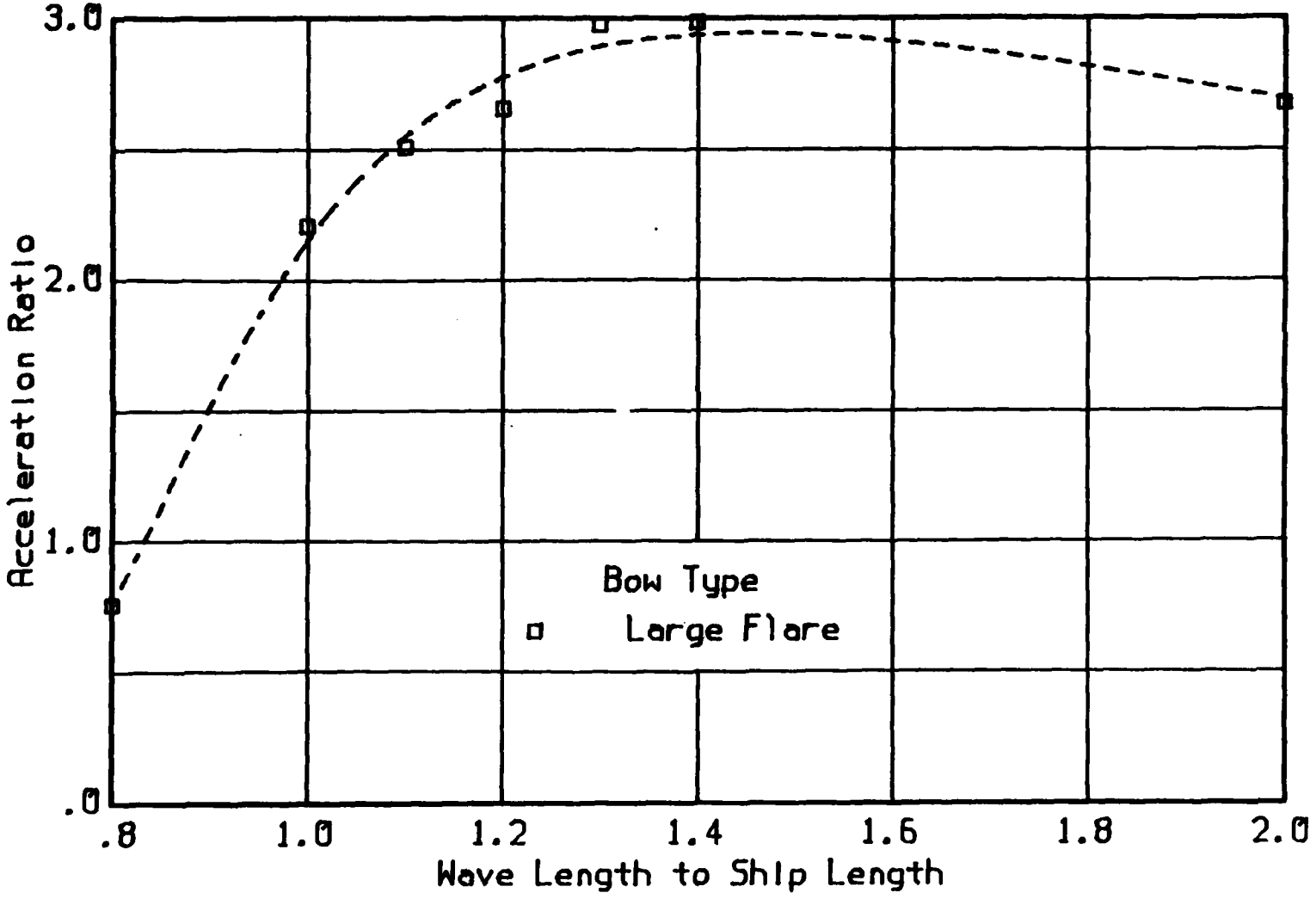

Figure A27c. Acceleration Ratio

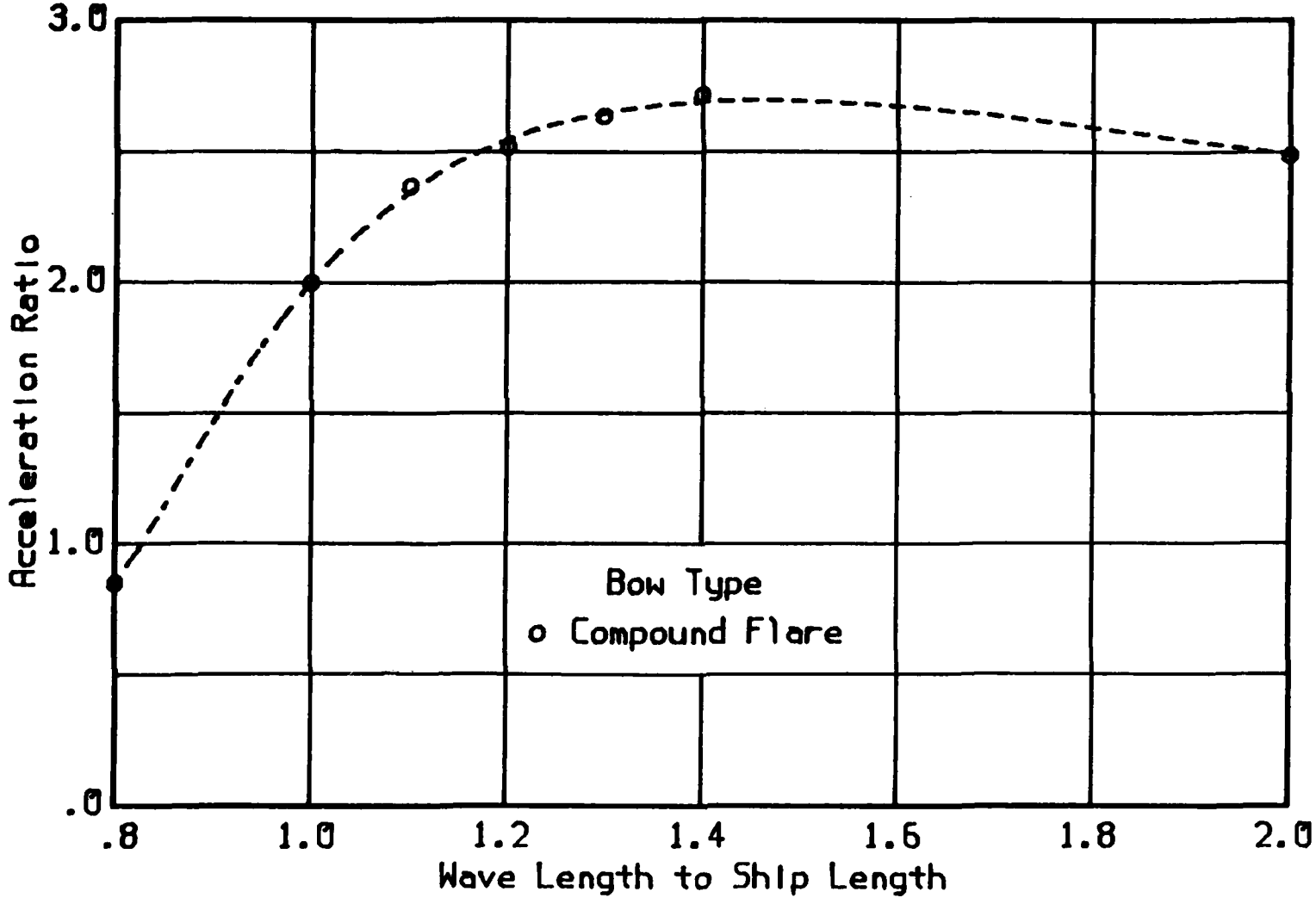

Figure A27d. Acceleration Ratio

DISTRIBUTION LIST FOR UNIVERSITY OF CALIFORNIA REPORT -

14 Commander
David W. Taylo r Naval
Ship R&D Center
Attn: Code 1505
Bethesda, Md 20084

8 Commander
Naval Sea Systems Command
Washington, D. C. 20362
Attn: 05R22 (J. Sejd)
55W (R. Keane, Jr.)
55W3 (W. Sandberg)
50151 (C. Kennell)
56X1 (F. Welling)
63R31 (T. Peirce)
55X42 (A. Paladino)
99612 (Library)

1 Dr. C. M. Lee, Code 432
Office of Naval Research
800 N. Quincy Street
Arlington, VA 22217

ENCLOSURE (1)

END

FILMED

02 — 84

DTIC